Rajesh Koppolu

High-throughput Processing of Nanocelluloses into Barrier Coatings

A Focus on Nanocellulose Rheology and Multilayer Barrier Properties

Åbo Akademi University

Rajesh Koppolu

Born 1989 in Kothagudem, India

Received his B.Tech. degree in Pulp and Paper Engineering from Indian Institute of Technology Roorkee, India in 2011.

Rajesh joined the Laboratory of Paper Coating and Converting (PaF), currently Natural Materials Technology (NMT) in 2014. He received his M.Sc. (Tech.) degree in Chemical Engineering from Åbo Akademi University in 2016. He continued with his doctoral studies at PaF/NMT since 2016.

High-throughput Processing of Nanocelluloses into Barrier Coatings

A Focus on Nanocellulose Rheology
and Multilayer Barrier Properties

Rajesh Koppolu

Natural Materials Technology
Faculty of Science and Engineering
Åbo Akademi University
Åbo, Finland, 2024

Supervisor

Professor Martti Toivakka
Laboratory of Natural Materials Technology
Åbo Akademi University
Åbo, Finland

Pre-examiners

Dr. David Guérin
Packaging & Product Development
L'Oréal Packaging Science Center
Clichy, France

Professor Thaddeus Maloney
Bio-based Materials Technology
Aalto University
Espoo, Finland

Opponent for the public defense

Dr. David Guérin
Packaging & Product Development
L'Oréal Packaging Science Center
Clichy, France

ISBN printed Version: 978-952-12-4357-8
ISBN digital Version: 978-952-12-4358-5
Painosalama – Åbo, Finland 2024

To my father, Ravi Kumar and grand father, Hanumantha Rao

Acknowledgments

This work was conducted at the Laboratory of Natural Materials Technology (NMT), formerly known as the Laboratory of Paper Coating and Converting (PaF) at Åbo Akademi University. I am grateful for the financial support from the Åbo Akademi Graduate School in Chemical Engineering (GSCE), Magnus Ehrnrooth Foundation, Finnish Forest Products Engineers' Association (Puunjalostusinsinöörit), Walter Ahlström Foundation, and the Rector of Åbo Akademi University.

I am immensely indebted to my supervisor, Prof. Martti Toivakka, for his unwavering support, invaluable guidance, endless patience, and for being a vast source of knowledge throughout my entire academic journey. Your mentorship has been instrumental in shaping my path, and I admire your curiosity, passion for science, and meticulous attention to detail. You have consistently challenged me to strive for a better version of myself, while granting me the autonomy to explore at my own pace. Over the years, you have been both a mentor and a friend, and words cannot express the depth of my gratitude for the privilege of conducting my doctoral studies under your exceptional guidance.

I am also thankful to my collaborators, Prof. Douglas Bousfield, Prof. Tiffany Abitbol, Prof. Agne Swerin, Prof. Jurkka Kuusipalo, Prof. Julien Bras, Dr. Johanna Lahti, and Dr. Christian Aulin, for your support and guidance through various projects and publications throughout my doctoral studies.

My time at PaF has undoubtedly been one of the most fulfilling and joyous periods of my life. When I reflect on my experiences there, Mari is the first person who comes to mind. Your warm and caring nature made me feel welcome from the very first day. You always knew the best local activities to try out and played a vital role in introducing me to the Finnish culture. ÄV (Björn) and Carola, you both have been some of the happiest people I have ever known, and you have always been like a family to me. I hold dear the memories of the Christmases, barbecues, parties, and sailing trips we spent together.

I want to express my heartfelt gratitude to Diosa, Ruut, and Kofi, for being incredible colleagues and wonderful friends both within and beyond the workplace. The special bond we have cultivated over the years means the world to me, and I genuinely hope we can continue nurturing our friendship by meeting regularly to share our dose of 'gossip' and laughter. I also extend my sincere thanks to Joel,

Dimi, Peter, Jani, JP, Kena, Fuaad, Himal, Jarkko, Jan, Anna, Xiaoju, Chunlin, Qingbo, Luyao, Liqiu, Minette, and all the other amazing individuals at PaF and NMT. Your presence has made my time here truly memorable, and I am grateful for each and every one of you.

Vinay, you are my oldest and best friend, one of the kindest, most helpful, and down-to-earth person I know. I have always looked up to you like an older brother, both for the fun-filled "bakchodi" moments and your invaluable professional/personal advice. Aayush, with your helpful and quirky nature, and Naren, with your ability to find new and interesting activities, complete the "bakchod bruus" group with Vinay and me. Together, we share a lifetime of experiences and I am certain we will continue to create more in the future. I want to give a big shout out to Debanga, Susmita, Sonu, Alexandra, Deepika, Milla, Narahari, Saket, and Pyne for your amazing company and the countless memories we have shared over the years. Special thanks go to Ida and Lucas for all the Friday after-work beers, mushroom picking, and introducing me to Åland - I truly enjoyed our time together.

Amma, you instilled in me a deep appreciation for the world's renowned scientists during my childhood, while Nana, you consistently emphasized the immeasurable value of education. The person and scientist I have become today are a testament to the enduring love and unwavering support you provided throughout my life. Suresh babai, you have been a constant source of inspiration, and I hold deep gratitude for your invaluable advice and guidance during my educational pursuits.

To my wife, Keerthana, you entered my life during one of its most challenging phases, marked by pandemic uncertainty, the loss of a loved one, and the pursuit of my thesis and a new job. Your unwavering support has been my anchor, and I am profoundly thankful to have you by my side. Before our paths crossed, there were a very few places I considered calling home, but now, home is wherever you and Nemo are!

Åbo, January 2024
Rajesh

Contents

Abstract

Packaging is an integral part of our modern lives, especially in our interconnected world where nearly all products require some form of packaging. The global packaging market is currently valued at 1 trillion USD, with a substantial portion dedicated to barrier food packaging. This type of packaging is a complex structure, composed of multiple functional layers made from non-biodegradable plastics or metallic layers that pose challenges during recycling. Therefore, it is imperative to find sustainable alternatives to these materials. Nanocellulose is a nano-scale cellulose based natural polymer derived from plants, fungi, and bacteria. In addition to being bio-based and biodegradable, nanocellulose-based coatings and films have excellent barrier against oxygen, grease, and oils. Therefore, they are being investigated as potential alternatives to some of the non-biodegradable plastics and metallic layers in barrier food packaging.

There are several challenges that need to be addressed to enable high-throughput processing of nanocellulose into barrier coatings and films. Nanocellulose suspensions exhibit high viscosity and yield stress even at a low solid content, making it difficult to achieve thin uniform coatings, especially in high speed industrial roll-to-roll processes. In addition, nanocellulose is highly moisture sensitive, with most of its barrier properties deteriorating at high humidites. The current work aims to understand and address these challenges, and to develop high-throughput continuous process concepts required to convert a wide variety of nanocellulose suspensions into barrier coatings.

Flow properties of different types of nanocelluloses were examined across a wide range of shear rates, with special attention on the influence of dispersants such as carboxymethyl cellulose (CMC) and sodium polyacrylate (NaPA) on suspension processing and coating quality. A slot-die applicator was used to successfully apply different grades of nanocellulose suspensions onto paper substrates in a roll-to-roll process at speeds up to 6 $m.min^{-1}$. In addition, the impact of substrate properties, including contact angle, surface roughness,

porosity, and surface charge groups, on the nanocellulose adhesion and coating quality was investigated. For moisture protection, biodegradable polymers and dispersions were applied onto the nanocellulose-coated samples via extrusion or dispersion coating. The resulting multilayer structures were evaluated for barrier properties such as, water vapor, oxygen, grease, and mineral oils at different test conditions.

CMC addition reduced yield stress, increased water retention, and slowed down structure recovery (post high-shear) for nanocellulose suspensions and therefore had positive influence on coating quality and barrier properties. A new Casson-Power-Cross model was introduced to explain the flow behavior of cellulose nanofibrils (CNFs) across a wide shear-rate range, and Herschel-Bulkley model explained the flow behavior for cellulose nanocrystals (CNCs). Water vapor permeance of the multilayer coatings remained below the control single-layer moisture barrier materials, and oxygen permeance was similar or lower than that of pure nanocellulose films. Glycerol and sorbitol plasticizers further improved oxygen barrier and kaolin pigment addition enhanced the adhesion at nanocellulose/thermoplastic interface.

The results provide insights into the factors influencing the continuous processing of diverse nanocellulose suspensions into barrier coatings. Moreover, the approach of processing nanocellulose and moisture barrier materials together into multilayer structures complements the shortcomings of each layer and produces a paperboard with superior barrier properties that is both bio-based and biodegradable. In order to improve the commercial viability of nanocelluloses in barrier coatings, future research should prioritize achieving the required barrier properties with low coat weights and high suspension solid content. This entails exploring various avenues, such as investigating the use of different rheology modifiers, employing CFD modeling to create custom coating applicators tailored specifically for nanocelluloses, blending diverse grades of nanocelluloses to enhance barrier performance, and employing cross-linkers to mitigate swelling in high humidity conditions. Lastly, it is crucial to assess the barrier performance following various converting operations to provide comprehensive perspective on the final barrier properties.

Keywords: Nanocellulose, cellulose nanofibrils, cellulose nanocrystals, roll-to-roll coating, barrier packaging, rheology, yield stress, thixotropy, slot-die, oxygen barrier, water vapor barrier.

Svensk sammanfattning

Förpackningar är en väsentlig del av vårt moderna liv, där nästan alla produkter behöver skyddas eller förvaras på något sätt. Den globala förpackningsmarknaden omsätter för tillfället ungefär en triljon USD, och en betydlig del av detta utgör barriärförpackningar för livsmedel. Förpackningar av denna typ har en komplex struktur och består av flera funktionella skikt som är tillverkade av icke-bionedbrytbara plast- eller metallager som leder till utmaningar under återvinning. Det är därför viktigt att hitta hållbara alternativ till dessa material. Nanocellulosa, som består av cellulosafibriller i nanostorlek, baserar sig på naturpolymerer utvunna från växter, svampar och bakterier. Förutom att de är biobaserade och bionedbrytbara har nanocellulosabaserade bestrykningar och filmer utmärkt impermeabilitet mot syre, fett och oljor. Därför undersöks nanocellulosa som potentiell ersättare för icke-bionedbrytbara plaster och metallskikt i barriärförpackningar för livsmedel.

Det finns många utmaningar i att möjliggöra höghastighetsprocessering av nanocellulosa till barriärbestrykningar och filmer. Nanocellulosasuspensioner har hög viskositet och flytspänning redan vid låg torrhalt, vilket gör det svårt att uppnå tunna och enhetliga bestrykningsskikt, speciellt i industriella kontinuerliga processer. Dessutom är nanocellulosa extremt fuktkänslig och vid hög fukthalt försämras dess barriäregenskaper. Målet med detta arbete var att förstå och ta itu med dessa utmaningar, och att utveckla ett kontinuerligt processkoncept som behövs för konvertering av olika nanocellulosasuspensioner till barriärbestrykningar.

Flödesegenskaper av olika typer av nanocellulosa undersöktes vid olika skjuvhastigheter, och speciellt undersöktes inverkan av dispergeringsmedel som karboximetylcellulosa (CMC) och natriumpolyakrylat (NaPa) på processeringen av suspensionen och bestrykningskvaliteten. En slot die-applikator användes för applicering av nanocellulosasuspensioner på papper i en rulle-till-rulle process vid hastigheter upp till 6 m/min. Därtill undersöktes effekten av substratens ytegenskaper, såsom kontaktvinkel, ytråhet, porositet och ytladdning, på nanocellulosans adhesion och bestrykningskvalitet. Som fuktskydd applicerades bionedbrytbara polymerer och dispersioner på de nanocellulosabestrykta proven med dispersions- eller extrusionsbestrykning. Den resulterade flerskiktsstrukturens barriäregenskaper mot vattenånga, syre och mineraloljor utvärderades.

Addition av CMC minskade flytspänningen, ökade vattenretentionen och saktade ner strukturåterhämtningen (efter hög skjuvning) av nanocellulosasuspensioner och hade på grund av det en positiv inverkan på bestrykningskvaliteten och barriäregenskaperna. En ny Casson-Power-Cross-modell användes för att förklara flödesbeteendet av cellulosananofibrillsuspensioner (CNF) över ett brett skjuvhastighetsintervall, och en Hershley-Bulkley-modell förklarade flödesbeteendet för cellulosa nanokristallsupensioner (CNC). Vattenångspermeabilitet av flerskiktsbestrykningar var lägre jämfört med referensmaterialen med fuktbarriär, och syrepermeabiliteten var på samma nivå eller lägre jämfört med rena nanocellulosafilmer. Glycerol- och sorbitolmjukgörare förbättrade syrebarriären ytterligare, och tillsats av kaolinpigment förbättrade adhesionen vid gränsytan nanocellulosa/termoplast.

Resultaten indikerar vilka faktorer som påverkar den kontinuerliga processeringen av olika nanocellulosasuspensioner för barriärbestrykningar. Därtill visades att processering av nanocellulosa och fuktbarriärmaterial tillsammans till flerskiktsstrukturer kompletterar bristerna i de enskilda lagren och resulterar i en biobaserad och bionedbrytbar kartong med utmärkta barriäregenskaper. För att förbättra förutsättningarna för kommersialisering av nanocellulosa i barriärbestrykningar borde framtida forskning prioritera barriärbestrykningar med låga bestrykningsmängder och höga torrhalter av suspensioner som skulle resultera i de eftersträvade barriäregenskaperna. Detta kräver forskning på bred front, såsom undersökning av användning av olika reologimodifierare, användning av CFD-modellering för specifika bestrykningsapplikationer specifikt för nanocellulosa, blandning av olika nanocellulosor för förbättring av barriärprestandan, och användning av tvärbindare för att minska svällningen vid höga fukthalter. Slutligen är det viktigt att evaluera inverkan av olika konverteringsoperationer på barriäregenskaperna för att få en omfattande förståelse av användningen av nanocellulosamaterial i förpackningar.

Keywords: Nanocellulosa, cellulosa nanofibriller, cellulosa nanokristaller, rulle-till-rulle bestrykning, barriärförpackningar, reologi, flytspänning, tixotropi, slot-die, syrebarriär, vattenångsbarriä.

List of included publications

This thesis is based on the following 6 publications. The publications are reprinted here with permission from the publishers.

PAPER I. **Substrate role in coating of microfibrillated cellulose suspensions** *109*

V. Kumar, V.R. Koppolu, D.W. Bousfield, and M. Toivakka
Cellulose **24**, 1247-1260 (2017)

The author helped Vinay Kumar (first author of this paper) with all the coatings and characterization tests, except SEM and TEM imaging, which were done by Ruut Kummala and Linus Silvander, respectively. The author participated in reviewing the manuscript.

PAPER II. **Continuous roll-to-roll coating of cellulose nanocrystals onto paperboard** *125*

R. Koppolu, T. Abitbol, V. Kumar, A.K. Jaiswal, A. Swerin, and M. Toivakka
Cellulose **25**, 6055-6069 (2018)

The author planned the work together with all the co-authors. The author was responsible for all the experimental work. TEM, AFM, and peel test measurements were done by Tiffany Abitbol. The author analyzed the data and wrote the manuscript.

PAPER III. **Enzymatically pretreated high-solid-content nanocellulose for a high-throughput coating process** *145*

R. Koppolu, G. Banvillet, H. Ghimire, J. Bras, and M. Toivakka

ACS Applied Nano Materials **5(8)**, 11302-11313 (2022)

The author planned the work together with Martti Toivakka. The author was responsible for most of the experimental work and data analysis. Enzymatic CNF production and optical microscopy images were done by Gabriel Banvillet. SEM images were done by Linus Silvander. The author wrote the manuscript.

R. Koppolu, J. Lahti, T. Abitbol, A. Swerin, J. Kuusipalo, and M. Toivakka

ACS Appllied Materials & Interfaces **11(12)**, 11920-11927 (2019)

The author planned the work together with all the co-authors. The author was responsible for most of the experimental work. Extrusion coating, oxygen and grease barrier measurements were done by Johanna Lahti. TEM images were done by Ruut Kummala and Tiffany Abitbol. SEM images were done by Linus Silvander. The author analyzed the data and wrote the manuscript.

R. Koppolu, J. Lahti, T. Abitbol, C. Aulin, J. Kuusipalo, and M. Toivakka

Cellulose **30**, 6945-6958 (2023)

The author planned the work together with all the co-authors. The author was responsible for most of the experimental work. Extrusion coating and a few oxygen barrier measurements were done by Johanna Lahti. Peel test measurements were done by Tiffany Abitbol, and SEM images were done by Linus Silvander. The author analyzed the data and wrote the manuscript.

List of supporting publications

Articles in peer-reviewed international journals and conferences

1. Hu L., Xu W., Gustafsson J., **Koppolu R.**, Wang Q., Rosqvist E., Sundberg A., Peltonen J., Willför S., Toivakka M., and Xu C., "Water-soluble polysaccharides promoting production of redispersible nanocellulose", *Carbohydrate Polymers*, **297**, 119976 (2022).

2. Wang Q., Xu W., **Koppolu R.**, van Bochove B., Seppälä J., Hupa L., Willför S., Xu C., and Wang X.; "Injectable thiol-ene hydrogel of galactoglucomannan and cellulose nanocrystals in delivery of therapeutic inorganic ions with embedded bioactive glass nanoparticles", *Carbohydrate Polymers*, **276**, 118780 (2022).

3. **Koppolu R.**, Banvillet G., Ghimire H., Bras J., and Toivakka M. (Presenter), "Role of rheology in reel-to-reel coating of high-solids content nanocellulose", *Proceedings of TAPPICon*, Charlotte, USA (2022). Oral presentation.

4. Wang L., Tan, L., Hu L., Wang X., **Koppolu R.**, Tirri T., van Bochove B., Ihalainen P., Sobhana L., Seppälä J., Wilfor S., Toivakka M., and Xu C., "On laccase-catalyzed polymerization of bio refinery lignin fractions and alignment of lignin nanoparticles on nanocellulose surface via one-pot water-phase synthesis", *ACS Sustainable Chemistry & Engineering*, **9(26)**, 8770 - 8782 (2021).

5. **Koppolu R.** (Presenter), Abitbol T., Lahti J., Aulin C., Kuusipalo J., and Toivakka M., "Multilayer barrier paperboard based on nanocellulose and biodegradable thermoplastics", *Proceedings of TAPPICon*, Atlanta, USA (2021). Oral presentation.

6. Ahamed Kutty F.P., Toivakka M. (Presenter), **Koppolu R.**, Swerin A., and Lundell F., "Numerical analysis of slot die coating of nanocellulosic

materials", *Proceedings of TAPPICon*, Atlanta, USA (2021). Oral presentation.

7. Ahamed Kutty F.P., **Koppolu R.**, Swerin A., Lundell F., and Toivakka M., "Numerical analysis of slot die coating of nanocellulosic materials", *Tappi Journal*, **19(11)**, 575 - 582 (2020).

8. Unuma T., Kobayashi O., Kotaka S., **Koppolu R.**, Toivakka M., and Saarinen J.J., "Terahertz complex conductivity of cellulose nanocrystal based composite films controlled with PEDOT:PSS blending ratio", *Cellulose*, **27**, 10019 - 10027 (2020).

9. Wang L., Lagerquist L., Zhang Y., **Koppolu R.**, Tirri T., Sulaeva I., von Schoultz S., Vähäsalo L., Pranovich A., Rosenau T., Eklund P.C., Wilfor S., Xu C., and Wang X., "Tailored thermosetting wood adhesive based on well-defined hardwood lignin fractions", *ACS Sustainable Chemistry & Engineering*, **8(35)**, 13517 - 13526 (2020).

10. Spieser H., Denneulin A., Deganello D., Gethin D., **Koppolu R.**, and Bras J., "Cellulose nanofibrils and silver nanowires active coatings for the development of antibacterial packaging surfaces", *Carbohydrate Polymers*, **240**, 116305 (2020).

11. **Koppolu R.**, Blomquist N., Dahlström., and Toivakka M., "High-throughput processing of Nanographite-Nanocellulose-based electrodes for flexible energy devices", *Industrial & Engineering Chemistry Research*, **59(24)**, 11232 - 11240 (2020).

12. Blomquist N., **Koppolu R.**, Dahlström C., Toivakka M., and Olin H., "Influence of substrate in roll-to-roll coated nanographite electrodes for metal-free supercapacitors", *Scientific Reports*, **10**, 5282 (2020).

13. Rosqvist M., Niemelä E., Frisk J., Öblom H., **Koppolu R.**, Abdelkader H., Soto Véliz D., Mennillo M., Venu A.P., Ihalainen P., Aubert M., Sandler N., Wilén C., Toivakka M., Eriksson J.E., Österbacka R., and Peltonen J., "A low-cost paper-based platform for fast and reliable screening of cellular interactions with materials", *Journal of Materials Chemistry B*, **8**, 1146 - 1156 (2020).

14. Wickström H., **Koppolu R.**, Mäkilä E., Toivakka M., and Sandler N., "Stencil printing – a novel manufacturing platform for orodispersible discs", *Pharmaceutics*, **12(1)**, 33 (2020).

15. **Koppolu R.** (Presenter), Lahti J., Abitbol T., Swerin A., Kuusipalo J. and Toivakka M., "Nanocellulose and polylactic acid based multilayer coatings for barrier applications", *Proceedings of TAPPI Papercon*, Indianapolis, USA (2019). Oral presentation.

16. **Koppolu R.** (Presenter), Toivakka M., Salminen P., and Preston J., "Sequential water absorption into linerboard", *Proceedings of Cellulose Materials Doctoral Students Conference*, Graz, Austria (2017). Oral presentation.

Non-reviewed conference publications

1. **Koppolu R.** (Presenter), Banvillet G., Ghimire H., Bras J., and Toivakka M., "Role of rheology in reel-to-reel coating of high-solids content nanocellulose", *International Conference on Nanotechnology for Renewable Materials*, Helsinki, Finland (2022). Oral presentation.

2. Toivakka. M (Presenter), **Koppolu R.**, and Kutty F.P.A., "Role of rheology in slot-die coating of high-solids content nanocellulose", *International Coating Science and Technology Symposium*, Minneapolis, USA (2022). Oral presentation.

3. **Koppolu R.** (Presenter), Abitbol T., Lahti J., Aulin C., Kuusipalo J., and Toivakka M., "Multilayer barrier paperboard based on nanocellulose and biodegradable thermoplastics", *TAPPI Nano Virtual Conference* (2021). Oral presentation.

4. **Koppolu R.** (Presenter), Abitbol T., Lahti J., Aulin C., Kuusipalo J., and Toivakka M., "Multilayer barrier paperboard based on nanocellulose and biodegradable thermoplastics", *Speciality Papers Europe*, Amsterdam, The Netherlands (2021). Oral presentation.

5. **Koppolu R.** (Presenter), Blomquist N., Dahlström C., and Toivakka M., "Processability of nanographite-nanocellulose based electrodes for flexible energy storage applications", *International Conference on Nanotechnology for Renewable Materials*, Chiba, Japan (2019). Oral presentation.

6. Toivakka M. (Presenter), **Koppolu R.**, Blomquist N., and Dahlström C., "Slot die coating of nanographite/nanocellulose-based electrodes for metal-free supercapacitors", *European Coating Symposium*, Heidelberg, Germany (2019). Oral presentation.

7. **Koppolu R.** (Presenter), Kumar V., Toivakka M., Abitbol T., and Swerin A., "Coatability of CNC suspensions in a high-throughput continuous process", *International Conference on Nanotechnology for Renewable Materials*, Madison, USA (2018). Oral presentation.

8. Toivakka M. (Presenter), **Koppolu R.**, Abitbol T., Swerin A., Lahti J., and Kuusipalo J., "Slot die coating of nanocellulose for barrier applications", *AIMCAL R2R Conference*, Phoenix, USA (2018). Oral presentation.

9. Forsberg V. (Presenter), Maslik J., Andersson H., Hummelgård M., Dahlström C., Toivakka M., **Koppolu R.**, Olin H., and Norgren M., "Printability of functional inkjet inks onto commercial inkjet substrates and a taylor made pigmented coated paper", *European Materials Research Society Spring Meeting*, Strasbourg, France (2018). Poster presentation.

10. Kumar V. (Presenter), **Koppolu V. R.**, Bousfield D., and Toivakka M., "Substrate requirements for roll-to-roll processed nanocellulose coatings", *TAPPI International Conference on Nanotechnology for Renewable Materials*, Montreal, Canada (2017). Oral presentation.

Immaterial property rights

Koppolu R. and Toivakka M., Method for producing nanocellulose films

- PCT/FI2020/050842 (filing date - 16.12.2020)
- FI129375 (granted date - 14.01.2022)
- US17/785,934 (pending)
- EP20838589.8 (pending)

Abbreviations

ÅAGWR	Åbo Akademi gravimetric water retention
AFM	Atomic force microscopy
AKD	Alkene ketene dimer
AlOx	Aluminum oxide
APAM	Anionic polyacrylamide
ATR-FTIR	Attenuated total reflectace - Fourier transform infrared spectroscopy
BNC	Bacterial nanocellulose
CHP	CH Polymers
CMC	Carboxymethyl cellulose
CNC	Cellulose nanocrystals
CNF	Cellulose nanofibrils
CP	Cone-plate
CPAM	Cationic polyacrylamide
DMSO	Dimethyl sulfoxide
DS	Degree of substitution
-E	Expandable
EU	European Union
EVA	Ethylene-vinyl acetate
EVOH	Ethylene-vinyl alcohol
FF	FINNFIX®
HC	Hydrocarb
-HD	High density
HDPE	High density polyethylene
HPH	High-pressure homogenizer
HVTR	Heptane vapor transmission rate
-LD	Low density
LDPE	Low density polyethylene
LLD	Linear low density

LVE	Linear viscoelastic region
MCR	Modular compact rheometer
-MD	Medium density
MFC	Microfibrillated cellulose
NaPA	Sodium polyacrylate
OCT	Optical coherence tomography
OP	Oxygen permeance
PA	Polyamide
PBAT	Polybutylene adipate terepthalate
PBS	Polybutylene succinate
PE	Polyethylene
PET	Polyethylene terephtalate
PHA	Polyhydrodxy alkanoate
PLA	Polylactic acid
PolyDADMAC	Polydiallyldimethylammonium chloride
PP	Polypropylene
PP	Parallel-plate
PPS	Parker print surf
PPWD	Packaging and packaging waste directive
PS	Polystyrene
PUR	Polyurethane
PVC	Polyvinyl chloride
PVDC	Polyvinylidene chloride
PVOH	Polyvinyl alcohol
R2R	Roll-to-roll
RH	Relative humidity
SEM	Scanning electron microscopy
SiOx	Silicon oxide
TEM	Transmission electron microscopy
TEMPO	2,2,6,6-tetramethylpiperidine-N-oxyl
TP	Thermoplastic
UHT	Ultra high temperature processed
UVP	Ultrasound velocity profiling
WD	Water-based dispersion
WVP	Water vapor permeance

Chapter 1

Introduction

We have come a long way from using animal skins and textiles as packaging materials during hunter-gatherer societies, to the modern packaging technology that uses a variety of materials viz., paper, plastic, glass, metal, and wood for specific end-use applications.[1–3] In 2021, the global packaging market was estimated to be about 1 trillion USD, and approximately 35% of all packaging was used for food packaging.[4] Efficient packaging protects the food, extends its shelf life, and therefore, plays a vital role in reducing food waste throughout the supply chain.[2] Most often, food packaging is a multilayer structure comprising of paper, paperboard, plastics, and metals as functional layers, for providing mechanical stability, barrier properties (water vapor, oxygen, grease, and mineral oils), printability, and sealability.[5,6] Figure 1.1 shows a schematic of different functional layers in a typical multilayer food packaging structure, and the most common material choices for each layer.

A majority of the functionality of a packaging structure depends on different types of fossil-fuel derived plastics such as, L/HDPE, PET, PP, PA, EVA, EVOH, and PVDC (figure 1.1).[2] Plastics in general are versatile materials that play a vital role in our daily lives, but more than 90% of them are derived from non-renewable fossil-based resources (figure 1.2a).[11] One of the major drawbacks of fossil-fuel derived plastics is that they do not biodegrade naturally, and have traditionally been discarded, incinerated, or sent to landfills after use.[12] Between 1950 and 2015, about 70% of the total plastics produced worldwide were used only once before being discarded (figure 1.2b), and only a small fraction (ca. 9%) was recycled.[11–13] It is estimated that approximately 40% of the total plastics produced are used for packaging applications and 17-20% of that consists of multilayer packaging.[1,12,14,15] While it is easy to recover and recycle mono-component

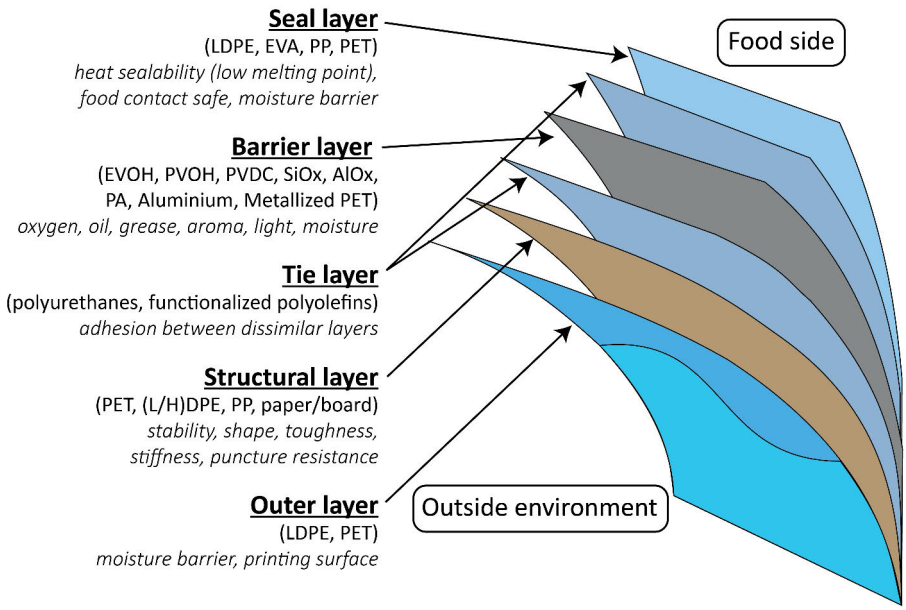

Figure 1.1 Schematic of different functional layers in a typical multilayer food packaging structure, and the most common material choices for each layer (based on Schmidt et al.,[1] Bauer et al.,[6] Kaiser et al.,[5] Morris,[7] Anukiruthika et al.,[8] Fereydoon and Ebnesajjad,[9] Marsh and Bugusu.[10]
Abbreviations: LDPE (low-density polyethylene), HDPE (high-density polyethylene), PP (polypropylene), EVA (ethylene-vinyl acetate), PET (polyethylene terephtalate), EVOH (ethylene-vinyl alcohol), PVOH (polyvinyl alcohol), PVDC (polyvinylidene chloride), SiO_x (silicon oxide), AlO_x (aluminium oxide), PA (polyamide).

packaging, it is very challenging to recycle the multilayer structures due to difficulty in separating the packaging into individual components, especially when they contain metal foils or metallized plastics as functional layers.[2,16] Therefore, most of the multilayer packaging is discarded or incinerated, which puts a considerable strain on natural resources and energy use.[5,17]

The issue of packaging waste has gained widespread attention, prompting many countries to introduce policy changes aimed at reducing the use of non-biodegradable fossil-fuel plastics, improving collection, reuse, and recycling systems, and promoting the use of bio-based and biodegradable (or compostable) materials.[1,6,14,18,19] For example, the European Union's (EU) "New circular economy action plan" (a building block of European Green Deal, adopted in March 2020) emphasizes the transition to a circular economy through legislative and non-legislative actions covering the entire life cycle of products.[20] And in November 2022, the European Commission proposed

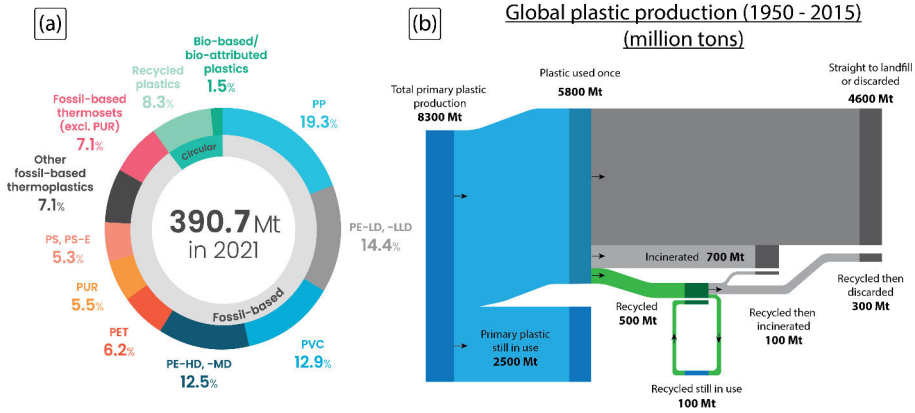

Figure 1.2 (a) Distribution of global plastic production by type during 2021 [adapted from Plastics Europe -"Plastics - the facts 2022" [11]]; (b) Global plastic production and its fate between 1950 and 2015 [adapted from Ritchie and Roser [13] and Geyer et al. [12]].
Abbreviations: PP (polypropylene), PE (polyethylene), -LD (low density), -LLD (linear low density), -HD (high density), -MD (medium density), PVC (polyvinyl chloride), PET (polyethylene terephtalate), PUR (polyurethane), PS (polystyrene), -E (expandable).

changes to the EU Directive (94/62/EC) on Packaging and Packaging Waste (PPWD) that aim to prevent packaging waste, boost reuse and refill, and make all packaging recyclable by 2030. [21,22] Other similar initiatives include the Ellen MacArthur Foundation's New Plastics Economy Global Commitment (launched in 2018 in collaboration with the United Nations Environment Program) [23] and the Protecting Communities from Plastics Act (introduced in the United States' senate in January 2022) [24]. In recent years, consumer preferences have also shifted towards using more bio-based and sustainable packaging alternatives. [25,26]. Despite legislations forcing the adoption of non-fossil fuel-based materials, bio-sourced materials remain too expensive for mainstream use due to higher raw material costs and lack of sufficient barrier properties, thus, keeping biodegradables and compostables a niche. [2]

The last two decades have seen an increasing interest from both the industry and academia in finding sustainable barrier packaging solutions that incorporate bio-based and biodegradable materials. [14,27–29] These materials are commonly derived from naturally occurring polymers found in plants, animals, and proteins, or synthetically produced from the fermentation of

biomass-based raw materials.[29–32] Some examples of naturally derived polymers that have demonstrated promising barrier properties include cellulose-based polymers (nanocelluloses[27,33,34] and hemicelluloses[35,36]), lignin,[37,38] chitosan,[39] starch,[40,41] alginate,[42–44] casein,[45] polyhydroxy alkanoates (PHAs),[46,47] whey,[48,49] and soy proteins[50]. On the other hand, polylactic acid (PLA)[51,52] and polybutylene succinate (PBS)[53,54] are examples of synthetic polymers (manufactured from bio-based sources) that are gaining popularity as barrier materials in packaging applications.

Nanocellulose is a nano-scale cellulose-based natural polymer derived from plants, fungi, and bacteria.[55] The development of nanocellulose can be traced back to Turbak et al.[56] and Herrick et al.[57] in 1983, who produced it by repeatedly passing cellulose pulp through a homogenizer to achieve a high degree of fibrillation. The resulting suspension mainly consisted of cellulose nanofibrils, which had diameters ranging from 25 to 100 *nm* and aspect ratios greater than 100.[56] Since then, the interest in nanocellulose has been steadily growing and it has become one of the most widely researched biomaterials in recent times, due to its abundance, renewability, biocompatibility, biodegradability, barrier properties, and high functionalization potential.[58,59]

Nanocelluloses have been extensively studied for various applications, such as barrier coatings, strength additives for paper and board making, drug delivery, printed electronics, composites, cosmetics, hygiene products, additives for paints and coatings, energy storage, and rheology modifiers (figure 1.3).[59–68] Among the demonstrated applications, nanocellulose-based barrier coatings and films have received the most attention from academia and industry due to their exceptional barrier properties against oxygen, grease, and mineral oils.[34,59] In addition, due to its bio-based and biodegradable nature, nanocellulose-based coatings and films are being investigated as a potential replacement for non-biodegradable plastics and metallic aluminum layers in food packaging applications.[27,62] It is estimated that the demand for nanocellulose will have a compound annual growth rate (CAGR) of approximately 18% over the next decade, with paper and board packaging being the largest share (figure 1.3).[69] Consequently, many companies have started producing nanocellulose at a pilot or commercial scale primarily for barrier packaging applications.[69]

Despite their immense potential as barrier packaging films and coatings, there are still challenges that need to be addressed before nanocelluloses can be commercialized for barrier coating applications. The high specific surface area, aspect ratio, and interfibril/fiber hydrogen bonding of nanocellulose suspensions

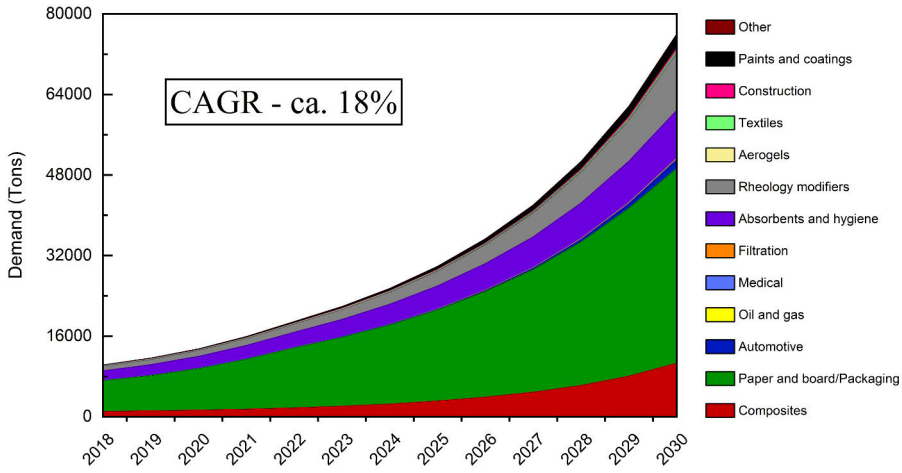

Figure 1.3 Global nanocellulose market demand by end user application, 2018-2030. [69]

result in high viscosities, which scale according to a power function with the solid concentration (power index of 2 – 4.5). [70,71] As a result, they are typically produced at low suspension solid contents of less than 3% to prevent clogging of the fibrillation equipment. [72] Nanocellulose suspensions also have complex rheology, which makes it difficult to apply them as thin uniform layers in a continuous roll-to-roll (R2R) process. [73] The yield stress and viscosity both scale according to a power function with the solid concentration, causing issues during pumping of the suspensions and leveling off of the wet coated layer. [74,75] Furthermore, most coating applicators are not designed to handle such high-viscosity suspensions. In addition, the high water content causes runnability issues during roll-to-roll coating as the wet strength of the paper substrate is greatly reduced [76], and also increases the drying energy demand.

Nanocellulose suspensions have high gel strength (storage modulus), which recovers rapidly after exposed to high shear and also scales according to power function with suspension solids. [67] This causes quick immobilization of the wet nanocellulose coating and results in poor coating quality. As a result, most research on nanocellulose-based barrier coatings is demonstrated using laboratory-scale batch processes such as solvent casting, filtration, and draw-down coating (at very low solid contents, <2%), often followed by slow drying at ambient conditions. [77] There are only a few examples in the

literature on roll-to-roll coating of nanocelluloses on paper/paperboard using slot-die,[73] gravure,[78] spray coating,[79,80] and wet lamination methods[81]. More research is needed to understand the role of nanocellulose type, its rheological parameters and additives, suspension solid content, and coating applicator design in the context of R2R coating before nanocelluloses can be used industrially as a barrier coating material.

Another challenge that is deterring the industrial adaptation of nanocellulose for barrier coatings is the material's extreme moisture sensitivity, with most of the barrier properties degrading, or even disappearing completely, at higher humidities.[34,82,83] However, one approach to protect nanocellulose from moisture is by using a multilayered structure consisting of nanocellulose and a moisture barrier top coating.[27,62] Some researchers have demonstrated this multilayer concept by using various biopolymers such as guar gum,[84] alginate,[85] alkyd resins,[86] polyglycolic acid,[87] PHAs,[88] shellac,[89] chitin,[90] and polylactic acid (PLA)[91]. Except for the work by Vartiainen et al.,[92] most of the nanocellulose-based multilayer coatings were again demonstrated using laboratory-scale batch processes. Several issues such as compatibility and adhesion between nanocellulose and moisture barrier materials, roll-to-roll application of top coating without destroying the nanocellulose layer underneath, and flexibility of the multilayer structure still need to be studied to produce nanocellulose-based sustainable packaging in a continuous roll-to-roll process.

Research objectives and thesis structure

The main objective of this work was to understand and address the challenges that arise during high-throughput roll-to-roll processing of nanocelluloses into barrier coatings on paper substrates, and to demonstrate biodegradable multilayer structures containing nanocelluloses and biopolymers, with barrier properties comparable to commercial references. This will lay the foundation for industrial adaptation of nanocelluloses as a barrier layer for sustainable packaging applications. In order to achieve the main objective, the research work was divided into the following sub-tasks:

(i) Investigate the rheology and suspension properties of different nanocellulose grades, and understand the impact of dispersants, suspension solid content, fiber to water ratio, and water release

properties in relation to roll-to-roll processing. This task also involved high shear rheology measurements and development of a viscosity model for nanocelluloses that cover a wide shear rate range.

(ii) Coat different nanocelluloses on paperboard using roll-to-roll processes and evaluate the resulting barrier properties. An additional task was to optimize the substrate properties to improve the coating quality.

(iii) Demonstrate multilayer structures by coating various biopolymers on the nanocellulose-coated paperboards using suitable coating techniques. Emphasis is on examining the impact of multilayer coating and nanocellulose's additives, such as pigments and plasticizers on the overall barrier properties.

This thesis is the summary of six publications addressing the research objectives and sub-tasks mentioned above. Chapter 2 provides a brief overview of the literature on nanocelluloses with a focus on their rheology, coating applications, and barrier properties. Chapter 3 describes various materials, coating methods, and characterization techniques used in this work. Chapter 4 discusses the main results followed by concluding remarks in Chapter 5. More details can be found in the attached publications.

Chapter 2

Literature Review

This chapter offers a brief overview of the existing research on the subject, without attempting an exhaustive review of the extensive literature. Instead, the focus is specifically on the essential topics that are pertinent to the discussion of the results in this thesis. For additional information on each topic, recent reviews are cited as appropriate.

2.1 Nanocellulose

Cellulose is a naturally occurring polymer that is widely present in plants, trees, algae, fungi, and some bacteria, and serves as the primary structural component in their cell walls.[72] Traditionally, industrial cellulose has been obtained from wood, which is composed of composite cell walls containing cellulose fibers, hemicelluloses, and lignin (figure 2.1).[93] These three components make up more than 90% of a tree's dry mass, with cellulose accounting for 45-50%, hemicellulose for 20-25%, and lignin for 20-25%.[94] Other components make up the remaining 5-10%, and the exact composition varies depending on the source.[94]

The cellulose fibers in the plant cell wall are made up of several microfibril bundles, which in turn are composed of elementary fibrils that are approximately 3 nm in diameter, and are considered the smallest morphological unit within a fiber (figure 2.1).[95,96] Cellulose polymer is made of linear chains of β-D-glucopyranose molecules linked by β-1,4-glucosidic bonds (figure 2.1b),[72] with the degree of polymerization ranging from 1000 to 30 000 depending on the source.[97] The cellulose molecules form strong intra- and inter-chain hydrogen bonding networks between hydroxyl groups of the

D-glucopyranose molecules.[98] The inter-chain hydrogen bonding together with the van der Waals forces promote parallel stacking of multiple cellulose chains, and contribute to its relatively stable polymer structure.[98]

Cellulose fibrils with at least one nanoscale (<100 nm) dimension are referred to as nanocelluloses.[72] Depending on the fibril size, crystallinity, and synthesis route, nanocelluloses can be broadly classified into three types.[55,58] These include cellulose nanofibrils (CNFs), cellulose nanocrystals (CNCs), and bacterial nanocellulose (BNC).[34] CNFs are produced by mechanical defibrillation of chemical pulp[93], but chemical or biological pretreatments such as TEMPO-oxidation,[99] periodate-chlorite-oxidation,[100] carboxymethylation,[101] phosphorylation,[102] and enzyme-mediated hydrolysis[103] are often utilized to reduce energy consumption during mechanical defibrillation and/or to enhance the final properties of CNFs. The diameters, lengths, and crystallinities of CNFs typically range from 10-100 nm, 100 nm to over 1 μm, and 60-70%, respectively.[72]. CNCs, on the other hand, are produced via strong acid (HCl, H_2SO_4, and H_3PO_4) hydrolysis of chemical pulp and have rice-like structures with lower aspect ratios compared to CNFs.[104] The diameters, lengths, and crystallinities of CNCs typically range from 3-35 nm, 200-500 nm, and >90%, respectively.[104] BNCs are high-purity nanocelluloses produced by various bacterial species and have high crystallinities, with longer fibrils than CNCs.[66]

2.2 Production methods

CNFs and CNCs are typically produced through top-down processes using cellulose pulp as the starting material.[72] The raw materials commonly used are woods, including both hardwood and softwood, as well as non-woods such as bagasse, cotton, kenaf, bamboo, jute, reed, hemp, flax, and coir.[58] As mentioned above, in nature, cellulose exists in plant cell walls along with hemicelluloses and lignin, and the first step in producing nanocellulose is to separate cellulose from the lignocellulosic biomass. Kraft pulping is one of the most commonly used methods by the pulp and paper industry to extract cellulose from wood pulp.[106] This involves subjecting wood chips to water, sodium hydroxide (NaOH), and sodium sulfide (Na_2S) at high temperatures and pressures to obtain pure cellulose fibers.[106] A bleaching step is also often used to remove any remaining lignin or hemicelluloses in the pulp. Various other chemical approaches such as sulfite process, soda pulping, and

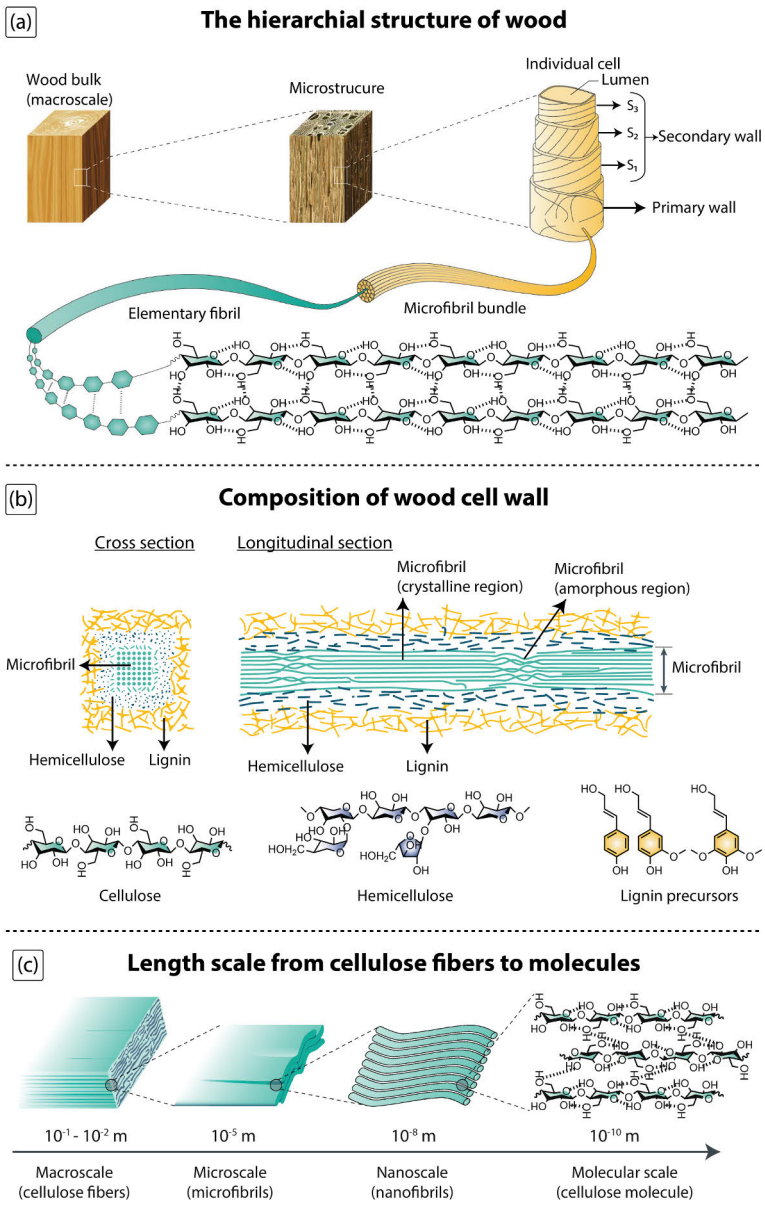

Figure 2.1 (a) The hierarchial structure of wood; (b) Composition of wood cell wall; (c) Length scale from cellulose fibers to molecules [adapted from Chen et al. [105]].

organosolv process are also commonly used to obtain cellulose pulp from wood.[106]

The cellulose pulp is subsequently subjected to mechanical pretreatment using disc refiners to delaminate or defibrillate the cellulose fibers. This is an energy intensive process and the degree of defibrillation achieved typically depends on the grade of paper that is produced using the pulp. In order to produce CNFs, the cellulose pulp must be defibrillated to the extent that microfibrils with diameters less than 100 nm are achieved.[58] Chemical or biological pretreatments are often used to reduce the energy consumption during defibrillation process, or to obtain finer fibrils.[93,107] CNCs are produced by subjecting cellulose pulp to strong acids, which degrade the amorphous regions of cellulose fibrils, leaving behind rigid cellulose crystals, and thus, do not require any mechanical treatments.[104] The following subsections briefly discuss the various mechanical, chemical, and biological treatments used to produce different grades to nanocelluloses.

2.2.1 Mechanical treatments

Mechanical treatment is a universal step during the production of CNFs, in which cellulose fibers are defibrillated into micro/nano-sized fibrils using mechanical forces. This was first demonstrated by Turbak et al.[56] and Herrick et al.[57] in 1983, who passed cellulose pulp with a concentration of 2% through a homogenizer multiple times (10-20 passes) at a pressure of 55 MPa and temperature of 80 ^oC, resulting in cellulose nanofibrils with diameters ranging from 25 - 100 nm. To distinguish between coarser and finer grades, the authors used the terms micro fibrillated cellulose (MFC) and nano fibrillated cellulose (NFC), which have since been used interchangeably by different researchers and in a few papers in this work (Papers I, IV, and V). To maintain consistency in nomenclature, the International Organization for Standardization (ISO) has defined the terms for various cellulose nanomaterials in their document, "ISO/TS 20477:2023(en) Nanotechnologies – Vocabulary for cellulose nanomaterial". According to this document, CNF is used for cellulose nanofibrils, and CNC is for cellulose nanocrystals, which will be followed throughout the rest of this thesis.

Mechanical defibrillation of cellulose fibers into CNFs can be achieved by grinding, homogenization, microfluidization, refining, extrusion, blending, ultrasonication, cryocrushing, steam explosion, ball milling, and aqueous counter collision.[72] However, the most commonly used methods are grinding,

homogenization, and microfluidization, which will be briefly discussed below (figure 2.2).

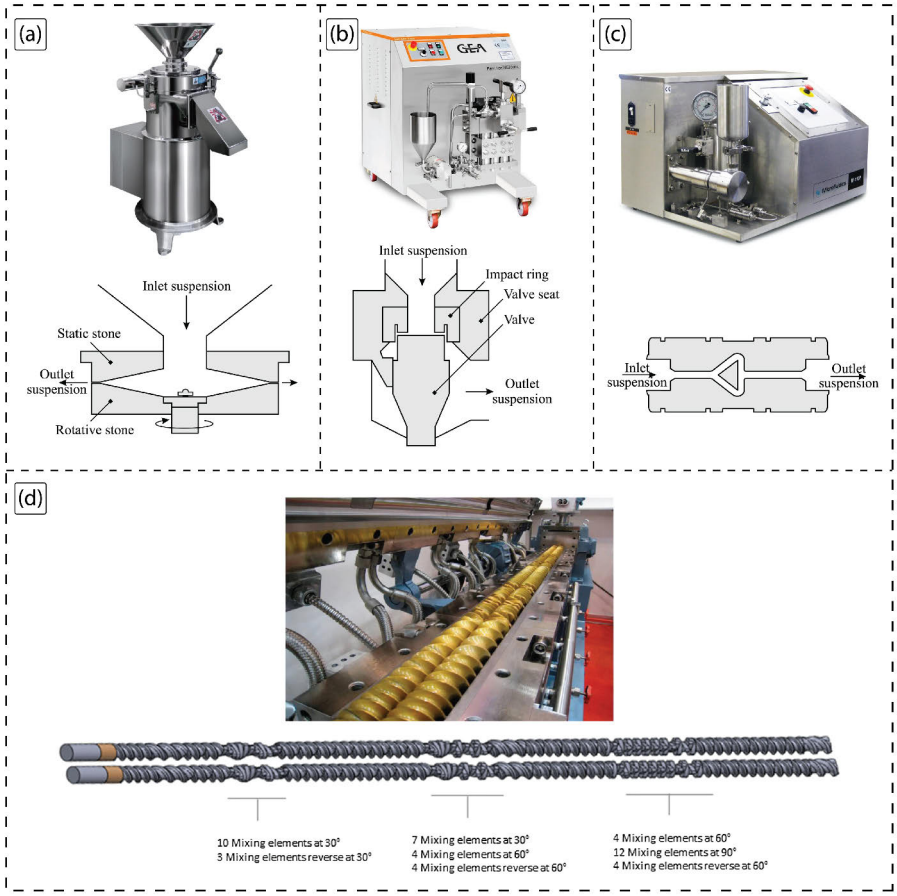

Figure 2.2 Commonly used mechanical methods for the production of CNFs, (a) Grinding; (b) High-pressure homogenization; (c) Microfluidization; (d) Twin-screw extrusion. [Schematics adapted from Nechyporchuk et al.[72], Rol et al.[108]. Photographs adapted from www.masuko.com, www.microfluidics-mpt.com, www.gea.com, and www.xindacorp.com].

Grinding

Ultrafine friction grinding is a commonly employed method in laboratories and pilot facilities to generate cellulose nanofibrils (CNF) from chemical pulp.[72,93] One widely used equipment for CNF production is the supermasscolloider (Masuko Sangyo Co. Ltd., Japan) [figure 2.2a]. This grinder consists of stationary and rotating stones (or discs), with an adjustable gap in-between

them. Typically, cellulose pulp, whether never-dried or once-dried, is introduced to the grinder at approximately 3-5% concentration.[82,109] The friction and high-shear forces between the discs delaminate and defibrillate the cellulose fibers into micro and nanofibrils. The suspension is typically passed multiple times (upto 10 times) through the grinder, while gradually reducing the gap between the discs. Initially, a higher gap is maintained to prevent clogging the grinder. A notable feature of this grinding process is the ability to set the gap as low as -100 μm, where zero gap represents the position where the discs touch each other when there is no pulp between them.[110] The negative gap configuration is adopted after loading the cellulose pulp to prevent physical contact between the discs, thus increasing the applied pressure on the fibers, enhancing friction, and improving the degree of defibrillation. Consequently, CNF with diameters ranging from 20 to 90 nm has been successfully produced using this method.

Another closely related technique involves the co-grinding of cellulose fibers with mineral pigments like kaolin or calcium carbonates. The presence of these hard minerals leads to increased friction, causing defibrillation of the cellulose fibers. As a result, a slurry comprising a composite of CNF and minerals is obtained after the grinding process. FiberLean Technologies Ltd. holds the patent[111,112] for this process, which has been successfully commercialized.

Homogenization

Homogenization is essentially the process of uniformly mixing different materials using mechanical means. Researchers often utilize high-pressure homogenizers (HPH) to produce CNFs.[56,93,107] The homogenizer consists of a high-pressure positive displacement reciprocating pump and a homogenization valve, which includes a spring-loaded valve, valve-seat, and impact ring (figure 2.2b). To create CNFs, a dilute cellulose pulp suspension (2% or lower) is subjected to high pressures ranging from 50 to 200 MPa as it passes through the homogenization valve. This high-pressure flow induces turbulence and generates high shear forces due to the narrow gap between the valve and the seat, leading to cavitation in the suspension after it exits the valve.[113] These combined forces significantly enhance the defibrillation of cellulose fibers, resulting in the production of CNFs with diameters between 5 and 90 nm.[93,114] Similar to other mechanical treatments, the process is typically repeated multiple times. However, studies have shown no significant improvement in fibrillation beyond 15 cycles.[93]

Microfluidization

Microfluidization is another homogenization technique employed to achieve defibrillation of cellulose fibers through the application of high pressure and high shear rates. During the process, the cellulose pulp suspension is directed through a narrow constriction with a specific geometry, such as Z or Y-shaped, featuring an orifice width ranging from 100 to 400 μm (figure 2.2c).[72,115] In this orifice, shear rates can reach remarkably high values of up to $10^7\ s^{-1}$. Moreover, the unique geometry of the constriction generates significant impact forces. Consequently, this intricate combination of shear and impact forces leads to the delamination and defibrillation of cellulose fibers, resulting in the formation of CNFs.[115]

Extrusion

Extrusion is a relatively less common method for the production of CNFs. The process involves feeding cellulose pulp into a twin-screw extruder where defibrillation occurs through the intermeshing, co-rotating screws inside a closed barrel (figure 2.2d). Ho et al.[116] were the first to demonstrate the use of twin-screw extrusion for CNF production, using bleached pulp at 28% and passing it through a twin-screw extruder for 14 passes to obtain CNFs at a solid content of 45% (some of the moisture evaporated due to heat generated during the extrusion process). Rol et al.[117] further optimized the screw profile to improve the quality of CNFs and reduce energy consumption. Compared to other methods, twin-screw extrusion produces CNFs at higher solid contents, which is beneficial for transportation of CNFs, and offers a promising approach for large-scale production.

2.2.2 Chemical and biological pretreatments

Pure mechanical treatments for CNF production are known to be energy intensive, with reported energy consumption ranging from 12 to 70 $MWh.tonne^{-1}$ (dry fiber), depending on factors such as type of raw material, number of passes, and defibrillation equipment.[118] Chemical or biological pretreatments are typically employed to reduce energy consumption. These pretreatments have the potential to significantly decrease energy requirements, sometimes achieving 20-30 fold reduction, resulting in energy consumption as low as 1 $MWh.tonne^{-1}$ (dry fiber).[93] Figure 2.3 shows the energy consumption as a function of suspension solid content for CNF

production using various mechanical, chemical, or biological pretreatments. Chemical pre-treatments typically introduce charged surface groups onto cellulose fibers. This induces swelling and fiber repulsion, thereby facilitating easier delamination of fibrils during mechanical treatments. Carboxylation [99,100] (such as TEMPO-mediated or periodate-chlorite oxidation), carboxymethylation, [119] sulfonation, [120] and quaternization [121] are commonly used chemical pre-treatment methods for producing CNFs. On the other hand, biological pre-treatments use enzymatic hydrolysis to delaminate cellulose fibers to enhance the efficiency of the defibrillation process. [103,122]

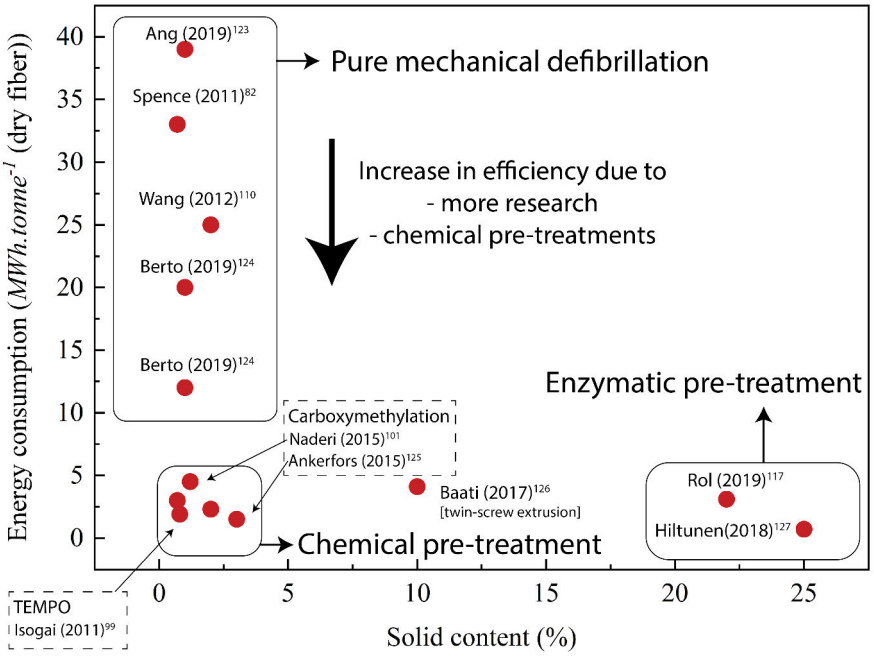

Figure 2.3 Energy consumption as a function of suspension solid content for CNF production using mechanical, chemical, or biological treatments. [Data sources: Ang et al. [123], Spence et al. [82], Wang et al. [110], Berto and Arantes [124], Isogai et al. [99], Naderi et al. [101], Ankerfors [125], Baati et al. [126], Rol et al. [117], Hiltunen et al. [127].]

TEMPO-mediated oxidation

Davis et al. [128] and De Nooy et al. [129] were among the first researchers to employ TEMPO (2,2,6,6-tetramethylpiperidine-N-oxyl), a water-soluble

radical, in conjunction with sodium bromide (NaBr) and sodium hypochlorite (NaClO) for the selective oxidation of primary alcohol groups in cellulose molecules, converting them into aldehyde groups that are subsequently oxidized into negatively-charged carboxylic groups. Building upon this, Saito et al.[130] utilized the TEMPO/NaBr/NaClO treatment to oxidize and defibrillate cellulose pulp under alkaline conditions, resulting in the production of CNFs with diameters ranging from 3 to 5 *nm*. However, it was later discovered that the presence of hydroxyl radicals in the alkaline conditions led to the unintended cleavage of anhydroglucose units in the cellulose polymer, thereby reducing the degree of polymerization (DP) of cellulose fibrils.[99] To address this issue, the TEMPO/NaClO/$NaClO_2$ system was introduced, and the reaction was carried out under neutral or weakly acidic conditions.[131,132] Notably, Prof. Akira Isogai's research group has made significant contributions to enhancing the energy efficiency and quality of CNFs produced through TEMPO-mediated oxidation, as outlined in the comprehensive review article by Isogai et al.[99]

Periodate-chlorite/bisulfite oxidation

Carboxylation through periodate-chlorite oxidation involves the utilization of sodium periodate ($NaIO_4$) to initially transform the secondary alcohols present in the cellulose molecule into aldehydes. Subsequently, these aldehydes are further oxidized to carboxyl groups by using sodium chlorite ($NaClO_2$).[100,133] Sulfonation process replaces $NaClO_2$ in the second step of periodate-chlorite oxidation with sodium bisulfite ($NaHSO_3$) to form sulfonated cellulose fibrils (negatively charged groups).[120,134] Additionally, the sulfonation procedure facilitates efficient recovery of sodium periodate, thereby presenting the potential for commercialization.

Carboxymethylation

Carboxymethylation is a widely used industrial process dating back to the 1920s, primarily employed for the production of Carboxymethyl cellulose (CMC) or other carboxymethylated polysaccharides.[135] It was first introduced by Wågberg et al.[136] as a pre-treatment method for the production of CNFs. The process involves several steps: first, cellulose fiber suspension is solvent-exchanged to ethanol, followed by impregnation with a solution of monochloroacetic acid in isopropanol. Subsequently, this mixture is combined with a solution of NaOH in methanol and isopropanol, allowing the

carboxymethylation reaction to proceed for approximately one hour, resulting in the formation of negatively-charged carboxymethyl-cellulose derivatives. Following the carboxymethylation step, the fibers are washed with water and acetic acid, and then treated with a $NaHCO_3$ solution to convert the carboxyl groups to their sodium form. Finally, the fibers are thoroughly rinsed with deionized water to eliminate any remaining solvents and reagents. The charge content of the carboxymethylated fibers typically ranges from 300 to 2000 $\mu eq.g^{-1}$, with higher charge contents leading to reduced energy consumption during the mechanical defibrillation step,[137] and CNFs with diameters as low as 5-15 nm have been reported with carboxymethylation pretreatment.[119] For comprehensive information on the carboxymethylation process for CNF production, refer to the work by Wågberg et al.[119] and Siró et al.[137]

Quaternization

In contrast to the above chemical pre-treatments, quaternization involves introducing positively charged groups onto the cellulose polymer, and the repulsion between these groups is utilized to enhance the efficiency of defibrillation. Various methods for quaternizing cellulose pulp have been proposed in the literature. Aulin et al.[121] employed (2-3-epoxypropyl) trimethylammonium chloride in water, isopropanol, and NaOH to quaternize bleached sulfite dissolving pulp, Ho et al.[138] utilized (2-chloroethyl) trimethylammonium chloride in dimethyl sulfoxide (DMSO) and NaOH with oat-straw pulp, and Liimatainen et al.[139] employed successive periodate oxidation and (2-hydrazinyl-2-oxoethyl)-trimethylazanium chloride (Girard's reagent T) with bleached birch pulp. These methods resulted in cationic CNFs with diameters ranging from 2.6 to 50 nm and cationic charge density varying from 0.35 to 2.13 $meq.g^{-1}$.[139,140] Furthermore, these cationic CNFs displayed antibacterial properties without leaching quaternary ammonium into the environment, and therefore, have the potential to be used for wound healing and tissue engineering applications.[141,142]

Enzyme-mediated hydrolysis

Cellulases are a group of enzymes primarily produced by fungi and bacteria, and are utilized to break down cellulose into smaller polysaccharides or monosaccharides.[143] There are three types of cellulases, each targeting different sections of the cellulose polymer. Endoglucanases hydrolyze

amorphous regions, cellobiohydrolases cleave the ends of crystalline or amorphous regions, and cellobioases break down smaller polysaccharides into glucose.[143] These enzymes can completely hydrolyze cellulose, with the resulting glucose used for bioethanol production, or subject the cellulose to mild hydrolysis to enhance defibrillation efficiency.[144,145] Pääkkö et al.[103] and Henriksson et al.[122] produced CNFs by mild hydrolysis of refined cellulose pulp with monocomponent endoglucanase, followed by defibrillation using a homogenizer or microfluidizer. While some researchers have employed all three cellulases together to produce CNFs, it was discovered that using monocomponent endoglucanase resulted in CNFs with minimal loss of DP.[146,147] Rol et al.[117], Hiltunen et al.[127] and Pere et al.[148] combined enzymatic hydrolysis with mechanical treatments such as twin-screw extrusion or sigma-type mixer, producing CNFs with solid contents exceeding 20% and reported energy consumption as low as 0.9 $MWh.tonne^{-1}$. Enzymatic CNFs produced at approximately 20% suspension solid content have the potential to be widely adopted by the industry due to reduced transportation and drying energy costs, especially when processed into barrier coatings and films. For more comprehensive information on enzymatic hydrolysis for nanocellulose production, refer to the review article by Arantes et al.[149]

2.2.3 Acid hydrolysis

Cellulose nanocrystals (CNCs) are extracted via strong acid hydrolysis of cellulose pulp.[104]. Nickerson et al.[150] and Rånby[151] were some of the earliest researchers to report the production of CNCs using acid hydrolysis. While sulphuric and hydrochloric acids are the most commonly utilized acids for this purpose, phosphoric, hydrobromic, oxalic, and nitric acids have also been employed.[152] During acid hydrolysis, the strong acids degrade the amorphous regions of cellulose fibrils, leaving behind the crystalline parts. Following acid hydrolysis, the mixture is diluted with water and subjected to centrifugation and dialysis to eliminate any residual acid molecules. Filtration and ultrasonication techniques are frequently employed to further disperse and break down the cellulose nanocrystals.[104] Depending on the cellulose source, CNCs typically have a L/D ratio of over 5, with widths, lengths, and crystallinities ranging from 3 to 10 nm, 100 to 500 nm, and 55% to 85%, respectively.[104,115,152]

2.2.4 Bacterial nanocellulose

Bacterial nanocellulose (BNC) is high-purity cellulose that is synthesized by various bacterial species, such as *Acetobacter, Agrobacterium, Alcaligenes, Pseudomonas,* and *Sarcina.*[153] Among these bacteria, *Acetobacter Xylinium* is the most efficient and commonly employed for the production of BNC.[154] Unlike other types of nanocelluloses, BNCs are characterized by their exceptional purity, devoid of lignins, hemicelluloses, pectins, or any functional groups other than alcohol. The nanofibrils of BNCs typically exhibit diameters of 3-4 nm and lengths exceeding 2 μm. BNCs possess high crystallinity and degrees of polymerization reaching up to 80-90% and 9000, respectively.[72,93] Due to their purity, BNCs are predominantly used in biomedical applications such as wound healing, tissue regeneration, and drug delivery.[154,155] On the other hand, CNCs and CNFs are produced from wood pulp, and their production processes can be scaled up, which is not the case for BNCs. Therefore, CNCs and CNFs are quickly becoming the preferred materials for high-volume commercial applications.

2.3 Suspension properties

Nanocellulose fibrils exhibit higher specific surface area and aspect ratios compared to pulp fibers, resulting in suspension properties that differ significantly from traditional pulp, which in turn have an impact on the handling and processability of these suspensions. The following section will explore relevant suspension properties that play a crucial role when processing nanocelluloses into barrier coatings using high-throughput methods.

2.3.1 Nanocellulose morphology

The morphology of nanocelluloses varies depending on the raw material source and its processing route. Figure 2.4 shows Atomic Force Microscopy (AFM) images of different grades of nanocelluloses. CNFs produced solely via mechanical treatment lie on the coarser side of the size spectrum with fibril diameters in the range of 25 to 100 nm and lengths exceeding 1 μm[109] (Figure 2.4a). Chemical pretreatments introduce charged functional groups on cellulose fiber walls and increase electrostatic repulsion between the nanofibrils, which in turn improve the efficiency of mechanical defibrillation.[118] Therefore, chemically pretreated CNFs show much finer

fiber structures than mechanical grades with fibril diameters as low as 3-5 nm, and in general have a narrower size distribution [99,100] (Figures 2.4b, c). The smaller size of chemically pretreated CNFs combined with higher relative surface area results in transparent films and higher barrier properties compared to mechanical CNFs. [59] However, they show higher viscosities than mechanical grades and are often limited to solid contents below 1–2%. [72] CNCs lie on the finer side of the size spectrum with diameters and lengths in the range of 3-35 nm and 200–500 nm, respectively. [104] They are stiffer and resemble rice like structures (Figure 2.4d), resulting in brittle films and coatings, and often require high amount of plasticizers to improve their flexibility. [59]

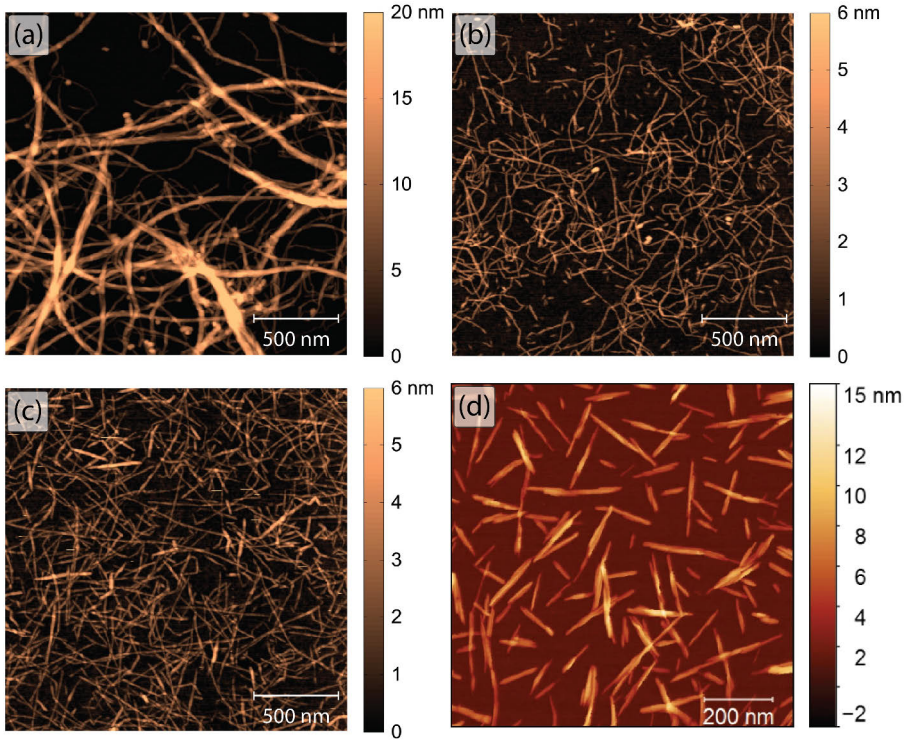

Figure 2.4 AFM images of (a) CNF produced via mechanical defibrillation only; (b) CNF produced by carboxymethylation pre-treatment; (c) CNF produced by TEMPO-mediated oxidation pre-treatment; and (d) CNCs produced via sulphuric acid hydrolysis. [CNF images adapted from Nechyporchuk et al. (2016) [72] and CNC image adapted from Chen et al. (2021) [156]].

2.3.2 Rheology

The rheology of nanocelluloses is a fascinating and important topic that is extensively documented in the literature.[67,70,71,74,75,157–162] Factors such as, cellulose feedstock, CNF production route, morphology, suspension solid content, chemistry, and measurement conditions, influence rheological parameters such as yield stress, gel strength, shear-thinning behavior, and structure recovery.[67,75] In industrial unit operations, a nanocellulose suspension may be exposed to a broad range of shear rates, starting from low to moderate-shear during pumping and mixing ($0.1 - 1000\ s^{-1}$), to high-shear during application and metering ($10^3 - 10^5\ s^{-1}$), and returning to rest/low-shear during leveling and consolidation of the coated layer. These transitions can occur within seconds in high-throughput processes. Therefore, a comprehensive understanding of the underlying principles governing the rheology of nanocellulose suspensions is crucial for the development of robust industrial processes.

Viscosity

Nanocellulose suspensions, characterized by strong inter-fibril networks and susceptibility to hydrogen bonding and van der Waals forces, exhibit high viscosities even at low solid contents below 3%.[67,159] CNFs in general have higher viscosities than CNCs due to the former's higher aspect ratio fibrils and mechanical interlocking between them. It is a well-established phenomenon that nanocellulose suspensions are highly-shear thinning. A typical viscosity curve of CNFs can be divided into three zones: low-shear, transition, and high-shear.[67,70,157,163] CNFs exist as loosely aggregated flocculated structures in aqueous media which results in a yield stress dominated microstructure. When subjected to shear, the flocs align with the shear direction (when shear stress is higher than yield stress), resulting in a drop in viscosity. As the shear rate increases, the hydrodynamic forces break down the flocs and the fibrils start aligning in the direction of the flow. This causes a momentary increase in viscosity due to the resistance (or turbulence) created during the breakup of the fiber bundles.[70,157] This 'kink' in the transition zone has become a characteristic feature of CNF suspensions. Beyond the transition zone, the fibrils align with the shear direction, leading to a continued drop in viscosity. Studies by Karppinen et al.[157] and Saarikoski et al.[164] visualized the development of the flocculated microstructure of mechanical CNFs at various shear rates using transparent measurement geometry and digital imaging. In

contrast to CNFs, the viscosity curve of CNCs does not exhibit a distinct transition zone, as the higher charge content and stiffer nature of CNCs cause the flocs to break more easily at very low shear rates. [159,163]

The viscosity of nanocelluloses is also strongly influenced by the solid content, and follows a power-law scaling, with a power-law index estimated to be around 2-2.6. [70,71,75] However, some studies have reported power-law indices ranging from 1.6 to 6, primarily due to differences in nanocellulose grades and measurement techniques. [75] This wide variation highlights the challenges in processing such complex suspensions for industrial applications. Nevertheless, the shear thinning behavior of nanocelluloses can be advantageous in high-throughput coating processes by utilizing applicators that can achieve high-shear rates. This approach lowers the apparent viscosity to sufficiently low levels, enabling the coating of thin, uniform layers.

Yield stress and thixotropy

Nanocelluloses are viscoelastic suspensions that form yield-stress gels already at low solid concentrations of 0.1-0.3% and 1.5-2% for CNFs and CNCs, respectively. [67,165] Evaluating the yield stress of these suspensions is commonly done through oscillatory amplitude sweep measurements at a constant angular frequency, where the yield stress represents the shear stress at the limit of the linear viscoelastic region (LVE). [166] Typical shear rates at the limit of LVE region are below 0.05 s^{-1} for CNFs and between 0.1 - 2 s^{-1} for CNCs. Yield stress, like viscosity, scales according to a power function with a power index estimated between 2 and 3 by various researchers. [67,74,158,160,161,167] Furthermore, the yield stress is influenced by factors such as aspect ratio and fibril morphology. For instance, Ciftci et al. [71] separated a mechanical CNF grade into different size fractions, and demonstrated that finer CNF fractions exhibit higher yield stress values. Higher yield stress is advantageous when nanocelluloses are used as stabilizers for dispersions and emulsions, as it hinders the sedimentation of larger particles. However, in coating applications, a high yield stress is undesirable as it can lead to cavitation during pumping due to increased resistance to flow. On the other hand, a low yield stress not only facilitates pumping but also improves coating quality by allowing the wet coated layer to reorganize into a uniform layer on the substrate.

Thixotropy is a reversible time-dependent shear-thinning property of certain suspensions. [168] When subjected to a shear load, these suspensions

experience a reduction in structural strength, such as viscosity or elastic modulus; once the shear load is removed, their strength is gradually regenerated over time.[166] Nanocellulose suspensions exhibit thixotropic behavior due to reversible non-covalent interactions between fibrils, and the elastic recovery is further aided by the highly branched and physically entangled fibril structure, even after significant deformations.[67,75] The thixotropic recovery time can be a useful parameter to predict the leveling properties of nanocellulose layer after application or metering.[75] A short thixotropic recovery time causes the viscosity of the coated nanocellulose layer to increase significantly, resulting in a poor coating quality due to the difficulty of the wet layer rearranging itself into a densely packed microstructure. Despite researchers demonstrating the thixotropic effects of nanocellulose suspensions, accurately measuring their recovery times poses a challenge since most grades of nanocellulose recover rapidly.[169–171] Consequently, research on this topic is scarce.

Rheology models

There are several rheology models available in the literature to elucidate the shear-flow behavior of fluids. These models offer valuable insights into predicting important parameters such as yield stress, flow point, and viscosity behavior through different geometries and shear rates; and are essential for designing pumps, mixers, approach flow systems, and related equipment. However, when dealing with nanocelluloses, their rheology becomes highly complex due to considerable variations arising from factors such as raw material source, production methods, fibril morphology (size distribution, aspect ratio, crystallinity, and flexibility), surface charges, and mechanical interlocking of fibers.

Table 2.1 lists some of the rheology models used by researchers for nanocelluloses. The power law model is a simple two-parameter approach frequently employed to fit viscosity data for nanocelluloses.[67,70,161,172] However, it only captures the shear-thinning region with a constant logarithmic decrease in viscosity and fails to accommodate viscosity plateaus at low and high-shear rates.[67,161] The Herschel-Bulkley model, a three-parameter variant of the power law model, is widely utilized and incorporates a yield stress component.[71,75,158,161] Additionally, Casson,[158] Sisko,[173] and vom Berg[174,175] models have been applied in a few cases. Nevertheless, most of these models fail to explain the behavior at the

transition zone and do not adequately fit the data at both the extremes of shear rates.[67]

Researchers have explored the use of Onsager,[176] Simha,[163,176,177] and Batchelor[178] models to predict the aspect ratio of dilute nanocellulose suspensions. While Onsager and Simha models demonstrated similar fitting results for CNFs, they overestimated the aspect ratio of the fibrils.[176] On the other hand, the aspect ratio predicted by the Batchelor model was closer to experimentally determined values.[178] Krieger-Dougherty model explains the relationship between viscosity and the volume fraction of suspension particles;[179,180] however, it is based on monodisperse hard spheres. Considering the heterogeneous nature of nanocellulose with flexible fibrils in CNFs and rigid elongated rods in CNCs, using models based solely on volume fraction and aspect ratio leads to significant deviations and necessitates bold assumptions.

Presently, no single model exists that can accurately fit viscosity data across a wide range of shear rates for nanocelluloses. Developing such a model would be a crucial tool for designing high-throughput unit processes for these materials, facilitating further advancements in their applications.

Measuring systems

Rotational rheometers are commonly utilized for measuring the rheology of nanocelluloses. Parallel-plate (PP), cone-plate (CP), and concentric cylinder (couette) geometries are typically used for these suspensions.[67] PP and CP are suitable for intermediate viscosity samples and require low sample volumes (less than 2 ml). However, they are prone to evaporation from the edges, and their low gap can cause water to be squeezed out from the suspensions, resulting in an increased actual solid content during measurement.[158,167] Measurement with CP is also hampered by sample extrusion from the gap.[167] Therefore, concentric cylinder geometry is preferred for nanocellulose rheology measurements.[67,75] Traditionally, smooth-walled bobs and cups are used in this geometry, but with fibrous suspensions, several factors such as wall slip, wall depletion (particles/fibers migrating away from surfaces, leaving behind water-rich boundary layers at the walls), and shear banding (fast and slow flowing regions in the geometry) can affect the rheology data.[75,164,167,188]

To mitigate these effects, a serrated bob with a roughened cylinder surface has been proposed, resulting in higher viscosity values at low shear rates.[70,160] This is mostly due to the rough surface preventing the formation

Table 2.1 Rheology models describing the shear-flow behavior of nanocellulose suspensions

Model name	Equation
Power-law [168]	$\tau = k\dot{\gamma}^n$
Herschel-Bulkley [168]	$\tau = \tau_y + k\dot{\gamma}^n$
Casson [181]	$\sqrt{\tau} = \sqrt{\tau_y} + \sqrt{\eta_p \dot{\gamma}}$
Sisko [182]	$\eta = \eta_\infty + k\dot{\gamma}^{n-1}$
vom Berg [183]	$\tau = \tau_y + b\sinh^{-1}(\frac{\dot{\gamma}}{c})$
Onsager [184]	$[\eta] = \frac{4}{15}\frac{f^2}{\ln f}$
Simha [185]	$[\eta] = \frac{f^2}{15(\ln(2f)-1.5)} + \frac{f^2}{5(\ln(2f)-0.5)} + \frac{14}{15}$
Batchelor [186]	$[\eta] = \frac{8f^2}{45\rho\ln(2f)}[\frac{\ln(2f)+0.64}{\ln(2f)-1.5} + \frac{1.659}{(\ln(2f))^2}]$
Krieger-Dougherty [187]	$\eta = \eta_o(1 - \frac{\phi}{\phi_m})^{-[\eta]\phi_m}$

τ - shear stress, τ_y - yield stress, $\dot{\gamma}$ - shear rate, η - viscosity, η_∞ - infinite viscosity, η_p - plastic viscosity (or Casson constant), $[\eta]$ - intrinsic viscosity, η_o - viscosity of fluid phase, k - consistency index, n - power-law index, b, c - vom Berg constants, f - aspect ratio, ϕ - volume fraction of disperse solid phase, and ϕ_m - maximum packing fraction of particles in disperse phase

of water-rich boundary layers and therefore reducing the wall slip. However, the viscosity gap between the two geometries narrows as shear rate increases. [169] Nevertheless, industrial equipment typically employs smooth surfaces; therefore, using such geometry might be more representative of actual industrial conditions. Alternatively, some researchers have explored the vane and cup geometry, which exhibits even less wall slip and wall depletion effects. [167,189,190] However, the larger gap between the vane edges and cup wall can lead to secondary flow or turbulent behavior, potentially yielding inaccurate results. [190]

Traditional rheometers are usually limited to shear rates below 1000 s^{-1}, but most industrial coating processes are high shear applications with shear rates reaching as high as 10^7 s^{-1} (under the blade in blade coating). [166] To study rheological behavior at these shear rates, capillary rheometers are used, but the high aspect ratio of CNF fibers tend to clog the entrances of the relatively small capillaries (diameters are less than 1 mm). Sutliff et al. [173] performed capillary

viscosity measurements for 3% CNC suspension and achieved shear rates upto 800 000 s^{-1}, where they observed a Newtonian plateau for the viscosity.

Fluid flow through pipes and narrow slits (a wide slot where slot gap $\ll$ width) is well documented, and the equations to calculate the respective shear stresses and shear rates are available in the literature.[168,191] By using large pipe/slot openings, it is possible to achieve shear rates higher than 1000 s^{-1} for CNF suspensions without obstructing the entrances.[158,161,192] Turpeinen et al.[161] and Salmela et al.[192] employed custom-built glass-pipe rheometers in conjunction with optical coherence tomography (OCT) and ultrasound velocity profiling (UVP) to investigate CNF suspensions. These investigations revealed wall depletion layers and provided insights into wall slip and yield stress for different CNF grades and concentrations. Kumar et al.[158] used pipe and slot rheometers and measured viscosity of mechanical CNF suspensions upto a shear rate of 10^5 s^{-1}. They also proposed that the slot-die could double as a coating applicator for nanocellulose suspensions.

Role of dispersants

Cationic polyelectrolytes such as cationic methacrylates and cationic polyacrylamide (CPAM) adsorb onto negatively charged nanocellulose fibrils, forming flocs, which in turn increase the gel strength and yield stress. However, beyond a certain addition level, the gel strength/yield stress decreases, indicating the formation of strong flocs with weak interactions in-between them.[193] Anionic polymers such as carboxymethyl cellulose (CMC), xanthan gum, and anionic polyacrylamide (APAM) have been proposed to stabilize nanocellulose suspensions through steric forces, where by the yield stress, gel strength, and low-shear viscosity are reduced.[169,194,195] CMC, in particular, has been extensively researched as a dispersant for nanocelluloses as its cellulose backbone is predicted to have positive dispersing capabilities.[169,194,196–199] Kumar et al.[73] demonstrated that CMC's dispersing effects contributed to improved coated layer uniformity during roll-to-roll processing. Overall, dispersants serve as valuable tools for controlling the rheology of nanocellulose suspensions and can greatly aid in the high-throughput processing of such complex suspensions.

2.3.3 Water retention

Water retention is a suspension's ability to resist dewatering. Nanocellulose suspensions, with their hygroscopic nature, high specific surface area, aspect ratio, and abundancy of hydroxyl groups, exhibit high affinity to water. Typical water retention of nanocellulose suspensions is at least one order of magnitude higher than paper pulps,[200] yet still one order of magnitude lower than traditional coating colors.[169] Chemical pre-treatments and the degree of defibrillation directly influence water retention, leading some researchers to employ it as a parameter to assess fibrillation degree.[201]

Water retention can have high impact on coating quality. High water retention results in better coating quality by allowing the wet layer to reorganize into a uniform and tightly packed microstructure. However, this leads to longer drying times and slower machine speeds. Conversely, very low water retention causes rapid water release, immobilizing the wet layer, causing non-uniformities, and coating defects. Moreover, fast water release compromises the wet strength of the paper substrate, particularly in low basis weight grades, potentially leading to runnability issues at high coating speeds. Thus, maintaining an optimal water retention level is vital for trouble-free runnability and uniform coating quality without compromising speed. While research on the influence of water retention on coating quality for nanocellulose suspensions is limited, Kumar et al.[73] demonstrated that adding CMC to mechanical nanocellulose increases water retention, leading to a positive impact on coating quality.

2.3.4 Charge and Zeta potential

The charge content of nanocellulose suspensions plays a crucial role in their processing conditions, stability, and flow behavior. Typically, cellulose fibers carry a slight negative charge, originating from ionizing groups during pulping and bleaching processes. Mechanical CNFs retain most of this charge, ranging from 20 to 300 $\mu eq.g^{-1}$.[202] With chemical pretreatments, the charge can significantly increase, ranging between 300 to 2000 $\mu eq.g^{-1}$ for CNFs and CNCs.[72,120,202] A high charge leads to repulsion between the fibers, resulting in low friction, reduced energy consumption and improved efficiency during defibrillation. For instance, the high charge of TEMPO-CNFs contributes to a 24 - 54% reduction in fibrillation energy.[203] Moreover, chemical CNFs tend to have finer fibrils, positively impacting the properties of films and coatings.

Additionally, these chemical CNFs exhibit lower flocculation, are more readily shear thinning, and show higher thixotropic effects than mechanical grades.[75]

Another crucial indicator of colloidal stability in nanocellulose suspensions is the zeta (ζ) potential. Higher absolute values of ζ potential indicate well-dispersed suspensions, and researchers often use it to assess the stability of nanocellulose suspensions.[204] Improved colloidal stability influences the yield stress, which decreases proportionally with the square of the ζ potential.[205,206] Understanding and controlling the surface charge and zeta potential are essential for optimizing nanocellulose processing and utilization in various applications.

2.4 Films and coatings

Nanocellulose finds diverse applications across several industries, including barrier coatings, paper additives, drug delivery, printed electronics substrates, composites, hygiene products, rheology modifiers, and energy storage.[59–68] Among these applications, nanocellulose-based barrier coatings and films have garnered significant attention from academia and industry due to their high resistance to oxygen, grease, and mineral oils.[34,59] Various methods have been employed to achieve these barrier properties, such as creating pure films from nanocellulose suspensions or applying thin, uniform layers onto substrates like paper, board, and plastics. While these methods are commonly used, there are also alternative approaches. For instance, nanocellulose has been utilized as a reinforcing component in thermoplastic resins and extruded into films.[207–213] However, this process is vulnerable to thermal degradation of cellulose fibers and suffers from compatibility issues between polar cellulose fibers and non-polar thermoplastic resins.[34] Another approach involves adding nanocellulose to ordinary pulp suspension to produce high-strength paper.[214–218] It is important to note that in both these cases, nanocellulose is a minor component, primarily serving as a reinforcing element. The full potential of barrier properties can be realized when nanocellulose becomes the main component, either in a high proportion or close to 100%. The following subsections will delve into more details regarding the various methods to produce nanocellulose-based films and coatings.

2.4.1 Film production process

Films made from pure nanocelluloses are strong, flexible (CNFs only), thermally stable, optically transparent, and exhibit excellent gas barrier characteristics.[219] Solvent casting or vacuum filtration (or papermaking) methods are commonly used to produce these films, which have thicknesses in the range of 25 - 100 μm.[34,219] It is possible to make thinner films but they are fragile and difficult to handle.

Solvent casting involves casting a dilute nanocellulose suspension (typical solid content less than 1%) into a petri dish, and allowing the water to evaporate at ambient or elevated temperatures.[220–222] Films produced by this method exhibit optimal properties, and are often used as a benchmark for a specific nanocellulose grade.[220] This is because the slow-drying conditions facilitate self-assembly of cellulose fibrils leading to a film with a dense and uniform micro-structure.

Vacuum filtration is a slightly faster process where the water from the nanocellulose suspensions is removed under vacuum through a porous polycarbonate or polyamide membrane. The wet cake can be air-dried or pressed and dried in an oven to produce films.[223–225] Nonetheless, these processes are time-consuming, and therefore, hinder their industrial adaptation.

Tammelin et al.'s[226] patent showcases a semi-continuous roll-to-roll production method of nanocellulose films by casting the suspension onto a polymer support (such as PET), and drying it at 30 - 60 $°C$. The low temperature tolerance of the base support restricts this process to low drying temperatures. Pihko et al.'s[227] patent overcomes this issue by using a metal belt as the support.

One challenge in the above processes is the need to use relatively low solid content of the nanocellulose suspensions (1% or lower). Increasing the solid content dramatically increases the viscosity of nanocellulose suspensions, and can be a limiting factor for most of the coating applicators used today. Kumar and Jaiswal's[228] patent application offers an alternative approach. They pass a nanocellulose suspension at 10% solid content through a nip formed by two porous polypropylene-based filter membranes. The nip pressure expels most of the water through the membranes, which then later act as a support, as the wet nanocellulose cake is dried using infrared and hot air dryers. The barrier properties of the resulting nanocellulose films were comparable to those produced via solvent casting method.

2.4.2 Coating methods

Coating methods play a vital role in incorporating nanocellulose as a functional layer on various substrates. These coatings are usually much thinner compared to films, as the underlying substrate provides the required mechanical strength. However, the process of coating is complex and influenced by multiple factors, including suspension properties, application principles, substrate characteristics, drying conditions, and machine parameters. The use of nanocellulose adds an additional level of difficulty due to its complex rheology and low solid content. Despite these challenges, nanocellulose coatings can find numerous valuable applications, driving researchers to employ various techniques for coating nanocelluloses. Several review articles in the literature delve deeper into this topic,[27,34,59,61,62,83] and some commonly used methods are discussed here.

Batch processes

One widely utilized method is rod (or 'bar') coating for nanocellulose suspensions. This approach uses a wire-wound rod with a predetermined surface volume to apply nanocellulose layers onto substrates. It is a straightforward batch process that requires minimal suspension amounts, making it a preferred choice by researchers for quick testing with small samples. The suspension's solid content usually ranges from 0.5% to 2%, resulting in coat weights below 2 $g.m^{-2}$.[86,220,229–231] Although some reports mention solid contents near 10%, these suspensions often contain other additives (such as pigments) mixed in.[232] For paper substrates, it is observed that low coat weights are insufficient to provide necessary barrier properties, as most of the coated material fills the substrate's surface roughness. Therefore, it is common to apply 5 - 10 layers, with reported coat weights ranging from 8 to 14 $g.m^{-2}$.[230] The need for higher coat weights can be alleviated by using a smooth-surfaced base paper with low surface porosity to retain the nanocellulose layer on the surface effectively.

Layer-by-layer assembly is another small-scale batch process where multiple thin nanocellulose layers are coated, with washing and drying steps between each layer. Spin coating[233–235] and dip coating[91,119,121,233,236] are commonly employed techniques in this method, enabling very thin-coated layers. The coat weight depends on the solid content, viscosity, surface energy, and roughness of the materials used. The solid contents are typically below 1% with each layer giving only a few nm thick coated layer.[91,233] Reports indicate that 5-10

layers are typical, with some instances using up to 50 layers, resulting in higher coat weights.[91] For example, Herrera et al.[233] coated mechanical CNF onto a filter paper and reported coat weights of 0.8 and 18 $g.m^{-2}$ for a 10-layer spin and dip coatings, respectively. Both the rod and layer-by-layer methods are valuable tools for laboratory-scale testing. However, scaling them up to industrial conditions proves impractical.

Continuous processes

Size press is a commonly used thin-layer coating method employed for surface sizing of paper, where starch and alkyl ketene dimers (AKDs) are utilized. It is an industrial process and can be used for nanocellulose coating as well. For instance, Lavoine et al.[230] successfully utilized size press to coat a 1.5% CNF suspension at speeds of up to 50 $m.min^{-1}$. They applied multiple layers and achieved coat weights of 3 and 4 $g.m^{-2}$ for 5 and 10-layer coats, respectively. Interestingly, the coat weight of CNF did not consistently increase with the number of layers, and was in-line with the findings reported by Boissard[237] and Richmond.[238]

Spray and foam coating are lesser-used techniques to coat CNF, but they are scalable processes as well. Beneventi et al.[80] employed spray coating with a 2% enzymatic CNF suspension on various paper substrates, achieving coat weights ranging from 3 to 14 $g.m^{-2}$ and speeds up to 12 $m.min^{-1}$. Satam et al.[90] and Shanmugam et al.[79] also used spray coating to effectively coat CNCs and CNFs, respectively. Kinnunen-Raudaskoski et al.[239] explored foam coating using a pilot-scale foam coater, applying 2-3% TEMPO and Enzymatic CNF foams (90% air content) on a paper substrate at a speed of 100 $m.min^{-1}$. The coat weights were 1 and 1-2.5 $g.m^{-2}$ for single and double layers, respectively.

Gravure coating relies on engraved microgravure rollers with predetermined surface volumes to pick up a wet suspension from a bath and apply it onto a moving web. Chowdhury et al.[78] used a reverse gravure coater to coat CNCs with 6 - 12% solid content onto a polyester substrate, resulting in coating thicknesses ranging from 2 - 5 μm. Due to their lower aspect ratios and stiff nature, CNCs are well-suited for gravure coating as they can be easily picked up by the roller. In contrast, CNFs, with their high aspect ratios, do not efficiently fill the gaps in the gravure roller and tend to be stuck under the doctor blade, making gravure coating more suitable for CNCs.

Guerin et al.'s[81] patent describes a continuous wet-on-wet lamination process, where CNF suspension is first deposited onto a moving filter

membrane (similar to a paper machine's forming section), and water is drained using a series of vacuum boxes to obtain a wet nanocellulose cake at 5 - 18% solid content. This is subsequently laminated with a hydrophilic paper substrate and dried using traditional drying methods used for drying paper.

Most of the coating methods described above were initially developed for traditional paper coatings with low suspension viscosities. For instance, a typical coating color containing 60% solid content exhibits a viscosity of approximately 100 $mPa.s$ at a shear rate of 100 s^{-1}. In contrast, a CNF suspension with just 2.5% solid content will show a viscosity above 1000 $mPa.s$ at the same shear rate. This necessitates reducing the solid content of nanocellulose suspensions when employing conventional coating systems. Consequently, it leads to lower coat weights and a requirement for multiple coating layers to achieve the desired coat weight range.

To address this issue, some researchers suggested employing a slot-die with a narrow gap as a coating applicator for nanocellulose suspensions.[73,169,240] With a gap size of 500 - 1000 μm, Kumar[169] achieved shear rates above 10^4 s^{-1} for 3% CNF suspensions, resulting in an apparent viscosity of approximately 30 $mPa.s$. This low-viscosity CNF suspension exiting the slot-die was then applied onto a paper substrate and dried in a roll-to-roll process. Remarkably, a single layer of this method yielded a coat weight of 16 $g.m^{-2}$. This approach therefore, shows a promising method for high-throughput processing of nanocelluloses into barrier coatings. Building on this work, the current study also utilizes slot-die coating, and its working principle will be explored further in subsequent chapters.

2.4.3 Multilayer coatings

As mentioned in the previous sections, nanocellulose-based coatings and films show excellent oxygen and grease barrier properties. However, due to cellulose's hygroscopic nature, these coatings and films suffer from poor water vapor barrier performance.[27,82] To address this challenge, researchers have explored various strategies to incorporate nanocellulose in multilayered systems, protecting it from exposure to a humid environment and mitigating the effects of moisture.[27,62] Vähä-Nissi et al.[241] achieved both oxygen and water vapor barrier by sandwiching a 0.5 - 1 μm thick TEMPO-CNF layer between HDPE and LDPE layers. Similarly, Pasquier et al.[60] developed multilayer films containing mechanical CNF, carnauba wax, and lignin nanoparticle-chitin nanofibrils. Aulin et al.[91] utilized a layer-by-layer

assembly technique, applying 50 layers of CNF and polyethyleneimine pairs on PLA films, resulting in enhanced oxygen barrier properties. Moreover, a variety of other materials such as alkyd resins,[86] guar gum,[84] alginate,[85] polyglycolic acid,[87] PHAs,[88] and shellac[89] have been explored for multilayer coating of nanocelluloses. The successful implementation of these multilayer approaches brings nanocellulose films and coatings closer to the current state of the art, supporting their potential for industrial adoption in barrier packaging applications.

2.4.4 Additives

Various additives serve different purposes in improving the properties of nanocellulose coatings and films. Kumar[169] used CMC as a rheology modifier, and found that at a 3% or higher addition, it acts as a dispersant, reducing CNF fibril aggregation and enhances coating quality. Plasticizers are employed to enhance flexibility, a crucial aspect for CNCs due to their inherent brittleness. Glycerol, sorbitol, ethylene glycol, and PVOH are some examples of plasticizers used for nanocellulose films/coatings, with sorbitol showing an added benefit of improved oxygen barrier properties.[34,233,242,243] However, excessive plasticizer addition can lead to migration issues due to their small size.[34,244] Several researchers have explored blending pigments such as, kaolinite or montmorillonite with nanocellulose and reported improved barrier properties.[245–247] Additionally, the use of mineral pigments can be a cost-effective option that can partially replace some of the more expensive nanocellulose. As this field continually evolves, researchers employ diverse additive combinations and processing conditions for various applications. Thus, readers are encouraged to refer to multiple sources to explore relevant literature on this subject.

2.5 Barrier properties

Barrier packaging plays a crucial role in preserving food freshness and preventing spoilage. Its primary function is to create a barrier against oxygen and water vapor, which are essential for the growth of most microorganisms that can lead to food spoilage.[248] Figure 2.5 lists a few examples of barrier requirements for different food products. For long shelf life products like coffee, baby products, nuts, and UHT (ultra-high temperature processed) milk, low oxygen and water

vapor permeance values are typically necessary. On the other hand, short shelf life products, such as fruits, vegetables, and bakery items, do not demand such stringent requirements. Figure 2.5 also illustrates the oxygen and water vapor permeance values for some common barrier materials.

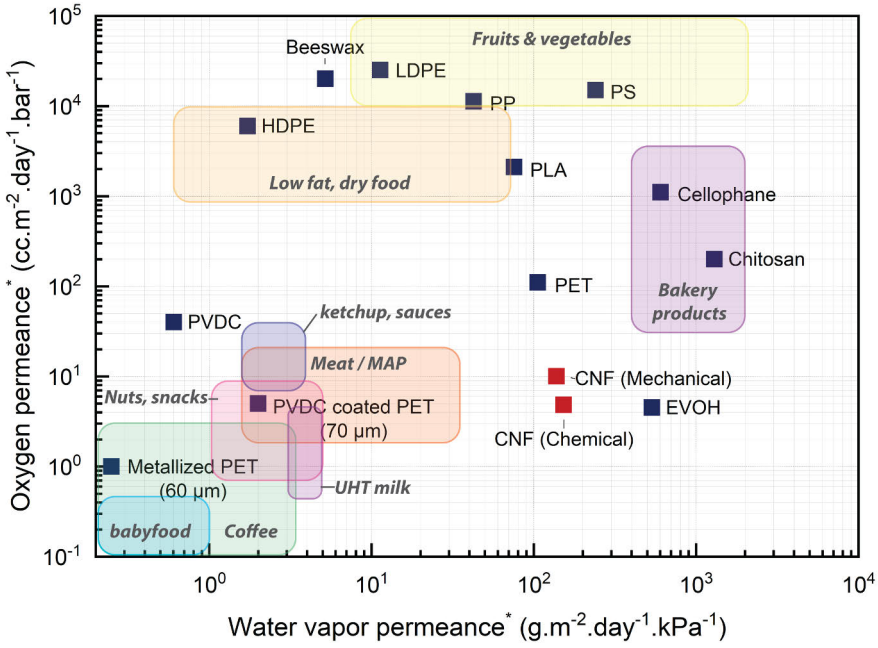

Figure 2.5 Oxygen and water vapor permeance for common packaging materials, and requirements for different food types. The permeance values for pure CNF films are shown in red markers. [Data sources: Lindström and Österberg (2020) [249], An et al. (2018) [250], Schmid et al. (2012) [49], Bauer et al. (2021) [6], Lange and Wyser (2003) [251], Adibi et al. (2023) [252], and Nair et al. (2014) [33] *Permeance values normalized for 10 μm films at 23 $^{\circ}C$ / 50% RH.

The recent attention for nanocellulose-based packaging is due to its remarkable ability to block the passage of oxygen. This can be attributed to the contrasting nature of oxygen, a non-polar compound, with the nanocellulose fibrils, which are enriched with polar groups. [34] Furthermore, the highly fibrillated structure of nanocellulose enables the formation of dense films and coatings, effectively eliminating any gaps in the structure. [220] The cohesive energy density resulting from hydrogen bonding between the molecular chains of cellulose further reinforces the molecular-level integrity, enhancing its capability to block gases. [220]

The oxygen permeance (OP) of nanocellulose films typically ranges from 1 to 10 $cc.m^{-2}.day^{-1}.bar^{-1}$, with finer CNF grades (TEMPO or Carboxymethylated) exhibiting even lower permeance values.[27,33,83,220,249,252,253] Some researchers have reported OP values below 1 $cc.m^{-2}.day^{-1}.bar^{-1}$, but these are typically observed at 0% relative humidity (RH).[220] Due to the inherent brittleness of CNC films and coatings, measuring oxygen barrier becomes challenging, as the measurement is highly sensitive to any defects. As a result, there is limited information regarding the barrier characteristics of pure CNC-based films or coatings.

The polar functional groups and dense structure of nanocellulose films/coatings also provide barrier against grease and mineral oils. Grease barrier is measured as a rate of penetration of oils (castor, olive, and turpentine) through a substrate. Aulin et al.,[220] Lyytikäinen,[254] and Kyllönen[255] reported high grease barrier values for nanocellulose-based coatings. KIT test is also frequently utilized to check the grease resistance of these coatings, and high KIT values over 10 are typically reported.[169,254] Additionally, Kumar[169] evaluated mineral oil barrier by measuring heptane vapor transmission rate (HVTR), and showed that nanocellulose-based coatings/films exhibit a near-zero HVTR.

Sensitivity to moisture poses a significant challenge for nanocellulose-based packaging, primarily due to the hygroscopic nature of cellulose fibers and the presence of polar groups that result in a poor water vapor barrier. It is predicted that water molecules create a plasticizing effect on the cellulose fibrils, weakening the densely packed structure.[34] Moreover, moisture absorption causes the cellulose fibers to swell, leading to breakage of the microstructure.[256] As humidity increases, the oxygen and other barrier properties of nanocellulose films and coatings deteriorate considerably, with OP increasing by up to 20 times when the relative humidity goes from 0 to 80% RH.[220,257]

To address this issue, researchers have explored the application of moisture barrier layers on nanocellulose, creating a multilayer structure. Positive results have been reported by several studies adopting this technique. For instance, Pasquier et al.[60] achieved OP and WVP (water vapor permeance) of 3 $cc.m^{-2}.day^{-1}.bar^{-1}$ and 5 $g.m^{-2}.day^{-1}.kPa^{-1}$, respectively, at 50% RH using a wax coating on CNF. Österberg et al.[258] also obtained an OP of less than 1 $cc.m^{-2}.day^{-1}.bar^{-1}$ with the wax coating on CNF, while Jung et al.[240] achieved an OP below 1 $cc.m^{-2}.day^{-1}.bar^{-1}$ by coating a double layer of chitin nanofibers and CNCs on cellulose acetate films.

The ongoing research efforts focused on improving both oxygen and water vapor barriers for nanocellulose-based packaging have shown steady progress, and it is expected that commercial products utilizing this material will become available in the future.

2.6 Biodegradability and recyclability

Cellulose is naturally biodegradable; and even when broken down into nano-scale components, retains its biodegradability.[83] In Europe, the suitability of a packaging material's biodegradability is assessed using the EN standard 13432 (Requirements for packaging recoverable through composting and biodegradation - Test scheme and evaluation criteria for the final acceptance of packaging).[259] To meet this standard, a packaging material must disintegrate by over 90% within 3 months into pieces smaller than 2 mm, biodegrade and release more than 90% of its theoretical CO_2 maximum within 6 months, have no negative effects on composting process, and not be ecotoxic to plant growth.

Vikman et al.[260] confirmed that nanocellulose meets all EN 13432 criteria and found that it biodegrades faster than the reference control. However, biodegradation rates slow down with increasing degree of substitution (DS), particularly when DS is higher than 0.5.[261,262] Chemically pre-treated CNFs (like TEMPO or carboxymethylation) typically have DS below 0.5, and therefore are fully biodegradable, though slightly slower than unmodified grades.[261]

Aside from being biodegradable, nanocellulose can also be recycled using traditional paper recycling methods.[263–265] In a study by Al-Gharrawi et al.,[247] it was demonstrated that having a nanocellulose layer in-between polyethylene coated paperboard improved the separation of the polyethylene layer during the recycling process. This finding holds promise for the separation and recovery of thermoplastic coatings in nanocellulose-based multilayer packaging structures.

Chapter 3

Materials and Methods

This chapter summarizes the different materials and the most relevant experimental methods used in this work. Further details on the methods can be found in the attached scientific articles (Papers I-VI).

3.1 Materials

3.1.1 Nanocellulose

Six different nanocellulose grades were used in this work, and Table 3.1 lists the nanocellulose type, their corresponding labels, supplier information, production method, and suspension solid content used for coating trials. The suspensions are labelled as nanocellulose type (CNF or CNC) followed by a letter that indicates either their production method or supplier information. For example, CNF-C indicates cellulose nanofibrils with carboxymethylation pre-treatment. In Papers I, IV, and V, the term 'MFC' was used to represent CNF resulting from pure mechanical defibrillation. However, to ensure adherence to the supplier's designated terms and align with the nomenclature specified in ISO/TS 20477:2023 (en) Nanotechnologies - Vocabulary for cellulose nanomaterial, the term CNF-M will be utilized instead to denote MFC. More details on the production process for CNF-M and CNF-C can be found in the supporting information of Paper V and for CNF-E in Paper III.

3.1.2 Additives to nanocellulose

Five different additives were used to study their influence on rheology and water retention of nanocellulose suspensions, as well as multilayer interfacial

Table 3.1 List of nanocellulose grades used in this work.

Label	Nanocellulose type	Supplier	Production method	Coating solid content[a]
CNF-M	CNF	University of Maine, U.S.A	Pure mechanical defibrillation	2.5 %[b]
CNF-C	CNF	RISE-Research Institutes of Sweden	Carboxymethylation followed by microfluidization	2 %
CNF-S	CNF	SAPPI Ltd., Netherlands	Commercial grade; Pre-treatment with swelling agents followed by mechanical defibrillation	2.5 %
CNF-E	CNF	Université Grenoble Alps, France	Enzymatic hydrolysis followed by defibrillation using twin-screw extrusion at 22 %	12.5 %[c]
CNC-M	CNC	Melodea Ltd., Israel	Commercial grade; Sulphuric acid hydrolysis	3 %
CNC-C	CNC	Celluforce Inc., Canada	Commercial grade; Sulphuric acid hydrolysis	7 %

[a]Unless otherwise stated, all solids content percentages are by weight.
[b]Pipe rheology of CNF-M was done at 3% solid content.
[c]Rheology of CNF-E was additionally done at 7.5 and 10% solid contents.
Note: CNF-M, CNF-E, and CNC-C were supplied at 20%, 22%, and 96%, respectively, and were diluted to their respective solid contents given in the table above for coating trials.

adhesion and flexibility of the nanocellulose coatings. Table 3.2 lists the additives and their corresponding suppliers, intended use, and addition levels. Nanocellulose films with and without additives were also prepared by casting 0.5% nanocellulose suspensions into polystyrene petri-dishes. The wet suspension was dried at 23 $°C$ and 50% RH to obtain the films. The amount of suspension was calculated to achieve a targeted film weight of 30 $g.m^{-2}$ (with a thickness of ca. 20 μm for fully dense films).

3.1.3 Substrates for coating

Three different substrates were used for the nanocellulose coating trials. In Paper I, two substrates, a recycled fiber liner board (Dong Il Paper, South Korea; 178 ± 4 $g.m^{-2}$ and 190 ± 5 μm) [referred to as *'linerboard'* from here on], and a packaging paperboard (Trayforma^{TM} Natura, Stora Enso, Finland;

Table 3.2 List of additives used to study rheology and water retention of nanocellulose suspensions, as well as multilayer interfacial adhesion and flexibility of nanocellulose coatings.

Additive	**Supplier**	**Intended use**	**Addition level**[a]
CMC - FINNFIX® 4000G[b]	CP Kelco, Finland	Dispersant and water retention aid	2 - 10 % (on dry CNF)
NaPA[c] - Sokalan® CP10	BASF, Finland	Dispersant	2 - 10 % (on dry CNF-E)
Hyperplaty Kaolin - Barrisurf™ HX	Imerys, U.K	Adhesion at nanocellulose / extrusion-polymer interface	10-50 % (blended into CNF-M)
Glycerol	Sigma Aldrich, Finland	Plasticizer for CNF-C and CNF-E	2-10 % (on dry CNF-C and CNF-E)
Sorbitol	Sigma Aldrich, Finland	Plasticizer for CNC	20 % (on dry CNC-M and CNC-C)

[a]Unless otherwise stated, all solid content percentages are by weight.
[b]DS - 0.8, M_w - 450 000$g.mol^{-1}$
[c]Sodium polyacrylate, M_w - 4000 $g.mol^{-1}$

190 ± 3 $g.m^{-2}$ and 250 ± 5 μm) [referred to as *'paperboard'* from here on] were first used to assess the role of substrate in coating nanocellulose suspensions.

The paperboard was further coated with various primer materials listed in Table 3.3 to investigate the impact of surface roughness, porosity, surface energy, and water absorption capacity on the coatability and quality of CNF coatings. The findings showed that a pigment-coated paperboard offered optimal surface properties for CNF coatings (see Chapter 4 for further information). Therefore, a pigment coated paperboard (Trayforma™ Special, Stora Enso, Finland; 205 ± 2 $g.m^{-2}$ and 270 ± 5 μm) [referred to as *'baseboard'* from here on], was used for the rest of the coatings in Papers II – VI.

In Paper II, more materials were pre-coated on the baseboard (see Table 3.3) to enhance the adhesion between nanocellulose and the baseboard (see Chapter 4 for further information). Based on the results, cationic starch was selected as the preferred primer material for all the roll-to-roll slot-die coating of nanocelluloses throughout Papers II-VI.

Table 3.3 List of primer-coating materials used for paperboard and baseboard.

Primer coatings on *paperboard*[a]			
Material	**Supplier**	**Description**	**Solid content**
HYDROCARB® (HC-60)[b]	Omya, Switzerland	$CaCO_3$ pigment (d_{50} - 1.4 μm)	60%
HYDROCARB® (HC-90)[b]	Omya, Switzerland	$CaCO_3$ pigment (d_{50} - 0.7 μm)	60%
FINNFIX® 10 (FF10)	CP Kelco, Finland	Carboxymethyl cellulose (DS - 0.8, M_w - 60 000 $g.mol^{-1}$)	5%
CNF-T	NTNU and PFI, Norway	TEMPO-oxidation pre-treated CNF (charge content - ca. 900 $\mu mol.g^{-1}$)	1%
CHP 585	CH Polymers, Finland	Acrylate latex (T_g - 0 $°C$, particle size - 50 nm)	5%
POVAL® 6-98	Kuraray Europe, Germany	Polyvinyl alcohol (PVOH, degree of hydrolysis 98.0 - 98.8 mol%)	3%
Primer coatings on *baseboard*[c]			
Material	**Supplier**	**Description**	**Solid content**
FINNFIX® 10 (FF10)	CP Kelco, Finland	Carboxymethyl cellulose (DS - 0.8, M_w - 60 000 $g.mol^{-1}$)	5%
Omyajet® 5010FL[d]	Omya, Switzerland	Cationically dispersed $CaCO_3$ (particle size - 2 μm)	30%
Superfloc C-592	Kemira, Finland	PolyDADMAC (Polydiallyldimethylammonium chloride — cationic polymer)	1%
Raisamyl® 135	Chemigate, Finland	Cationic starch (DS - 0.035)	0.3%

[a]Coating method - roll-to-roll reverse gravure coating (MiniLabo, Yasui Seiki, Japan).
[b]Contains styrene acrylate latex binder (DL1066, Trinseo, Finland) added at 10% addition level (on dry pigment).
[c]Coating method - benchtop metered rod coating.
[d]Contains styrene acrylate latex (DL1066, Trinseo, Finland) as binder, and CMC (FINNFIX® 10) as rheology modifier added at 5% addition level (on dry pigment) each.

3.1.4 Moisture barrier materials for multilayer coatings

Nanocellulose-coated baseboards were further coated with biodegradable thermoplastics or water-based dispersions to protect the nanocellulose-layer from humidity. Table 3.4 lists the moisture barrier materials and their corresponding labels and coating methods. LDPE was used as the reference coating to compare the barrier properties with the biodegradable grades. All the moisture barrier materials are commercial grade and their exact

formulations are withheld by the suppliers. Only the main material type has been disclosed for better interpretation of results.

Table 3.4 Moisture barrier materials used to protect nanocellulose-based coatings from humidity.

Thermoplastic materials (Extrusion coated)		
Label	**Material type**	**Supplier**
TP1	LDPE	Borealis, Finland
TP2	PLA	NatureWorks, USA
TP3	ecovio® - PLA, PBAT blend	BASF, Finland
TP4	BioPBS™ - PBS	PTT MCC Biochem, Thailand
Water-based dispersions (Reverse gravure coated)		
Label	**Material type**	**Supplier**
WD1	Pigment containing polymer dispersion	Commercial grade[a]
WD2	PLA-based dispersion	Commercial grade[a]
WD3	PHA-based dispersion	Commercial grade[a]

[a]Supplier's name withheld to comply with non-disclosure agreements.
Abbreviations: LDPE - low density polyethylene, PLA - polylactic acid, PBAT - Polybutylene adipate terephthalate, PBS - Polybutylene succinate, PHA - Polyhydroxyalkanoate.

3.2 Suspension characterization

3.2.1 Nanocellulose structure

The fibril structure of the different grades of nanocelluloses was imaged using a transmission electron microscope (TEM), JEOL JEM-1400 Plus (JEOL, Japan) operated at 80 kV acceleration voltage. Prior to TEM imaging, 5 μl of 0.01% nanocellulose suspension was drop cast on carbon-coated, glow-discharged copper grids (200 mesh from Ted Pella Inc., U.S.A), and negatively stained with 1% (w/v) uranyl acetate.

3.2.2 Rheology

A modular compact rheometer, MCR 702 (Anton-Paar, Austria) was used to measure rotational, oscillatory, and thixotropic rheology parameters for the nanocellulose suspensions using a Couette geometry (bob diameter - 26.65 mm, effective bob length - 40 mm, cup diameter - 28.93 mm, working

gap - 5.7 mm) with smooth surfaces at 25 $°C$. Prior to each measurement, the samples were pre-sheared at 100 s^{-1} for 60 s and allowed to equilibrate for 120 s to remove any pre-existing heterogenities in the suspension, as suggested by Naderi et al.[266] All the measurements were done in triplicate to ensure repeatability.

Rotational viscosity measurements were performed in controlled shear rate mode with logarithmic shear rate ramp-up/down from 0.01-1000-0.01 s^{-1} (10 points/decade) with dynamic acquisition time that changes logarithmically from 60-1-60 s and an additional 4 s at 1000 s^{-1}, and data from the ramp-down curve was considered for analysis.

Oscillatory strain sweep measurements were performed to evaluate linear viscoelastic (LVE) range and yield stress of the suspensions. Oscillatory strain was logarithmically varied from 0.01 to 100% (10 points/decade) with logarithmic decrease in acquisition time from 100 to 10 s at a constant angular frequency of 10 $rad.s^{-1}$.

Three-interval oscillatory-rotational-oscillatory test was performed to measure thixotropic behavior of the suspensions. As the name suggests, the test has three intervals: (i) Rest - oscillatory mode with constant strain and angular frequency (in LVE range) of 0.1% and 10 $rad.s^{-1}$, respectively, for 60 s (15 points with 4 s/point); (ii) High shear - rotational mode with constant shear rate of 1000 s^{-1} for 40 s (10 points with 4 s/point); and (iii) Recovery - oscillatory mode with constant strain and angular frequency (in LVE range) of 0.1% and 10 $rad.s^{-1}$, respectively, for 120 s (120 points with 1 s/point). Time taken for the elastic modulus (G') in the recovery interval to reach 50% of the rest-interval's steady-state G' value is reported as the relative thixotropy time. Choice of the test parameters for the above rheology measurements were based on the information available in the literature and the author's experience with measuring fiber-based nanocellulosic suspensions.[67,70,75,166,169]

3.2.3 High-shear pipe and slot rheometry

Custom-built pipe and slot rheometers were used to measure the viscosity of CNF-M (3%) and CNF-E (7.5%, 10%, 12.5%) suspensions at high shear rates. A schematic of the experimental setup is shown in Figure 3.1. Briefly, pressurized CNF suspensions were fed into a pipe or slot via a pneumatically actuated ball valve, while an electronic controller measured the time duration for which the valve was open. Suspensions exiting the pipe or slot were collected into a vessel and weighed to obtain the mass flow rate (Q), while a pressure gauge recorded

the pressure drop (ΔP) across the pipe or slot. Two pipes [length (L) = 750 mm] with internal radii (r) of 2 and 3 mm (Figure 3.1b), and three slots [L = 50 mm; width (w) = 100 mm] with slot gaps (h) of 500, 750, and 1000 μm (Figure 3.1c, d) were used in this work. The experimental setup was first tested using silicone oil (V350 and V100, Pentisol, Finland), with a Newtonian kinematic viscosity of 350 and 100 $m^2.s^{-1}$ for pipe and slot configurations, respectively. The resulting viscosity values agreed well with the target range specified by the supplier. These findings were further validated through rotational rheology measurements, which corroborated the obtained values.

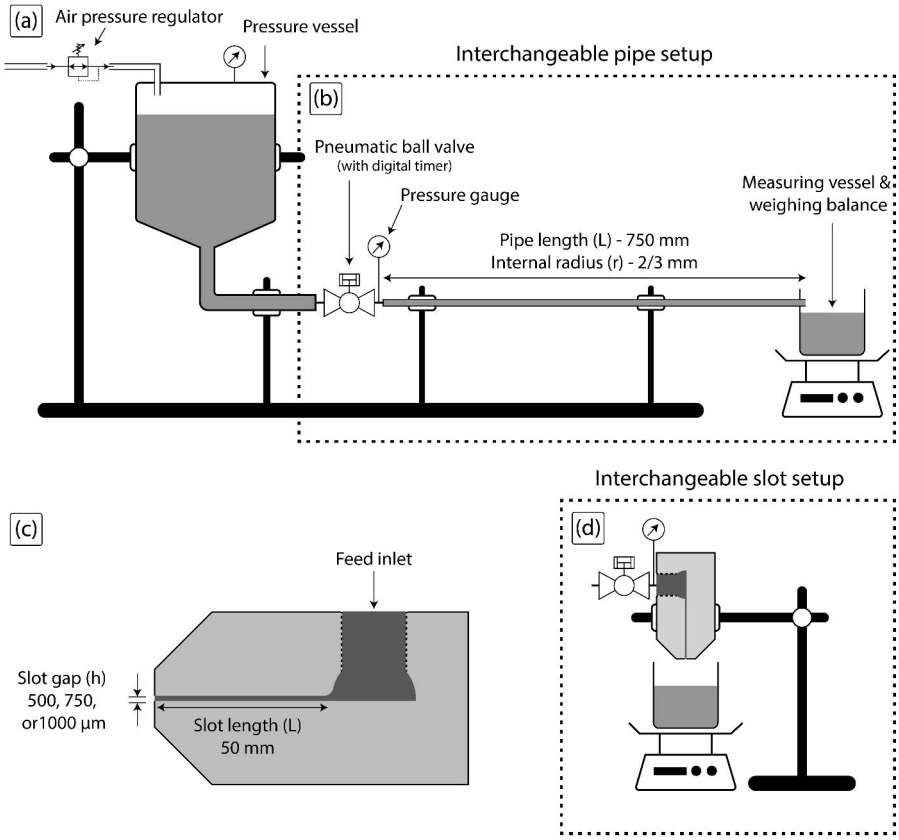

Figure 3.1 (a) Schematic of pipe and slot rheometer setup; (b) pipe setup; (c) slot-die cross-section; (d) slot setup

Equations 3.1 and 3.3 were used to calculate the wall shear stress (σ_w) and equations 3.2 and 3.4 to calculate the non-Newtonian wall shear rate ($\dot{\gamma}_w$) for flow through the pipe and slot, respectively.[191,267] The power-law index (n)

in equations 3.2 and 3.4 was obtained from Casson-Power-Cross-fit parameters (discussed in Chapter 4).

$$\text{Wall shear stress (pipe)} : \sigma_w = \frac{\Delta P r}{2L} \tag{3.1}$$

$$\text{Wall shear rate (non-Newtonian (pipe))} : \dot{\gamma}_w = \frac{(3 + \frac{1}{n})Q}{\pi r^3} \tag{3.2}$$

$$\text{Wall shear stress (slot)} : \sigma_w = \frac{\Delta P h}{2L} \tag{3.3}$$

$$\text{Wall shear rate (non-Newtonian (slot))} : \dot{\gamma}_w = \frac{(2 + \frac{1}{n})2Q}{wh^2} \tag{3.4}$$

As the fluid entering the pipe or slot-die accelerates to its final velocity, a portion of the pressure drop is lost as kinetic energy. The pressure loss due to kinetic energy is given by Equation 3.5 [267], where ρ, ν, and α are fluid density, average fluid velocity and kinetic energy correction factor (given by Equation 3.6), respectively.

$$\text{Kinetic energy pressure loss} : \Delta P_{KE} = \frac{\rho \nu^2}{\alpha} \tag{3.5}$$

$$\text{Kinetic energy correction factor} : \alpha = \frac{2(2n+1)(5n+3)}{3(3n+1)^2} \tag{3.6}$$

Entrance and exit pressure losses and boundary slip are some of the potential errors that could arise while calculating the shear stress and shear rates for flow through the pipe/slot, and several experimental methods exist to evaluate such errors. However, accounting for these errors requires a significantly higher number of experimental parameters and goes beyond the scope of this work, and therefore, have been neglected.

3.2.4 Water retention and zeta (ζ) potential

A gravimetric water retention test (Åbo Akademi type method – ÅAGWR) was performed according to TAPPI T701 pm-01. The test simulates a suspension's dewatering rate in a coating process by measuring the amount of water released from a 10 ml sample through a 5 μm filter membrane at a pressure drop of 0.5 bar during a 90 s time interval. The amount of water released per unit area was reported as an average from three parallel measurements. ζ potential for the nanocellulose suspensions diluted to 0.05% was measured using a Zetasizer 3000 (Malvern Instruments Ltd., U.K), and the average from six parallel measurements is reported.

3.3 Coating methods

3.3.1 Primer coating

In Paper I, different materials (listed in Table 3.3) were coated on paperboard (Trayforma^{TM} Natura) to explore the impact of substrate properties on nanocellulose coating quality. The primers were coated using a desktop roll-to-roll reverse gravure coater, MiniLabo (Yasui Seiki, Japan), and dried inline using a combination of infrared and hot-air dryers. The web speed was 1.5 $m.min^{-1}$, and the gravure roll has a surface volume of 82.8 $cm^3.m^{-2}$ (75 lpi x 165 μm), and applies a wet coating thickness of ca. 20 - 30 μm (transfer fraction - 0.33). After analyzing the results (as detailed in Chapter 4), a pigment coated board (Trayforma^{TM} Special - *baseboard*) was chosen as the preferred substrate for the rest of the work (Papers II – VI).

In Paper II, the baseboard was further coated with additional materials (refer to Table 3.3) to improve the adhesion of nanocellulose with the baseboard. These primers were coated using a bench-top metered rod coater, K202 control coater (RK PrintCoat instruments, U.K.), and dried using a combination of infrared and hot-air ovens. The coatings were done at 3 $m.min^{-1}$ and the metered bar applies a wet coating thickness of ca. 25 μm. Based on the results, cationic starch was selected as the primer material for the rest of the work.

Cationic starch primer coating on the baseboard was carried out using a laboratory-scale mini-pilot roll-to-roll coater (Rotary Koater, RK PrintCoat Instruments, U.K.), which can be fitted with different coating applicators based on the requirement. The coater has operating speeds between 1 - 50 $m.min^{-1}$, maximum drying capacity of 43 kW, and a maximum coating

width of 300 mm. Cationic starch coating was done using reverse-gravure method. The gravure roll has a surface volume of 78.5 $cm^3.m^{-2}$ (70 lpi x 127 μm) and applies a wet coating thickness of 16 - 25 μm (transfer fraction 0.32). Due to the low solids content of cationic starch solution (0.3%), it is difficult to accurately determine the dry thickness/coat weight of the starch layer. Therefore, it is assumed that the coat weight of starch layer is less than 1 $g.m^{-2}$.

3.3.2 Slot-die coating of nanocellulose

The same Rotary Koater was modified in-house and fitted with a custom-built slot-die applicator to coat nanocellulose suspensions onto the starch-coated baseboard. Figure 3.2a shows the schematic of the slot-die coating process. Nanocellulose suspension is fed to the slot-die from a pressurized feed vessel via a gear pump. Inside the slot-die, the suspension first enters into a distribution channel (diameter - 25 mm) and then passes through a narrow gap (slot-gap) before exiting the slot-die. Pressure drop across this gap results in high-shear rates, which reduces the apparent viscosity of shear-thinning nanocellulose suspension. Shear rate in the slot-die is directly proportional to the flow rate (controlled by the gear pump) and inversely proportional to the square of the slot gap (Equation 3.4). Typical shear rates achieved during slot-die coating of nanocelluloses in this work are in the range of 500 - 20 000 s^{-1}.

The fluidized suspension exiting the slot-die is applied onto a moving substrate to obtain a uniform wet coating layer. The slot-die has a coating width of 100 mm and length of the narrow slot-gap region is 50 mm (In Papers I, II, and IV, the slot-die's length, width, and distribution channel's diameter were 34, 74, and 16 mm, respectively). Depending on nanocellulose's fibril size, suspension solids content, and viscosity, slot-gap is adjusted between 500 - 1000 μm to avoid clogging the slot entrance. Figures 3.2b and c show a close-up and cross-section of the slot-die applicator, respectively.

The slot-die is fixed at a 3 o'clock position with a downward offset of 5 mm against the backing roll's center-line. This results in a converging geometry between the backing roll and the slot-die's top lip, thus allowing the top lip to function as a metering device to remove excess applied coating. The advantage is that, this allows the coater's line speed to be set independent of the minimum flow rate required to achieve sufficient fluidization (low viscosity) of the nanocellulose suspension. Wet coating thickness is set by the gap between

substrate and slot-die's top lip, and coating speed depends on the wet coating thickness, suspension solid content, and maximum drying capacity of the coater. Table 3.5 lists the different nanocellulose coatings done in this work along with their wet-coating thicknesses (set value), line speeds, and dry-coating thicknesses (measured value). All the nanocellulose-coated baseboards were calendered at 100 $kN.m^{-1}$ and 60 $°C$ using a laboratory-scale soft-nip calender (DT Paper Science, Finland).

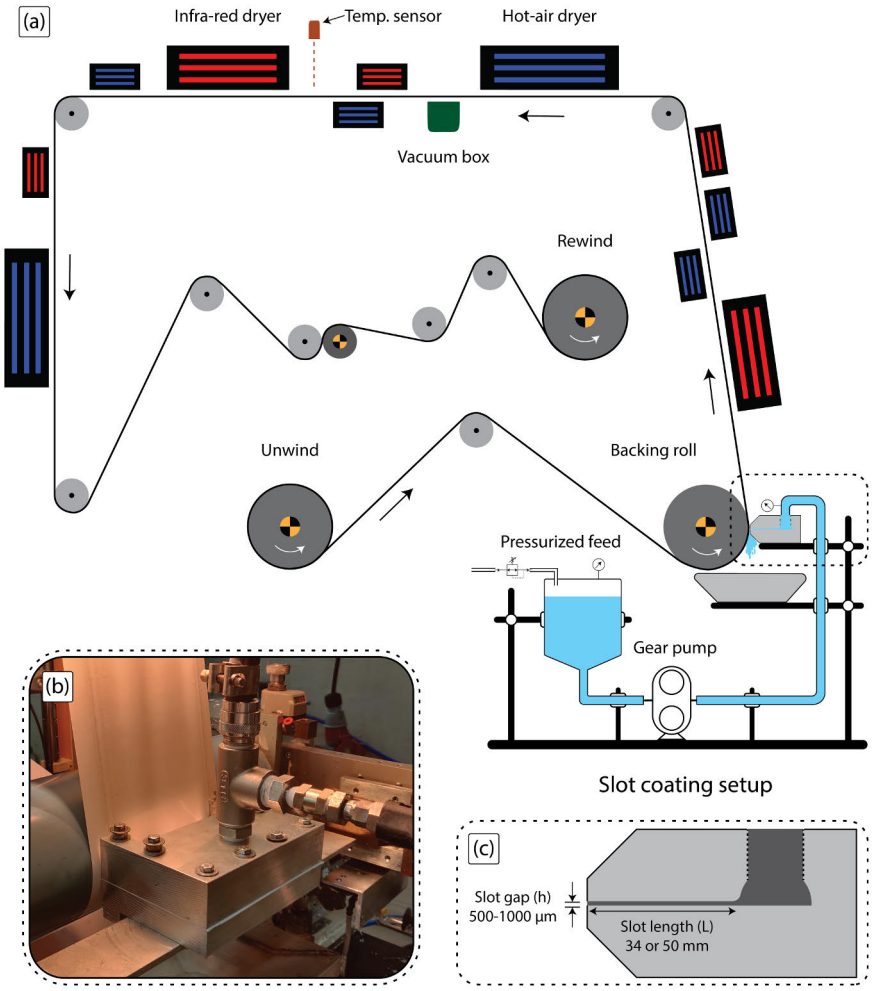

Figure 3.2 (a) Schematic of roll-to-roll slot-die coating of nanocellulose; (b) Slot-die coating applicator; (c) Cross-section of the slot-die.

Table 3.5 List of nanocellulose coatings produced in this work.

Nanocellulose[a]	**Solid content**	**Line speed**	**Wet thickness**[b]	**Dry thickness**[c]
CNF-M	2.5%	3 $m.min^{-1}$	400 μm	8 ±2 μm (≈12 $g.m^{-2}$)
90%CNF-M + 10%Kaolin	2.8%	3 $m.min^{-1}$	400 μm	10 ±2 μm (≈16 $g.m^{-2}$)
60%CNF-M + 40%Kaolin	4%	3 $m.min^{-1}$	400 μm	8 ±1 μm (≈15 $g.m^{-2}$)
CNF-C	2%	6 $m.min^{-1}$	250 x 2 μm[d]	5 ±1 μm (≈7 $g.m^{-2}$)
CNF-C + 2%Glycerol	2%	6 $m.min^{-1}$	250 x 2 μm[d]	5 ±1 μm (≈8 $g.m^{-2}$)
CNF-C + 10%Glycerol	2%	6 $m.min^{-1}$	250 x 2 μm[d]	4 ±1 μm (≈7 $g.m^{-2}$)
CNF-S	2.5%	3 $m.min^{-1}$	450 μm	8 ±1 μm (≈12 $g.m^{-2}$)
CNF-E[e]	12.5%	4 $m.min^{-1}$	200 μm	ca. 16 μm (≈24 $g.m^{-2}$)
CNC-M + 20%Sorbitol	3%	3 $m.min^{-1}$	400 μm	7 ±1 μm (≈11 $g.m^{-2}$)
CNC-C + 20%Sorbitol	7%	4 $m.min^{-1}$	300 μm	4 ±1 μm (≈6 $g.m^{-2}$)

[a]CNF-M, CNF-C, and CNF-S have 5% CMC added as dispersant.
[b]Wet thickness is the set value between slot-die's top lip and paper substrate.
[c]Dry thickness is measured value from SEM cross-sections, and coat weights are calculated assuming a density of 1.55 $g.cc^{-1}$ and fully dense coating.
[d]Double coated.
[e]Three different coatings were produced. Pure CNF-E, CNF-E + 5%CMC, and CNF-E + 5% NaPA.

3.3.3 Multilayer coatings

The nanocellulose-coated baseboards were further coated with moisture-barrier materials from Table 3.4 to obtain multilayer-coated structures. Depending on the type of moisture-barrier material, two different coating methods, hot-melt extrusion for thermoplastics and reverse-gravure coating for water-based dispersions were used. Extrusion coating was done using a pilot-scale extrusion coater at Tampere University, Finland. Coating speed was set at 70 $m.min^{-1}$ and coating thickness was chosen according to supplier's recommendation for each material type. Prior to extrusion coating, nanocellulose-coated baseboards were corona treated (inline) to improve the adhesion between nanocellulose and thermoplastic layers. Reverse gravure coating for water-based dispersions was done using the Rotary Koater at 5 $m.min^{-1}$ with

the same gravure roll used for cationic starch primer coatings. Table 3.6 lists the moisture-barrier top coatings done on different nanocellulose-coated boards along with their corresponding measured dry-coating thicknesses.

Table 3.6 List of multilayer coatings produced in this work.

Extrusion coated samples			
Mositure barrier coating	**Line speed**	**Dry thickness[a]**	**Nanocellulose base layer**
TP1 - LDPE	$70\,m.min^{-1}$	$17\,\mu m$	CNF-M (with/without Kaolin), CNF-C (with/without glycerol), CNC-M
TP2 - PLA	$70\,m.min^{-1}$	$19\,\mu m$	CNF-M (with/without Kaolin), CNC-M
TP3 - ecovio®	$70\,m.min^{-1}$	$38\,\mu m$	CNF-M (with/without Kaolin), CNF-C (with/without glycerol)
TP4 - PBS	$70\,m.min^{-1}$	$22\,\mu m$	CNF-M (with/without Kaolin), CNF-C (with/without glycerol)
Reverse gravure coated samples			
Mositure barrier coating	**Line speed**	**Dry thickness[a]**	**Nanocellulose base layer**
WD1 - Pigment, latex blend	$5\,m.min^{-1}$	$22\,\mu m$	CNF-M (without Kaolin), CNC-C
WD2 - PLA-based dispersion	$5\,m.min^{-1}$	$12\,\mu m$	CNF-S
WD3 - PHA-based dispersion	$5\,m.min^{-1}$	$12\,\mu m$	CNF-S

[a]Dry thickness is the measured value from SEM cross-sections

3.4 Characterization of coated samples

Prior to characterization, all the coated samples were conditioned at 23 $°C$ and 50% RH for at least 24 hours.

3.4.1 Characterization of primer coatings

Air permeability of the coatings was measured using an air permeability tester, SE-166 (Lorentzen & Wettre, Sweden) with a measurement range of 0.003 - 100 $\mu m.Pa^{-1}s^{-1}$. Average value from ten parallel measurements is reported. Surface roughness was measured using a Parker Print-Surf smoothness tester, PPS ME-90 (Messmer Büchel, The Netherlands), and the average from five

parallel measurements is reported in μm. Cobb-60 was determined according to TAPPI T-441 standard test method and the average from three parallel measurements is reported in $g.m^{-2}$. Dynamic contact angle for the substrates and primer coatings was measured using an optical contact angle goniometer, KSV CAM 200 (KSV Instruments, Finland). A 4 μl water droplet was placed on the substrate's surface, and a high-speed camera recorded the dynamic wetting of the water droplet for a duration of 60 s. An image analysis software, OneAttension® (Biolin Scientific, Finland) was used to determine the contact angle of the droplet as a function of time. Average contact angle at 1 s, from three parallel measurements is reported. A tape test (Standard: IPC-TM-650) was used to qualitatively measure the adhesion of CNF-M and CNC-M to various primer coated substrates in Papers I and II, respectively.

3.4.2 Coating structure

Surface and cross-section images for the coated samples were obtained using a field-emission scanning electron microscope (FE-SEM), LEO Gemini 1530 (Carl Zeiss, Germany). Prior to imaging the cross-sections, coated samples were embedded in an epoxy resin (Epon epoxy embedding kit, Sigma-Aldrich, Finland), polished using a grinder/ polisher (Phoneix BETA grinder/polisher, Buehler, USA), and sputter-coated with carbon (Temcarb TH500, Emscope Laboratories, U.K.). More information on embedding and grinding/polishing is given in Paper III. In addition, broad-ion beam cutting was used to prepare a few samples for SEM cross-sections in Papers IV and V. Dry coating thicknesses for each layer was obtained from the cross-section images. An average of 10 points from three images is reported. Due to the baseboard's variation in basis weight compared to the nanocellulose coatings, traditional gravimetric methods do not give accurate values for the coat weights. Therefore, they were calculated by multiplying the coating thicknesses with density of nanocellulose (1.55 $g.cm^{-3}$), and assuming a densely packed structure.

Adhesion at nanocellulose/cationic starch-coated baseboard and nanocellulose/thermoplastic interfaces was quantified by measuring the force required to peel off a tape, TZe-C51 (Brother, U.K.) attached to the coated surface using an SP-2000 peel tester (IMASS, USA). One edge of the tape was attached to the surface of the substrate, while the opposite edge was clamped to a 50 N load cell. The tape was pulled at an angle of 180° over a length of 26 mm at a speed of 5 $mm.s^{-1}$, and the force required to peel the tape was

measured as a function of peeling distance. There is an initial force peak as the coated layer fractures at the weaker interface, after which the force plateaus to a lower value as the fractured-layer is peeled off. The average peak force from five parallel measurements is reported.

Attenuated total reflectance – Fourier transform infrared spectroscopy (ATR-FTIR) was used to determine the orientation of kaolin-pigment particles in both CNF-M-kaolin composite films and roll-to-roll (R2R) coated samples according to the method described by Elton et al.[268] and Bollström et al.[269]. Nicolet™ iS50 FTIR Spectrometer (Thermo Scientific, USA) with a diamond KRS5 ATR crystal and an incidence angle of 45° was used for ATR-FTIR measurements. The particle alignment factor ($k = I_{3695}/I_{3620}$) of kaolin pigments on the surfaces of the films and coated samples was determined by comparing the –OH absorption peaks of kaolin above 3500 cm^{-1}. The peak at 3695 cm^{-1} (I_{3695}) shows the –OH group that is perpendicular to kaolin surface; and the peak at 3620 cm^{-1} (I_{3620}) shows the –OH group that is at a shallow angle to the kaolin's surface. A low value of k indicates higher alignment to the surface and vice-versa.

3.4.3 Barrier properties

Water vapor permeance (WVP) was determined according to ASTM E96/E96M-05 at two different conditions, 23 ^oC/50% RH and 38 ^oC/90% RH, and an average from three parallel measurements is reported as $g.m^{-2}.day^{-1}.kPa^{-1}$. Oxygen permeance (OP) was measured according to ASTM F1927-07 (coulometric method) [Ox-Tran 2/21 MH/SS, Mocon, U.S.A] or ASTM F3136-15 (dynamic accumulation method) [OpTech-O2 Model P, Mocon, U.S.A] at 23 ^oC/50% RH. A few multilayer-coated samples were also measured at 25 ^oC/75% RH and 38 ^oC/90% RH. F3136 is a relatively fast method to determine oxygen barrier for medium to low barrier materials, and was first used to screen out low oxygen-barrier samples. F1927 is more sensitive to defects and is used for high oxygen-barrier samples. OP from two parallel measurements is reported as $cc.m^{-2}.day^{-1}.bar^{-1}$.

Grease barrier was evaluated according to ASTM F119-82 using olive oil at 40 $^\circ C$, and the average value from three parallel measurements is reported in hours (in the interest of time, the test was stopped after 500 hours). Mineral oil barrier (Heptane vapor transmission rate - HVTR) for the coated samples was determined according to the method suggested by Miettinen et al.,[270] and the average value from three parallel measurements is reported as

$g.m^{-2}.day^{-1}$. Additionally, grease resistance (KIT-test) for the coated papers was evaluated according to a TAPPI test method, T559 cm-12, and reported as KIT numbers from 1 to 12, with higher numbers indicating higher grease resistance. Detailed experimental procedures for the barrier tests can be found in the attached Papers I-VI.

Chapter 4

Results and Discussion

This chapter discusses the findings related to the processing of various grades of nanocelluloses into multilayer barrier coatings. Emphasis is placed on the factors that influence the roll-to-roll processability of nanocelluloses on a large scale and the resulting barrier properties. Readers are encouraged to refer the attached Papers I-VI for additional details.

4.1 Nanocellulose structure

Morphology of nanocelluloses can be considered as a spectrum that depends on the raw material source and the processing route. Figure 4.1 shows the TEM images of all the six nanocellulose grades from Table 3.1. CNF-M is produced with just mechanical defibrillation and therefore shows relatively coarse fibers compared to the rest. CNF-C and CNF-S are chemically pre-treated with carboxymethylation and swelling agents (Morpholine, Potassium Hydroxide, Calcium Thiocyanate), respectively, before undergoing mechanical defibrillation. These chemical treatments aid in delaminating cellulose fiber walls and enhance electrostatic repulsion among the nanofibrils. Consequently, CNF-C and CNF-S exhibit finer fiber structures than CNF-M due to improved mechanical defibrillation efficiency.[72]

Enzymatic hydrolysis typically uses single-component endoglucanase-based enzymes that are known to have high specificity towards disordered (amorphous) regions of the cellulose.[149] This enzymatic process weakens the amorphous regions within cellulose fibers, and subsequent mechanical defibrillation severs these weakened regions, resulting in smaller fibrils with lower degrees of polymerization compared to other CNF grades. Figure 4.1d

shows that CNF-E has shorter fibers that resemble CNCs but are relatively thicker. This could potentially yield stiff and brittle coatings with diminished barrier properties, as will be discussed later in this chapter.

CNCs are on the finer end of the nanocellulose spectrum as acid hydrolysis removes most of the amorphous regions, leaving behind predominantly crystalline segments of cellulose fibers (average length and diameter of CNCs in Figures 4.1e and f is between 60 - 250 and 7 - 15 nm, respectively). Due to this selective removal, CNCs have lower yield than that of CNFs. The crystalline nature of CNCs might also result in brittle coatings and therefore need higher amount of plasticizer to deliver their barrier properties.

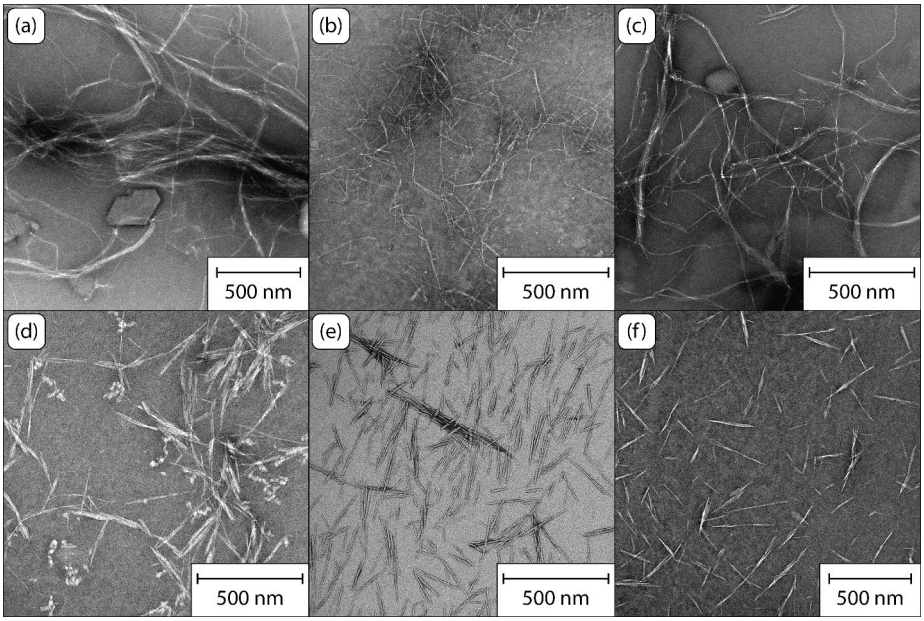

Figure 4.1 TEM images of, (a) CNF-M, (b) CNF-C, (c) CNF-S, (d) CNF-E, (e) CNC-M, and (f) CNC-C.

4.2 Rheology

4.2.1 Yield stress

Nanocellulose suspensions exhibit high yield stress due to inter-fibril hydrogen bonds and mechanical entanglement of high-aspect ratio fibers. This high yield stress can give rise to various challenges during a coating process. For instance,

it can lead to cavitation during pumping due to increased flow resistance, formation of non-yielding areas within the coating head resulting in coating defects, and compromised barrier properties arising from the nanocellulose layer's inability to restructure itself into a densely packed microstructure. Yield stress can be determined through oscillatory amplitude sweep measurements performed at a constant angular frequency, and plotting the storage modulus (G') against shear stress. Yield stress corresponds to the shear stress at the limit of the linear viscoelastic (LVE) region.[166] Figure 4.2a shows an example of yield stress assessment for CNF-E suspensions (containing 5% CMC or NaPA dispersants) at 12.5% solid content.

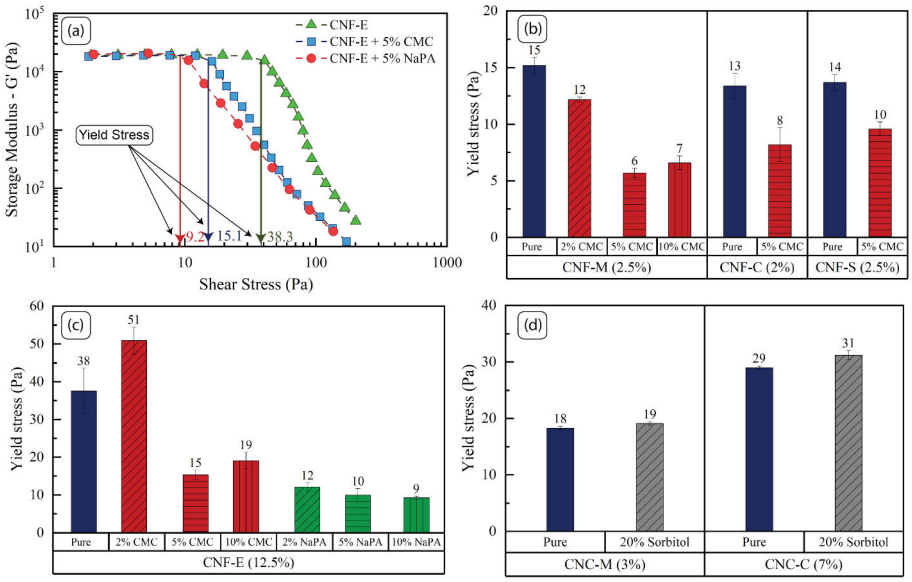

Figure 4.2 (a) Storage modulus (G') versus shear stress for CNF-E suspensions (containing 5% CMC or NaPA addition level) at 12.5% solid content; (b) Yield stress of CNF-M, CNF-C, and CNF-S with CMC as dispersant; (c) Yield stress of CNF-E with CMC and NaPA dispersants; (d) Yield stress of CNC-M and CNC-C with sorbitol.
Note: For CNC suspensions in (d), CNC to water ratio was kept constant due to higher contribution of sorbitol towards the total suspension solid content.

Figures 4.2b, c, and d show the yield stress for all the nanocellulose suspensions used in this work along with different dispersant additions. For CNF suspensions (Figures 4.2b and c), it is evident that the yield stress reduces with the addition of dispersants. CMC and NaPA are conventionally used dispersants in mineral pigment coating formulations to improve the colloidal stability via electro-steric stabilization.[271] Therefore, the reduction

in yield stress can be attributed to the increased repulsion between the charged CNF fibers due to the presence of adsorbed dispersants.

The impact of dispersant levels on yield stress was further explored for CNF-M and CNF-E (Figures 4.2b and c). With increasing CMC addition, the yield stress initially decreases, followed by an increase, indicating an optimal addition level around 5%. Excessive addition can lead to unabsorbed dispersant, which increases the ionic concentration in the water phase and promotes flocculation due to compressed electric double layers.[271] In the case of CNF-E suspensions, NaPA addition produces the most significant reduction in yield stress (Figure 4.2c), continuing to decrease with higher addition levels. This behavior persists across different solid contents of CNF-E suspensions (Paper III). This trend suggests the possibility of either an unreached optimum dispersant loading or an excess that forms smaller, more robust flocs, which flow as separate entities. Such a scenario could create a misleading perception of lower yield stress, ultimately compromising coating quality, as will be demonstrated later on.

In contrast, sorbitol addition to CNC suspensions has minimal influence on the yield stress (Figure 4.2d). This is attributed to sorbitol's small molecular size, which is unlikely to cause steric stabilization of CNCs. Instead, sorbitol primarily serves as a plasticizer to reduce the brittleness associated with CNC coatings.

Solid content or consistency is another factor that effects the yield stress of nanocellulose suspensions. Existing literature reveals that yield stress (τ_y) of nanocellulose suspensions scales according to a power function with the consistency (c) (Equation 4.1), with a typical exponent of 2.3.[74] The constants 'τ_o' and 'm_τ' in Equation 4.1 are suspension-specific parameters that can vary significantly across different nanocellulose grades. Figure 4.3a shows normalized yield stress ($\overline{\tau} = \tau_y/\tau_o$) plotted against solid content for CNF-E suspensions along with 5% CMC and NaPA dispersants. CNF-E with 5% CMC exhibits a lower m_τ value (2.5) compared to pure CNF-E ($m_\tau = 3.8$) and CNF-E with 5% NaPA ($m_\tau = 4.7$). This means that, as the solid content increases, yield stress increases much more rapidly for pure CNF-E and CNF-E with NaPA compared to CNF-E with CMC. This can have an adverse effect on the coating layer. This is because, as the wet coated layer dries, the yield stress increases with a power of m_τ, implying that suspensions with higher m_τ will immobilize more rapidly, potentially leading to uneven or cracked coating layers.

Figure 4.3b shows the evolution of m_τ as a function of increasing dispersant loading for CNF-E suspensions. CMC-containing suspensions display an initial

decrease in m_τ followed by an increase, confirming the optimal addition level at 5%, as mentioned earlier. Conversely, NaPA-containing suspensions show an upward m_τ trend with higher addition levels, suggesting a possible optimum level between 0% and 2%.

$$\text{Yield stress: } \tau_y = \tau_o c^{m_\tau} \tag{4.1}$$

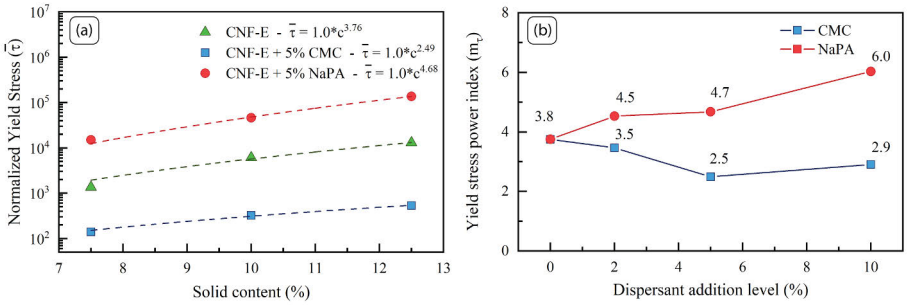

Figure 4.3 (a) Normalized yield stress versus solid content for CNF-E suspensions (with 5% CMC and NaPA addition levels); (b) Yield stress power-law index versus dispersion addition level for CNF-E suspensions.

4.2.2 Viscosity

Nanocellulose suspensions exhibit a well-established shear-thinning behavior,[67,75] as demonstrated by Figures 4.4a and b, which present viscosity versus shear rate plots for CNF and CNC suspensions used in this work. The shear-thinning phenomenon is evident in both figures, where the viscosity drops by approximately four orders of magnitude as the shear rate transitions from 0.1 to 1000 s^{-1}. Despite the CNF-E grade having a significantly higher solid content than other CNF grades, the difference in viscosity is not substantial. This could be attributed to the finer and longer fibrils found in CNF-M, -C, and -S (as depicted in Figure 4.1), resulting in enhanced mechanical interlocking and hydrogen bonding, thereby leading to higher viscosity already at a low solid content.

Figure 4.4a further shows that the viscosity profile of CNFs can be categorized into three distinct zones: low-shear, transition, and high-shear, with the characteristic nanocellulose 'kink' noticeable in the transition zone. A possible explanation is that, CNFs exist as loosely aggregated flocculated microstructures (fibril flocs) within the suspension, mostly due to mechanical

interlocking and inter-fibril hydrogen bonding. At low shear rates, these flocs congregate and align in the direction of shear, leading to a decrease in viscosity. With increasing shear rates and stress, the flocs disintegrate, and the fibers align with the flow direction. The transient viscosity increase within the transition zone results from the resistance and turbulence arising during the breakdown of fibril flocs.[70,75,157]

In contrast, CNCs do not exhibit a distinct transition zone (Figure 4.4b) due to their reduced flocculation tendency stemming from the smaller, stiffer, and crystalline fibers. The short and stiff cellulose nanocrystals align more readily with the flow direction compared to longer fibrils, and any flocs that may be present are broken down already at low-shear rates. Additionally, the higher charge of CNCs (as shown in Figure 4.10b) contributes to a relatively stable suspension with reduced flocculation tendency.

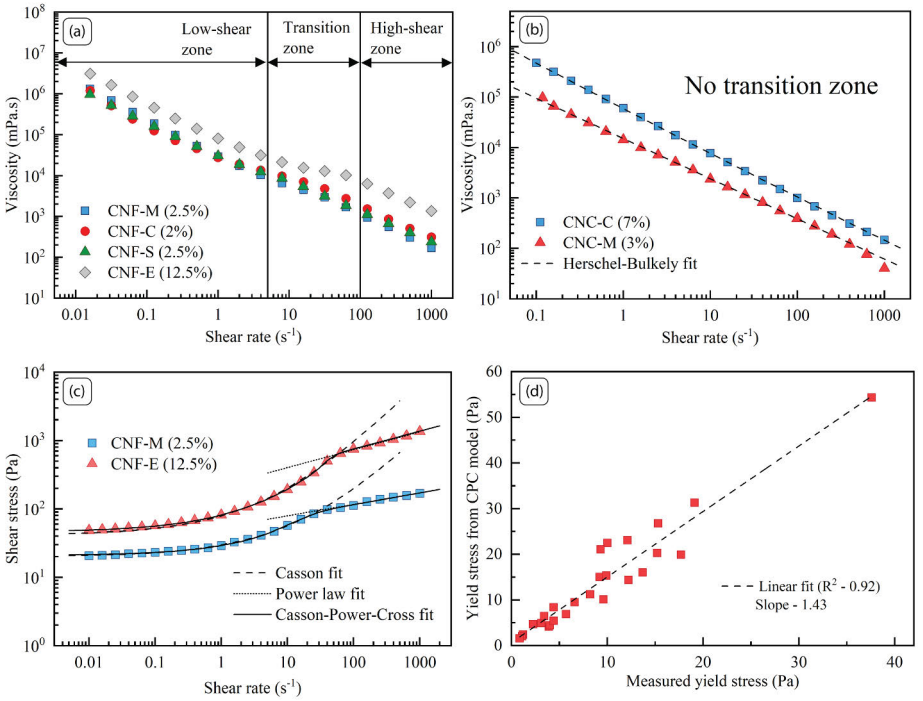

Figure 4.4 (a) Viscosity versus shear rate for CNF suspensions; (b) Viscosity versus shear rate for CNC suspensions with Herschel-Bulkley fit; (c) Shear stress versus shear rate for CNF-M and CNF-E suspensions with Casson, Power-law, and Casson-Power-Cross fits; (d) Yield stress from Casson-Power-Cross model versus yield stress from oscillatory strain sweep measurements for all the CNF suspensions.

Rheological modeling

During a roll-to-roll coating process, nanocellulose suspensions experience rapid changes in shear rates, ranging from rest to as high as $10^5\ s^{-1}$, and back to rest in under a second. Therefore, it is important to understand the rheological behavior of nanocellulose suspensions across this entire shear rate range. Several rheology models have been proposed in the literature to describe the shear-thinning behavior of nanocellulose suspensions and are briefly summarized in chapter 2.3. However, these models have certain shortcomings. For instance, they fit the viscosity data within a specific shear-rate range or necessitate the evaluation of additional parameters such as, volume fraction and aspect ratio of the fibrils, which can be difficult to determine accurately.

For example, the Casson model (Equation 4.2),[166] which is often used to describe the behavior of yield stress suspensions fits the shear stress/shear rate curve of CNF suspensions only at low shear rates and deviates considerably beyond the transition zone (Figure 4.4c). At low shear rates, the flow is also influenced to an extent by the dynamic yield stress resulting from fibril flocculation and entanglement, which is not entirely mitigated by the applied shear forces. Conversely, at high shear rates, the fibrils move unrestrictedly, and the flow resistance is primarily governed by hydrodynamic forces. A power-law model (Equation 4.3)[166] fits the shear stress data at higher shear rates, but deviates at shear rates preceding the transition zone (Figure 4.4c).

The Cross model (Equation 4.4)[191] is an interesting viscosity model that explains the behavior of suspensions characterized by two distinct Newtonian viscosities [zero-shear viscosity (η_o) and infinite shear viscosity (η_∞)], separated by a power-law region that describes the transition from low to high-shear zones. By substituting shear stress, Casson, and power-law equations for η, η_o, and η_∞ in the Cross-model equation, a novel Casson-Power-Cross model emerges (Equation 4.5). In this model, the parameter λ, has the unit of time, and its inverse gives the inflection shear rate at which the transition from Casson to power-law behavior occurs, i.e., shear rate at the 'kink'.

$$\text{Casson model} : \sqrt{\tau} = \sqrt{\tau_y} + \sqrt{\eta_p \dot{\gamma}} \tag{4.2}$$

$$\text{Power-law model} : \tau = k\dot{\gamma}^n \tag{4.3}$$

$$\text{Cross model} : \eta = \frac{\eta_o - \eta_\infty}{1 + (\lambda\dot{\gamma})^m} + \eta_\infty \tag{4.4}$$

$$\text{Casson-Power-Cross model} : \tau = \frac{(\sqrt{\tau_y} + \sqrt{\eta_p\dot{\gamma}})^2 - k\dot{\gamma}^n}{1 + (\lambda\dot{\gamma})^m} + k\dot{\gamma}^n \tag{4.5}$$

τ, τ_y, η_p, k, n, λ, m, and $\dot{\gamma}$ are shear stress, yield stress, plastic viscosity (Casson constant), consistency index, power-law index, relaxation time, cross exponent, and shear rate respectively.

The proposed Casson-Power-Cross model fits the shear stress data with high R^2 values of approximately 0.999 across the entire shear rate range for CNF-E and CNF-M suspensions (Figure 4.4c). The model also agrees with the shear stress data for all the CNF suspensions used in this work that span across a wide range of solid contents. Additionally, the model exhibits a strong fit for suspensions containing CMC and NaPA dispersants, across various levels of addition and consistencies. A table with Casson-Power-Cross fit parameters for CNFs used in this work is available in Papers III and VI.

In the high-shear zone, power-law indices ranging from 0.18 to 0.39 were observed for pure CNF suspensions, accompanied by corresponding inflection shear rates spanning from 10 to 58 s^{-1}. The relationship between yield stress values, as determined through Casson-Power-Cross fits and oscillatory amplitude sweep measurements, is depicted in Figure 4.4d. The slope of this fit is 1.43 with a reasonable R^2 value of 0.92. These results highlight the close agreement between the model-derived parameters and the actual measured values. The model's accuracy can be further improved by refining rotational test parameters. This involves extending measurement time durations, employing stress-controlled measurements at low-shear rates, and incorporating roughened geometries to mitigate potential wall slip effects and averting the development of water-rich boundary layers.

This Casson-Power-Cross model can be a useful tool for computational fluid dynamics for the design and optimization of novel coating applicators tailored for nanocellulosic materials. Additionally, this model enables the extraction of vital characteristic parameters (yield stress, transition shear rate, and power-law index at high shear rates) from a single flow curve. An in-depth understanding on the correlation between CNFs' physical properties and

variables from Casson-Power-Cross model requires additional suspension characterization and significant time resources, and therefore, goes beyond the scope of this work.

Since CNC suspensions do not have the transition zone, a yield stress-based power-law model such as Herschel-Bulkley (Equation 4.6) fits the data very well (Figure 4.4b). Herschel-Bulkley fit parameters for CNC suspensions are given in the Paper VI.

$$\text{Herschel-Bulkley model} : \tau = \tau_y + k\dot{\gamma}^n \tag{4.6}$$

High-shear pipe and slot rheometry

In conventional rheometers measurements are typically limited to shear rates up to 1000 s^{-1} due to viscous heating, air entrapment, and material expelling out from the geometries at high shear rates. However, shear rates in high-speed coating processes far exceed this limit, reaching up to 10^5 s^{-1}. Therefore, rheology of CNF-M (3%) and CNF-E (7.5, 10, and 12.5%) suspensions was further measured using custom-built pipe and slot viscometers, where high shear rates are possible. The choice of slot rheology was driven by its suitability as a coating applicator. Figures 4.5 and 4.6 show the combined rotational, pipe (r = 2 mm), and slot (h = 500 and 750 μm) viscosity data for CNF-M (3%) and CNF-E (7.5%, 12.5%) suspensions. These results are accompanied by Casson-Power-Cross fit curves spanning shear rates from 10^{-2} to 10^6 s^{-1} (similar curves for other CNF-E suspensions can be found in Paper III).

Beyond the transition zone, the pipe and slot data aligned with the rotational data up to 1000 s^{-1}. Subsequently, the alignment shifted to the Casson-Power-Cross-fit curve, maintaining accuracy up to 10^5 s^{-1}, where the viscosity approaches that of water and therefore starts to level out. For CNF-M (3%), peak shear rates of 160 000 s^{-1} and 25 000 s^{-1} were attained in the slot (750 μm) and pipe (r = 2 mm), respectively. Similarly, for CNF-E (7.5%), peak shear rates reached 240 000 s^{-1} and 37 000 s^{-1} in the slot (500 μm) and pipe (r = 2 mm), respectively. Moreover, at shear rates above 10^5 s^{-1}, the Reynolds number approaches 2000, and the flow starts to transition from laminar to turbulent, rendering the equations used to calculate the shear stress/shear rates in the pipe and slot invalid. Nevertheless, shear rates of less than 10^6 s^{-1} are sufficient for most practical applications.

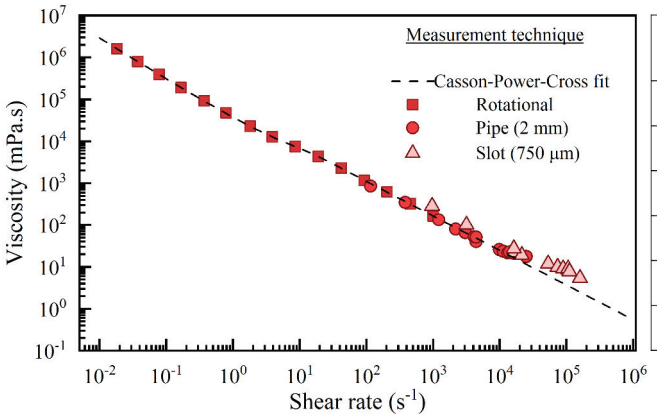

Fitted parameters from CPC model	
τ_y (Pa)	28.3
η_p (Pa)	0.7
k (Pa.s^n)	50.1
n	0.17
λ (s)	0.09
m	2.33

Figure 4.5 Viscosity versus shear rate for CNF-M (3%) from rotational, pipe, and slot rheology measurements, and from Casson-Power-Cross model.

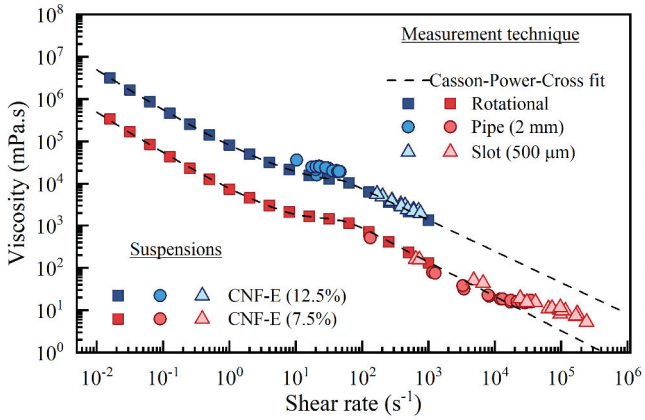

Fitted parameters from CPC model		
	CNF-E (12.5%)	CNF-E (7.5%)
τ_y (Pa)	45.9	4.6
η_p (Pa)	5.1	0.4
k (Pa.s^n)	227.4	37
n	0.26	0.19
λ (s)	0.02	0.02
m	4.86	2.43

Figure 4.6 Viscosity versus shear rate for CNF-E (7.5% and 12.5%) suspensions from rotational, pipe, and slot rheology measurements, and from Casson-Power-Cross model.

Below the transition zone, there is a slight deviation of the pipe and slot viscosity data from the rotational data, especially for CNF-E (12.5%). One reason for this deviation is that, shear-rate calculations for the pipe and slot (Equations 3.2 and 3.4) relied on the power-law index evaluated from Equation 4.5, which is applicable for the data after the inflection point.

Despite the noted disparities, the primary focus of pipe and slot rheometry was the study of flow behavior at high shear rates, alongside the slot-die's suitability as a coating applicator. An essential observation is the extended

applicability of the Casson-Power-Cross model in describing the behavior CNF suspensions (along with different dispersant types and addition levels) across a wider shear-rate range compared to traditional models. Furthermore, the empirical viscosity values obtained from rotational, pipe, and slot rheometers closely conformed to the model within their respective shear-rate ranges.

Coating windows

The advantage of using a slot-die as a coating applicator is that it is possible to achieve high shear rates in the narrow slot-gap. This in turn reduces the apparent viscosity of nanocellulose suspensions by several orders of magnitude and makes it possible to coat an otherwise high viscosity suspension. For a nanocellulose suspension, a specific viscosity threshold exists for each solid content and dispersant loading, below which, the suspension is adequately fluidized, leading to uniform coating quality. By identifying this critical viscosity level, one can utilize Equations 4.5 (or 4.6 for CNCs) and 3.4 to determine the necessary minimum flow rate through the slot-die. This will then establish a baseline minimum line speed for each desired coat weight, assuming no metering at the slot exit.

If one assumes that an effective viscosity of at least 1000 $mPa.s$ is required for achieving good quality nanocellulose coating, it becomes feasible to compute the minimum line speed required for various coat weights. Additionally, the maximum line speed for each coat weight is dictated by the coater's drying capacity. Figure 4.7 illustrates instances of these minimum and maximum line speeds, representing coating windows for CNF-M (2.5%) and CNF-E (12.5%) suspensions. Comparable coating windows can be graphed for different nanocellulose suspensions, provided the parameters within Equation 4.5 (or 4.6) are known. This could be a valuable tool for researchers and machine operators alike, particularly when coating nanocellulose suspensions on a pilot or industrial scale.

Influence of CNF to water ratio on viscosity

As mentioned multiple times in this section, the high viscosity of nanocellulose stems from the mechanical interlocking of high aspect ratio fibers and the formation of inter-fibril hydrogen bonds. The influence of these factors becomes more pronounced with increasing solid content, as higher number of fibers are interacting with each other, leading to intensified crowding. Conversely, a reduction in solid content results in decreased crowding, allowing

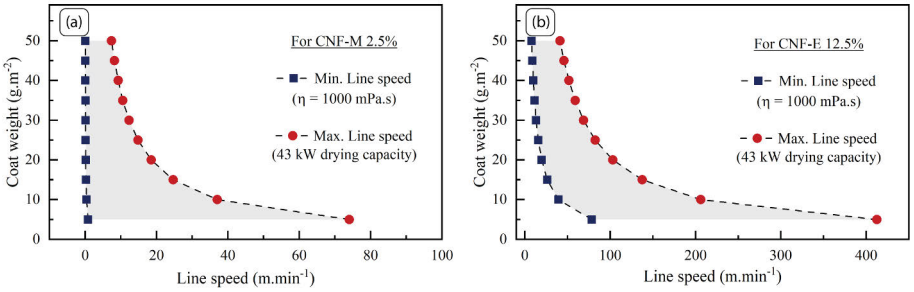

Figure 4.7 Slot-die coating windows for (a) CNF-M (2.5%), and (b) CNF-E (12.5%) suspensions. Assuming an effective viscosity of at least 1000 $mPa.s$, maximum drying capacity of 43 kW (90% drying efficiency), coating width of 100 mm, and slot-gap of 500 μm.

water molecules to participate in hydrogen bonding, thereby weakening the inter-fibril bonds and subsequently leading to a decrease in viscosity. Hence, the viscosity of nanocellulose suspensions highly depends upon the nanocellulose-to-water ratio.

This crucial aspect should be borne in mind particularly when incorporating additives. For instance, when kaolin is added to CNF-M while maintaining a constant total suspension solid content of 2.5%, the CNF-water ratio diminishes from 2.4% to 1.5% with increasing kaolin ratio from zero to 40%, leading to a lowered viscosity compared to the original suspension (Figure 4.8a). Conversely, by keeping the CNF-water ratio constant at 2.4%, an increase in kaolin percentage from 0 to 40% increases the total suspension solid content from 2.5% to 4%, while maintaining a constant viscosity for all suspensions (Figure 4.8b). Hence, cautious consideration is warranted when evaluating scenarios involving high additive levels. A similar trend was observed with CNC suspensions using 20% sorbitol. Refer to Paper II for details on the viscosity curves for varying CNC-water ratios.

4.2.3 Thixotropy

Thixotropy can be defined as the property where the initial structural strength of a suspension decreases during a high shear process, and then regenerates its structure upon removal of shear stress.[166] This phenomenon is particularly evident in CNF suspensions due to reversible non-covalent interactions between fibrils, and the elastic recovery is further aided by the highly branched and physically entangled fibril structure, even after significant deformations. As the

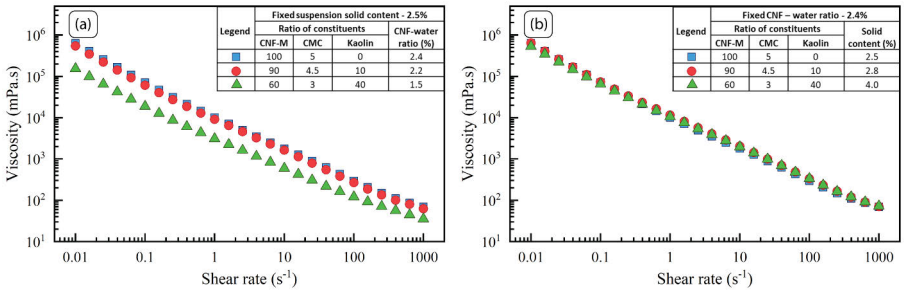

Figure 4.8 Viscosity versus shear rates for CNF-M + kaolin suspensions, (a) fixed suspension solids content of 2.5% with varying CNF-kaolin and CNF-water ratios; (b) fixed CNF-water ratio of 2.4% with varying CNF-kaolin ratio and suspension solid contents.

CNF suspension exits the slot-die and shear forces are completely removed, it then starts to regain its original structure and viscosity. A short recovery time leads to a sudden, significant increase in the viscosity and yield stress of the wet coated layer. Consequently, the wet layer struggles to reorganize into a densely packed microstructure, resulting in a poorly formed dry layer.

Figure 4.9a shows the normalized elastic modulus during rest and recovery intervals from a 3-interval oscillatory thixotropy test for CNF-E (12.5%) with 5% CMC or NaPA dispersants. The figure shows that the pure CNF-E suspension swiftly recovers its elastic modulus compared to that with CMC or NaPA, with CMC requiring the longest recovery period. Post the high-shear interval, charged dispersants adhering to CNF fibers hinder the structure regeneration due to electro-steric effects. This hindrance is more pronounced for CMC, attributed to its longer molecule chains. Figure 4.9b shows the time taken for the recovery interval's elastic modulus to reach 50% of the rest interval's steady-state value for CNF-M, -S, and -E suspensions with or without dispersants. In all cases, CMC addition substantially prolongs the recovery time by up to 5-fold, and therefore could positively affect the coating quality.

Additionally, Figure 4.9b presents the viscosity recovery time for CNC-M suspension from a 3-interval rotational thixotropic test. For CNC-M, the extended recovery time is possibly due to repulsion from highly charged cellulose crystals. Moreover, the stiff and short nature of CNCs lacks the same mechanical interlocking effect found in CNFs, resulting in a slower recovery. In addition, sorbitol being a small non-ionic molecule, does not contribute much to thixotropic effects for CNCs.

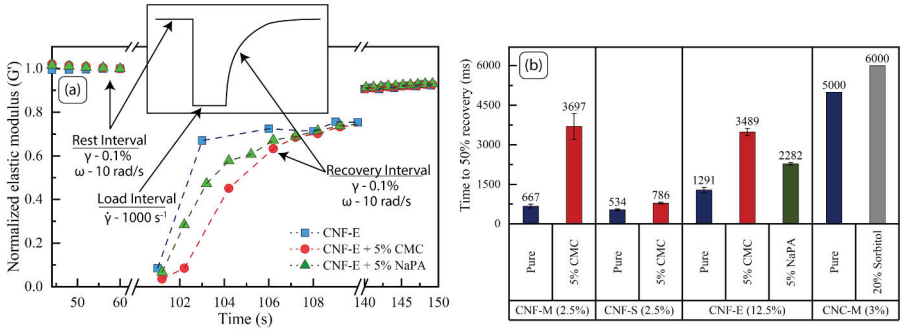

Figure 4.9 (a) Normalized elastic modulus versus time for rest and recovery intervals from a 3-interval thixotropy test (oscillatory-rotational-oscillatory) for CNF-E with 5% CMC and NaPA addition (insert shows a depiction of viscosity/complex-viscosity vs. time curve for this type of test); (b) Time taken for elastic modulus to recover to 50% of rest interval's steady state value for CNF-M, CNF-S, CNF-E, and CNC-M with/without dispersant addition.
Note: For CNC-M, the recovery was calculated for viscosity from a 3-interval rotational-rotational-rotational test.

4.3 Water retention and ζ-potential

Gravimetric water retention describes a suspension's ability to resist dewatering. A suspension with high water retention (low dewatering rate) grants the wet coated layer ample time to rearrange itself into a uniform and densely packed structure. However, this also slows down the drying process, resulting in reduced coating speeds. Conversely, low water retention (high dewatering rate) prompts rapid water release into the base substrate, quickly immobilizing the wet coated layer. This can lead to unevenness and defects in the coated layer. Furthermore, faster water release reduces the wet strength of the base paper leading to runnability issues such as web breaks at high speeds. Hence, an optimal water retention level is needed to achieve desired coating quality without compromising much on coating speeds.

Figure 4.10a shows the ÅAGWR values for CNF-M, -S, and –E suspensions both with and without dispersants. Nanocellulose suspensions generally exhibit water retention an order of magnitude higher than their precursor pulps, yet still an order of magnitude lower than traditional paper coating colors.[169,200] CMC, having cellulose as its backbone, has higher affinity to water, and therefore, increases the water phase viscosity of CNF suspensions. Consequently, this increases the water retention (lower ÅAGWR) for all CNF suspensions. Conversely, the addition of NaPA to CNF-E reduces the water retention (higher ÅAGWR). Despite NaPA's affinity to water, its

impact on water phase viscosity is lesser than that of CMC due to its lower molecular weight. Moreover, as discussed in the yield stress subsection above, a possible excessive NaPA addition might be forming strong and small CNF flocs, potentially weakening the hydrogen-bond network between CNF and water molecules, resulting in lower water retention.

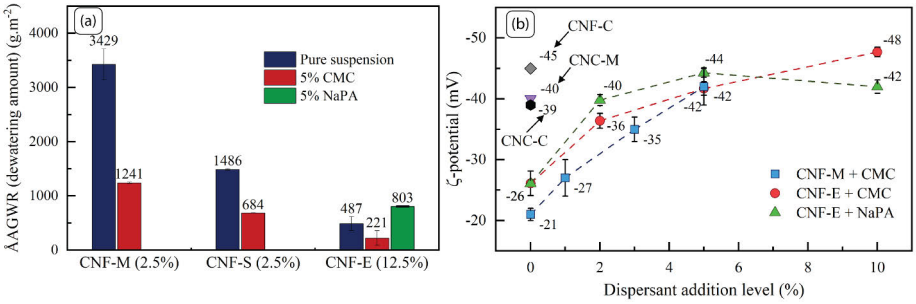

Figure 4.10 (a) ÅAGWR (water retention) for CNF-M, CNF-S, and CNF-E with/without dispersants; (b) ζ-potential for different nanocellulose suspensions.

Zeta potential is typically an indicator of a suspension's colloidal stability. A low zeta potential (absolute value) indicates poor suspension stability, often resulting in the flocculation of cellulose fibrils. Figure 4.10b shows the zeta potential for various nanocellulose grades used in this work along with CMC and NaPA dispersants for CNF-M and -E. Pure mechanical defibrillation and enzymatic pre-treatments do not introduce charged groups to cellulose fibers, resulting in a low zeta potential for CNF-M and CNF-E. In contrast, chemical pre-treatments or acid hydrolysis impart charged groups onto the cellulose fibers for CNF-C and CNC suspensions, respectively, which result in higher zeta potential. CMC and NaPA contain negatively charged groups; therefore adding them to CNFs increases the zeta potential, which in turn contributes to improved colloidal stability for these suspensions.

Overall, the addition of CMC had a positive impact on the coating quality for all CNF grades. This improvement can be attributed to a combination of factors such as, higher zeta potential, lower yield stress, higher water retention, and slower thixotropic recovery. Without CMC addition, the coating quality of CNFs was poor and the barrier properties were non-existent. Therefore, 5% CMC addition was set as standard for all CNF coatings in this work.

4.4 Substrate role in nanocellulose coatings

The selection of the substrate plays a vital role in ensuring high coating quality for nanocellulose suspensions. A hydrophilic surface is essential for uniform wetting and spreading of the wet coated layer. Given the substantial water content in nanocellulose suspensions, a porous structure is advantageous for efficient drying, particularly from the paper's reverse side. Additionally, the paper's wet strength is critical as it absorbs a significant portion of water from the nanocellulose coating upon application. This strength is vital for guiding the paper substrate through the entire coating line as the wet coating undergoes drying. Furthermore, a smooth surface requires less coated material to fill in the surface volume, enabling the attainment of desired barrier properties with minimal coat weights. Therefore, in Papers I and II, the role of substrate in nanocellulose coatings is looked into in more detail.

In Paper I, the role of substrate in coating CNF-M was investigated using linerboard and paperboard. The paperboard was further coated with various primers (see Table 3.1) to alter substrate properties such as surface roughness, water contact angle, air permeability, and Cobb. Table 4.1 lists the substrate properties for linerboard, paperboard, and different primer-coated paperboards. Linerboard's hydrophilic nature aids in spreading the nanocellulose coating, while its high air permeability and Cobb enhance water absorption and coating drying efficiency. Air permeability of CNF-coated linerboard is below the instrument's detection limit. This usually indicates a full coverage of CNF on the surface, because of CNF's ability to form a densely packed layer upon drying. However, a high surface roughness indicates that high amount of CNF is needed in order to achieve any useful barrier properties.

Paperboard has a hydrophobic surface that is attributed to surface sizing treatments in commercial grades. With the exception of latex, the primers effectively reduced the water contact angle of the paperboard, promoting better spreading of the CNF suspension. Cobb values for primer-coated paperboards remained relatively stable due to low primer coat weights, with bulk structure of paperboard primarily controlling the water absorption. Pigment primer coatings showed the greatest decrease in surface roughness by up to 40%, with potential for further reduction through calendering. Compared to HC-60, HC-90 has lower surface roughness due to its smaller particle size. This smoother surface will result in a uniform CNF-layer, as is

evident from the low air permeability, which is below the instrument's detection limit.

CMC primer coating also achieved low air permeability after CNF coating. This can be attributed to CMC's low water contact angle enabling easy spreading of wet CNF-layer. Moreover, the high molecular weight of CMC might have closed the surface of paperboard (as indicated by air permeability before CNF coating) thereby improving the holdout of CNF-layer. CNF-T primer in theory should behave similar to CMC, but the low coat weight of CNF-T might be limiting its performance. Latex, owing to its hydrophobicity might cause poor wettability, potentially resulting in pinholes or cracks in the dry CNF-layer. More details on the substrate role can be found Paper I. Based on these findings, the pigment-coated paperboard emerged as the ideal substrate for coating nanocellulose suspensions. Therefore, a pigment-coated paperboard (baseboard) was adopted as the main substrate for all subsequent coatings in this work.

Table 4.1 Substrate properties of linerboard, paperboard, and primer-coated-paperboards.

Substrate/ Primer	Coat weight ($g.m^{-2}$)	Cobb-60 ($g.m^{-2}$)	PPS roughness (μm)	Contact angle (at 1 s)	Air permeability ($\mu m.Pa^{-1}.s^{-1}$) [Before/after CNF coating[1]]
Linerboard	–	255	7.5	80°	1.8/Below detection limit
Paperboard	–	24	6.2	115°	2.1/0.018
HC-60	30	25	4.8	81°	0.16/Below detection limit
HC-90	30	32	3.5	79°	0.14/Below detection limit
CMC	2-3	24	7.1	51°	0.006/Below detection limit
CNF-T	1	27	7.5	51°	1.8/0.005
Latex	1	27	7.5	103°	2.8/0.015
PVOH	1	25	7.7	77°	1.2/0.005

[1]CNF-M was coated on these substrates using the slot-die process and approximate coat weight is 5-6 $g.m^{-2}$.

Most commercial baseboards have surface treatments to improve printing characteristics, but this can negatively affect adhesion to nanocelluloses. In Paper II, the pigment-coated paperboard (baseboard) was further coated with different primers (see Table 3.3) to improve the adhesion. Table 4.2 lists the substrate properties for different primer-coated baseboards. The baseboard has a surface roughness, air permeability, and water contact angle of 1.4 μm, 0.009 $\mu m.Pa^{-1}.s^{-1}$, and 72°, respectively, which already results in full

coverage of CNC layer on its surface. However, the CNC-coating easily peeled off with the tape indicating poor adhesion to the substrate.

All the primer coatings reduced the contact angle for the baseboard, further improving the wettability of the CNC-layer. The slight increase in air permeability is attributed to baseboard's fiber swelling during the primer coating step. This increase in air permeability can be beneficial in drying the nanocellulose coatings. Both CMC and cationic starch primers improved adhesion between the baseboard and the CNC-layer, with the latter showing higher adhesion performance. Both CMC and starch are natural carbohydrates that show high affinity to nanocellulose. Moreover, the positive charge of cationic starch might have further contributed to improved adhesion with negatively charged CNCs. Although PolyDADMAC and $CaCO_3$ were positively charged, they did not show much improvement in adhesion compared with just the baseboard. This shows that charge itself is not the only factor that influences the adhesion of nanocelluloses, but it is a combination of several factors ranging from surface functional groups, surface energy, porosity, and roughness.

To quantify adhesion, peel forces were measured for nanocellulose-coated baseboards with cationic starch primer coating. Peak peel forces were 10, 7, and 8 N for CNF-M, CNF-C, and CNC-M coated paperboards, respectively. These are not far off from the peak peel force of 12N for uncoated baseboard. Based on these findings, cationic starch primer coating was used for subsequent nanocellulose coatings in this study.

Table 4.2 Substrate properties of primer-coated-baseboards

Substrate/ Primer	**Coat weight** ($g.m^{-2}$)	**Air permeability** ($\mu m.Pa^{-1}.s^{-1}$)	**Contact angle (at 1 s)**	**Adhesion[1] (0-5)**
Baseboard	–	0.009	72°	1
CMC	2	Below detction limit	32°	4
Cat. $CaCO_3$	20	0.017	20°	2
PolyDADMAC	1	0.024	29°	1
Cat. starch	below 1	0.016	58°	5

[1]Adhesion from tape test for CNC-M coated baseboards.Scale goes from 0 = poor adhesion to 5 = strong adhesion (fiber tear).

4.5 Coating structure

Various grades of nanocelluloses, as listed in Table 3.1, were coated onto the cationic starch pre-coated baseboard. All the coatings were produced in a roll-to-roll process using a slot-die applicator, and Table 3.5 lists the parameters used to produce each of these single-layer nanocellulose coatings. Figure 4.11 shows the SEM cross-sections of the baseboards coated with CNF-M, CNF-C, CNF-E, and CNC-M. It is challenging to visualize cationic starch layer in the cross-sections due to its low coat weight (below 1 $g.m^{-2}$). Nevertheless, the nanocelluloses form uniform layers and show full coverage on the baseboard. The air permeability of all the single-layer nanocellulose coatings is below the instrument's detection limit, which is also an indicator for full coating coverage. This is because of the dense structure of the dry nanocellulose layer impeding the passage of air effectively. The solid contents, dry thicknesses, and coat weights of the nanocellulose coatings varied between 2 - 12.5%, 4 - 16 μm, and 6 - 24 $g.m^{-2}$, respectively. This demonstrates the slot-die's suitability as a coating applicator to handle a wide spectrum of nanocelluloses and solid contents.

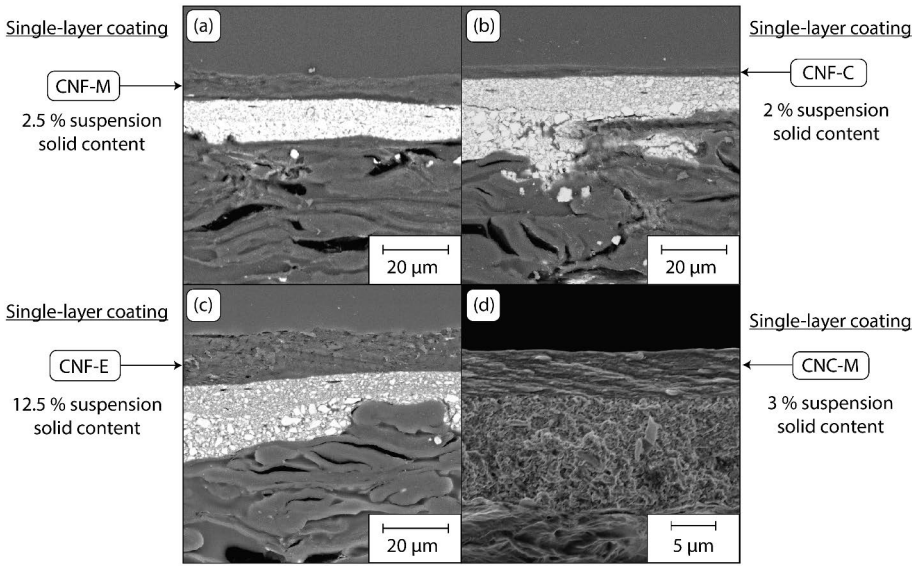

Figure 4.11 SEM cross-sections of the nanocellulose coated samples: (a) CNF-M (3%), (b) CNF-C (2%), (c) CNF-E (12.5%), and (d) CNC-M (3%).

As the inherent moisture sensitivity of the nanocellulose-based coatings negatively affects the barrier properties, a polymer-based top coating was added to provide moisture protection. Moreover, this top coating serves the

dual purpose of providing sealability for the packaging material during converting operations. One of the key drivers to employ nanocellulose for barrier coatings is its biodegradability. Guided by this principle, several biodegradable materials were chosen for the moisture-barrier top coatings. The multilayer paperboard can be made more sustainable if the top coating material is both bio-based and biodegradable. Among the options, PLA [272] (TP2, TP3, and WD2), PBS [273] (TP4), and PHA [274] (WD3) are both bio-based and biodegradable, while PBAT [275] (TP3), although biodegradable, is currently fossil fuel based. While the exact composition of WD1 is undisclosed, it is a commercial pigment containing polymer dispersion with certified compostability. Finally, LDPE, which is both fossil fuel based and non-biodegradable is used as a reference material.

Figures 4.12a, b, and c, show the SEM cross-sections of extrusion coated TP1 (LDPE), TP2 (PLA), and TP3 (ecovio®) on CNF-M, while Figure 4.12d shows the reverse gravure coated WD3 (PHA) on CNF-S. It can be seen that both coating methods form uniform multilayer structures without disturbing the CNF layer beneath. A similar behavior is seen when TP2 (PLA) and WD1 (pigment + latex) are coated with their respective coating methods on CNC-M and CNC-C (Figures 4.12e and f). Cross-section images for remaining multilayer-coated samples can be found in Papers IV, V, and VI.

4.6 Adhesion at CNF-thermoplastic interface

Insufficient adhesion between dissimilar layers is a common challenge in multilayer packaging structures. Figures 4.13a and b clearly show that that there is poor adhesion at CNF/TP4 interface, with visible delamination noticeable between thermoplastic layer and CNF-coated board. This is more pronounced in the case of CNF-C (Figure 4.13b), where the TP4 layer has entirely detached from the CNF-C coated board. Even though TP1, TP2, and TP3 (Figures 4.12a, b, and c) may not exhibit visible signs of delamination, the adhesion between CNF-M and the thermoplastics remained sub-optimal (see Figure 4.14a), which may cause serious problems during converting operations, such as creasing, folding, and sealing. This poor adhesion, despite corona pre-treatment could be attributed to the incompatibility between polar and non-polar groups of nanocellulose and thermoplastics, respectively.

The adhesion between such dissimilar materials can be either improved by using tie-layers (functionalized polyolefins, such as maleic anhydride-modified

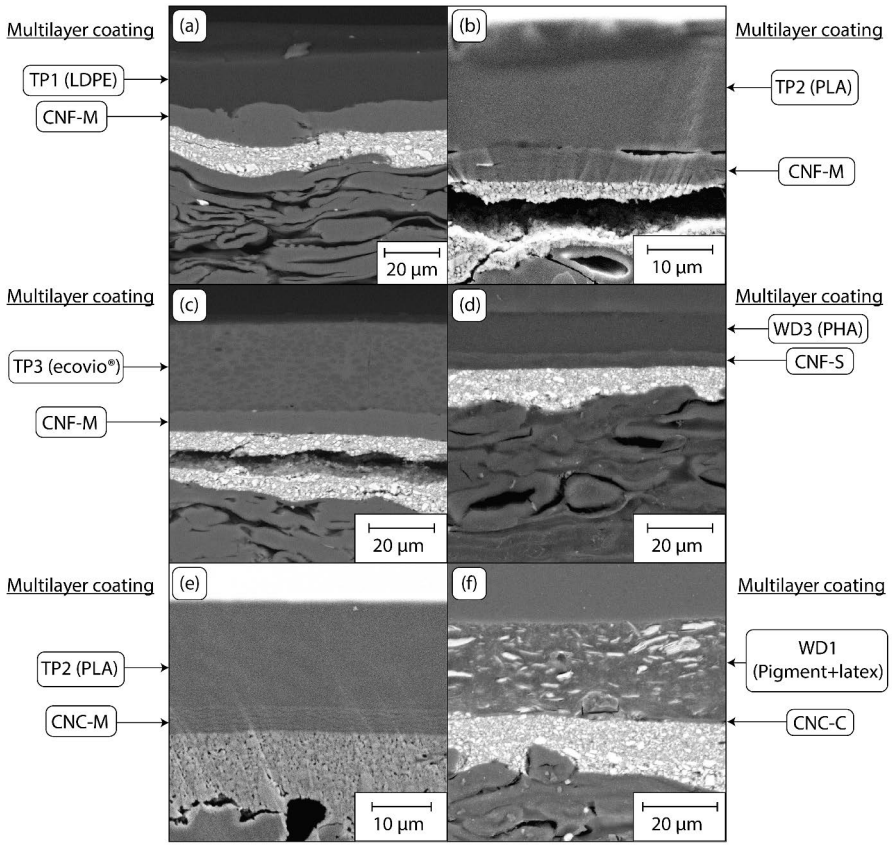

Figure 4.12 SEM cross-sections of the multilayer samples: (a) CNF-M + TP1 (LDPE), (b) CNF-M + TP2 (PLA), (c) CNF-M + ecovio®, (d) CNF-S + WD3 (PHA-based aqueous dispersion), (e) CNC-M + PLA, and (f) CNC-C + WD1 (pigment and latex based aqueous disperison).

linear-LDPE) or by promoting the mechanical interlocking by e.g., increasing the surface roughness.[7] Kaolin in different ratios was added to CNF-M to understand the effect of pigments on the adhesion with the thermoplastic top coatings. Figures 4.13c and d clearly indicate an improvement in adhesion at the kaolin-blended CNF-M and TP4 interface, compared to CNF-M without kaolin (SEM cross-sections of TP1 and TP3 coatings on kaolin-blended CNF-M are available in Paper V).

A tape test was further used to assess adhesion at the interface between thermoplastic and CNF-M by measuring the peak peel force required to fracture the interface (Figure 4.14a). Comparatively, the peel force decreased considerably when thermoplastics were coated solely onto CNF-M, as opposed to the single-layer thermoplastic coating on the baseboard. As the kaolin

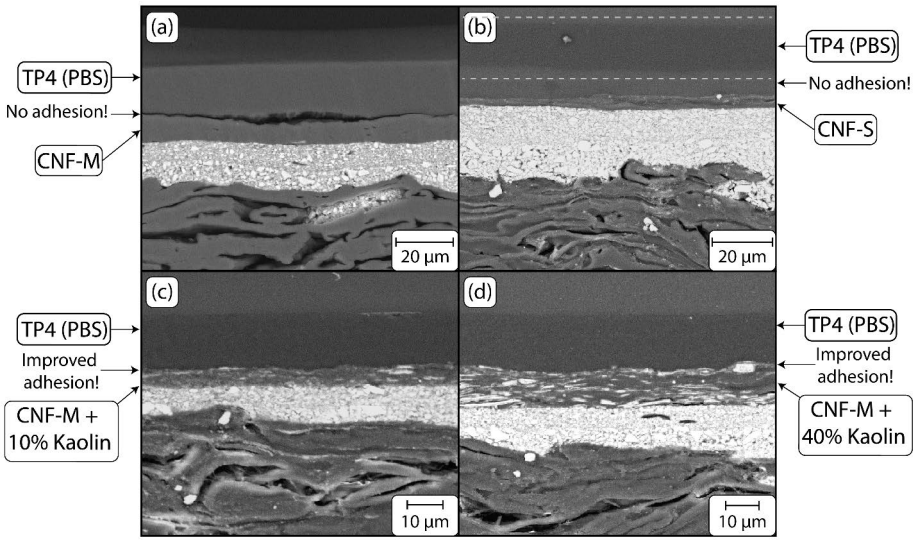

Figure 4.13 SEM cross-sections of the multilayer samples showing the adhesion at CNF-thermoplastic interface: (a) CNF-M + TP4 (PBS), (b) CNF-S + TP4 (PBS) [PBS layer is completely separated - shown between the dashed lines], (c) CNF-M + 10% Kaolin + TP4 (PBS), and (d) CNF-M + 40% Kaolin + TP 4 (PBS).

content in CNF-M increased, adhesion between CNF-M and thermoplastics also improved. Notably, for TP3 and TP4, a 2-fold increase in peak peel force occurred at 40% kaolin content, in comparison to coatings on pure CNF-M.

The alignment factor (k) of kaolin, determined through ATR-FTIR measurements, is shown in Figure 4.14b for CNF-M/kaolin composite films (produced on petri-dishes) and roll-to-roll coated samples. Lower 'k' values indicate greater particle alignment with the surface plane,[268,269] and it is evident that films have higher kaolin pigment alignment compared to R2R coated samples. The film preparation process allows the platy-pigment particles to align more readily due to low initial suspension solid content (ca. 0.5%) and less crowding of CNF fibrils around the pigment particles. Moreover, slow drying conditions during film preparation provides ample time for the platy particles to orient along the surface due to surface tension forces in the contracting layer. In contrast, R2R coating involves higher solids content (ca. 3 - 4%) and faster drying, thus, hindering kaolin pigment alignment and resulting in increased surface roughness of the coated CNF-M layer. This enhances mechanical interlocking with the thermoplastic layer, thereby improving adhesion (see Paper V for SEM surface images of

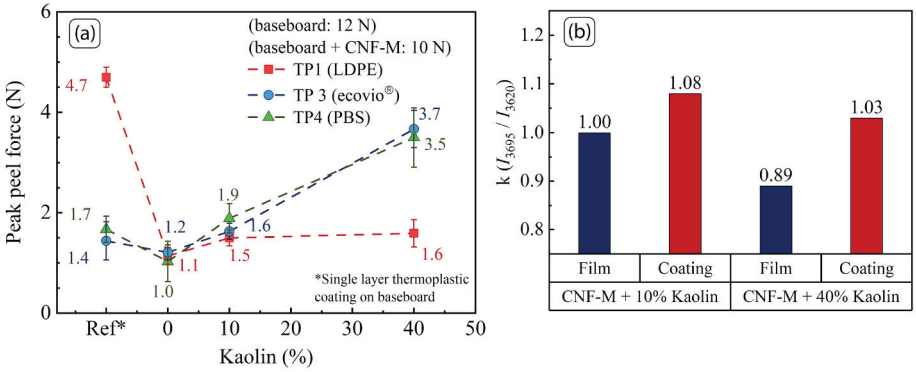

Figure 4.14 (a) Peak peel force for multilayer CNF-M coatings as a function of kaolin addition level; (b) Kaolin alignment factor ($k = I_{3965}/I_{3620}$) for films and roll-to-roll coated samples.

CNF-M/kaolin coated baseboards). It is important to note that blending pigments into CNF might disrupt the densely packed microstructure of the nanocellulose layer, potentially leading to reduced barrier performance, as will be discussed in the subsequent sections.

When water-based dispersions were applied onto CNFs, better adhesion was observed when compared to multilayer extrusion coated samples. This could potentially be attributed to water in the dispersions swelling the CNF layer, thereby increasing surface roughness and promoting adhesion. Additionally, the smaller particle size of the dispersion polymers likely facilitated better filling of surface roughness gaps, thereby augmenting mechanical interlocking of the dispersion-coated top layer.

4.7 Barrier properties

4.7.1 Water vapor barrier

A crucial property for barrier food packaging is the ability to resist water vapor transmission. If moisture infiltrates the packaging, it can dampen dry foods like coffee, crisps, and baby food, leading to both sogginess and potential spoilage. Conversely, moist food items face the opposite issue, where moisture loss can render the product unappetizing. Figure 4.15 shows the water vapor permeance (WVP) for single-layer nanocellulose and moisture barrier coatings on baseboards at two conditions, 23 $°C$ / 50% RH and 38 $°C$ / 90% RH. As

anticipated, the nanocellulose-coated baseboards do not show any improvement in water vapor resistance, with WVP levels akin to uncoated baseboard. At higher humidity, the nanocellulose-coated samples actually display elevated WVP compared to the baseboard. This is due to the hygroscopic nature of the cellulose fibers, whose water absorption rate increases with temperature and relative humidity.

In contrast, thermoplastic and water-based dispersion coated samples demonstrate a substantial reduction of over 70% in WVP compared to the baseboard, with LDPE (TP1) showing the highest reduction in WVP of 90% at both the test conditions. It is important to note that many biodegradable polymers are susceptible to hydrolysis, especially at elevated temperatures and humid conditions,[276] resulting in higher WVP values compared to LDPE. For multilayer-coated samples, the WVP follows that of the top-coated moisture barrier layer, underscoring the positive impact of the top coating on maintaining the overall water vapor resistance of the multilayer structure.

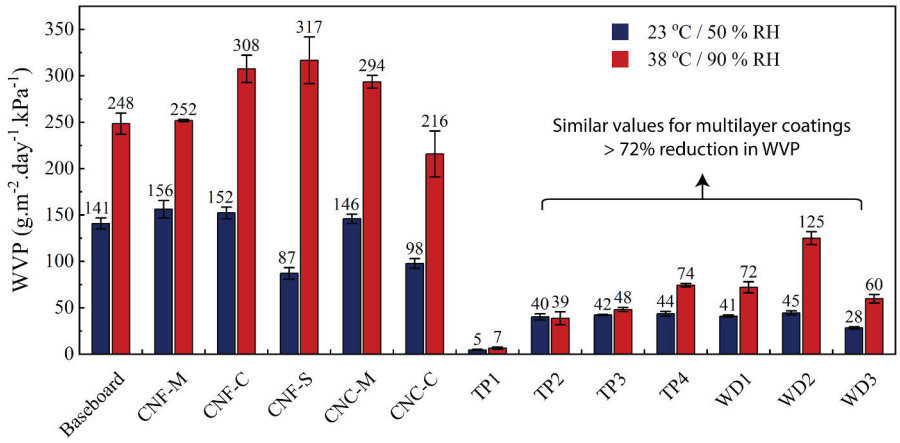

Figure 4.15 Water vapor permeance (WVP) for different single-layer roll-to-roll coated samples at 23 $^{\circ}C$ / 50% RH and 38 $^{\circ}C$ / 90% RH.

4.7.2 Oxygen barrier

Films versus R2R-coated samples

Oxygen is a very small molecule that can permeate even the tiniest gaps in coating structures and diffuse through most polymer-based moisture barrier materials. Therefore, achieving an effective oxygen barrier is a major challenge for bio-based materials. Nanocellulose films exhibit remarkable oxygen barrier

properties that are comparable to established materials like, PVDC, EVOH, and metallized PET, that are commonly used in high-barrier packaging applications (see Figure 2.5).

Figure 4.16a shows the oxygen permeance (OP) values for CNF films and single and multilayer CNF-coated boards at 23 $°C$ / 50% RH. Similarly, Figure 4.16b shows the OP for CNC-based coatings at the same test conditions. The OP of CNF films is normalized to the same thickness as that of the corresponding R2R coated samples, and is approximately 10 $cc.m^{-2}.day^{-1}.bar^{-1}$. This is in line with the OP values reported in the literature.[27,33,83,220] CNC films were too brittle to handle, therefore, the OP of the CNC-films could not be measured. Surprisingly, the R2R-coated single layer nanocellulose boards show poor barrier against oxygen, with OP values approximately two orders of magnitude higher than those of equivalent films. Furthermore, the OP values for these coated boards vary significantly, ranging from 200 to 6000 $cc.m^{-2}.day^{-1}.bar^{-1}$. This can be attributed to the rapid drying during R2R process, where the wet nanocellulose layer dries within a short time frame (less than 2 minutes) under harsh conditions where the temperature in the dryers could reach up to 200 $°C$. Consequently, cracks and pinholes form in the dry nanocellulose layer that compromise the oxygen barrier. In contrast, the slow drying and gentle self-assembly conditions in the film production results in a uniform and dense nanocellulose network that is essential for effective oxygen barrier properties.

Despite their barrier against water vapor, both extrusion and dispersion-coated boards show poor oxygen barrier, with OP ranging from 334 to 9428 $cc.m^{-2}.day^{-1}.bar^{-1}$ (Figure 4.16c). This is because of the non-polar nature of both oxygen and moisture-barrier polymers, which allows oxygen to easily diffuse through these materials.[53] Interestingly, applying these moisture-barrier materials onto the nanocellulose-coated boards seems to restore original OP values seen in the corresponding nanocellulose films (Figures 4.16a and b). Both extrusion and reverse-gravure coating methods have this effect, with the lowest OP of 2 $cc.m^{-2}.day^{-1}.bar^{-1}$ achieved for CNF-S + WD3 (PHA-based dispersion).

This improvement in OP for the multilayer-coated boards might be attributed to the moisture barrier material effectively filling in or sealing any pre-existing cracks or pinholes within the nanocellulose layer. If the effective area of these defects is small, just sealing them can be sufficient to restore the oxygen barrier. In addition, during reverse-gravure coating, the water from the dispersion might be having a plasticizing effect on the underlying

nanocellulose layer, effectively sealing the defects within the layer. Based on the observations above, it can be said that the integration of nanocellulose and moisture barrier materials in multilayer coatings results in a packaging structure with similar (or in some cases higher) oxygen barrier as pure nanocellulose films, while also having a high water vapor barrier.

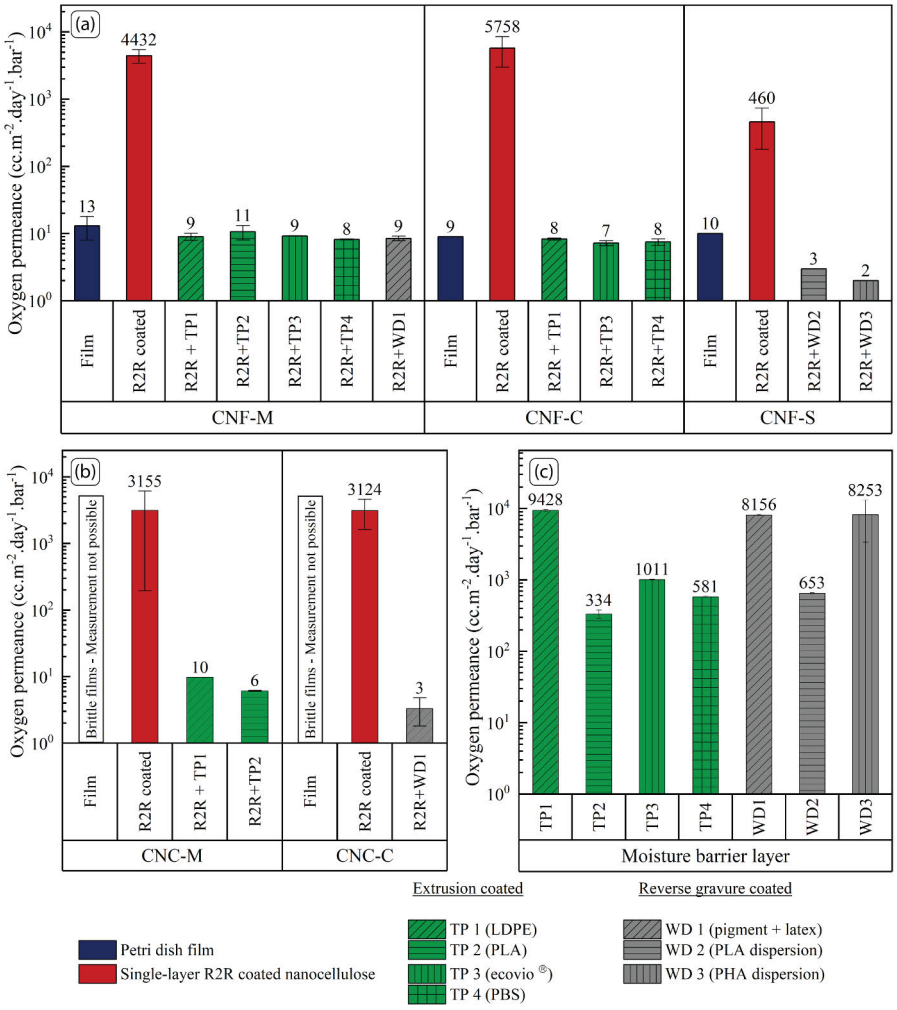

Figure 4.16 Oxygen permeance of nanocellulose films and single/multilayer roll-to-roll coated baseboards at 23 $°C$ / 50% RH for, (a) CNFs, (b) CNCs, and (c) single layer moisture barrier coatings.

Influence of pigments and plasticizers on oxygen barrier

In the preceding section, it was discussed that adding kaolin into CNF-M resulted in improved adhesion with the thermoplastic top layer. However, this might compromise the barrier properties due to potential interference from pigment particles with the densely packed nanocellulose microstructure. Figure 4.17a illustrates the OP for CNF-M containing multilayer boards with varying kaolin ratios. As anticipated, OP of these boards raises with increasing kaolin ratio. Notably, at 40% kaolin ratio, the OP is 1-2 orders of magnitude higher than that of pure CNF-M. However, at 10% addition level, there is only a minor increase in OP compared to the original value. This suggests that low addition levels could be suitable for applications with moderate oxygen barrier needs, as long as sufficient adhesion with the thermoplastic top layer is maintained. Therefore, by optimizing the pigment addition level, the multilayer architecture can be tailored to attain desired oxygen barrier and inter-layer adhesion, while reducing the amount of pricier nanocellulose. Furthermore, for demanding high-oxygen barrier applications, an option is to apply a separate thin layer of kaolin (or pigment) atop the nanocellulose coating to aid in the adhesion with the thermoplastic upper layer.

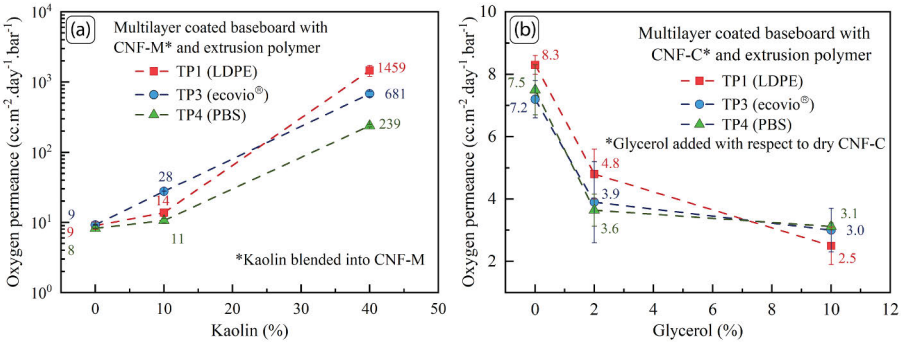

Figure 4.17 (a) Influence of kaolin addition on oxygen permeance of multilayer coatings with CNF-M at 23 $^{\circ}C$ / 50% RH; (b) Influence of glycerol addition on oxygen permeance of multi-layer coatings with CNF-C at 23 $^{\circ}C$ / 50% RH.

Plasticizers like glycerol play a crucial role in improving the flexibility of nanocellulose films. For instance, the addition of 2% and 10% glycerol increases the strain at break for 20 μm thick CNF-C films from 2.1% to 5.4% and 14.8%, respectively (refer to Paper V for more details on the influence of CMC, PVOH, and glycerol plasticizers on the mechanical properties of CNF-C films). This improved flexibility could reduce the likelihood of crack formation

in the nanocellulose layer during R2R coating. Figure 4.17b shows the OP of CNF-C containing multilayer boards with varying glycerol addition levels. The introduction of glycerol leads to a reduction in OP for CNF-C multilayer boards from ca. 7.5 $cc.m^{-2}.day^{-1}.bar^{-1}$ to a minimum value of 2.5 $cc.m^{-2}.day^{-1}.bar^{-1}$ at 10% glycerol addition. Surprisingly, this value aligns closely with the OP of pure CNF-C film with the same thickness at 0% RH (The OP of a 5 μm CNF film at 0% RH is 3.1 $cc.m^{-2}.day^{-1}.bar^{-1}$). Barrier packaging paper or paperboard is commonly shaped into various end-use product forms through creasing or folding. Therefore, beyond the flat samples, plasticizers could also offer an advantage in preserving the barrier properties of nanocellulose-based packaging during such converting operations.

Influence of temperature and humidity on oxygen barrier

As the humidity increases, cellulose fibers absorb moisture from the air and swell, loosening the dense microstructure formed by nanocellulose. Consequently, the barrier performance of nanocellulose coatings diminishes as the humidity raises, and this effect is further expedited by higher temperatures (or vapor pressure). Figure 4.18 shows the OP of CNF-M + LDPE coated boards at three different test conditions, 23 $°C$/50% RH, 25 $°C$/75% RH, and 38 $°C$/90% RH. As both temperature and humidity increase from 23 $°C$/50% RH to 38 $°C$/90% RH, the vapor pressure of water climbs from 1.4 to 6 kPa. This leads to a nearly 150-fold rise in the OP of the multilayer board, which increases from 9 to 1305 $cc.m^{-2}.day^{-1}.bar^{-1}$. Although the LDPE top coating protects the CNF-M from moisture, water vapor still manages to permeate through the backside of the baseboard, inducing swelling in the CNF-layer. In addition, the baseboard also swells at high humidity, which puts additional mechanical strain on the CNF layer.

To counter this, an additional layer of LDPE was coated on the backside of the baseboard. Even with this dual-sided LDPE coated board, the OP remains elevated at 38 $°C$/90% RH. Nevertheless, this increase in OP is only 50-fold (increase from 8 to 411 $cc.m^{-2}.day^{-1}.bar^{-1}$), which is much lower than the single side LDPE coated board. Despite this, an OP value of 411 $cc.m^{-2}.day^{-1}.bar^{-1}$ remains too high for most practical applications. One reason for this high OP even for double side LDPE coated board could be that the water vapor is diffusing in through the sample's cross-section.

It is important to acknowledge that measurement setup may not be optimized for high temperatures and humidities. Factors such as the sealing

grease and gaskets in the test cell might not provide an optimal edge seal, potentially contributing to edge leakage effects. In such circumstances, adopting specialized test cells that mitigate edge leakage by circulating inert N_2 gas along the outer edges could prove beneficial. The influence of humidity can be further reduced by sandwiching the nanocellulose layer between two moisture barrier layers, thereby reducing the cross-sectional area exposed to the external environment. Another approach entails integrating cross-linkers into the nanocellulose formulation to control swelling at elevated temperatures and humidity, thereby preserving the microstructure of the nanocellulose. Future work should address these issues.

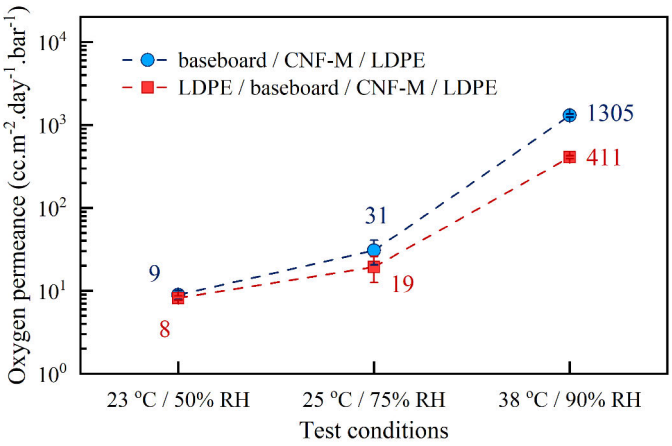

Figure 4.18 Oxygen permeance at different test conditions for CNF-M/LDPE and LDPE/CNF-M/LDPE multilayer coated baseboards.

4.7.3 Grease and mineral oil barrier

Figure 4.19 shows the grease barrier for single layer nanocellulose and thermoplastic-coated samples produced in this work. The starting point of the bar indicates the failure of the first sample and the end indicates the failure of the last sample. Similar to oxygen permeance, all the single layer nanocellulose coated samples show a wide variation in grease barrier, which is attributed to the cracks/pinholes in the dry nanocellulose layer. Despite the defects, CNF-M, CNF-C, and CNC-M coated samples show maximum grease penetration time of 270, 450, and 340 hours, respectively. CNF-C has finer fibrils than CNF-M and therefore shows higher grease barrier. CNC-M and CNF-E have shorter (and stiffer) fibrils (Figure 4.1), therefore, they are more

susceptible to defects, and should show lower grease barrier. However, CNC-M has higher crystallinity and has better barrier than CNF-E. The thermoplastic-coated boards did not show any failure within the 500-hour test period and the multilayer-coated samples followed the same trend.

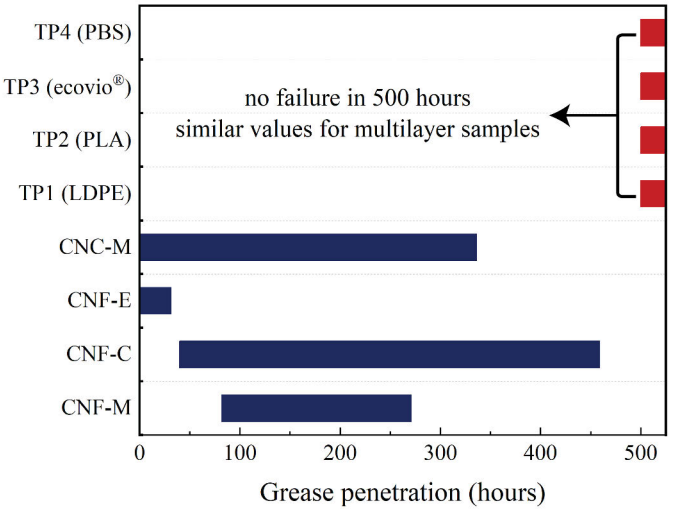

Figure 4.19 Grease barrier for single-layer roll-to-roll coated samples (start point of the bar indicates failure of first sample and end indicates failure of last sample).

All the single layer nanocellulose coated boards show excellent barrier against mineral oil (HVTR), with no n-Heptane vapors escaping through the sample during the test period. With the exception of TP1 (LDPE) and WD1 (pigment/polymer dispersion), the rest of the moisture barrier coatings also show high barrier against n-heptane. The HVTR for TP1 and WD1 coated boards is 640 and 800 $g.m^{-2}.day^{-1}$, respectively, but when coated on nanocellulose show zero HVTR. All the nanocellulose and multilayer-coated samples show a maximum KIT value of 12.

Table 4.3 shows the data on HVTR, KIT, and grease penetration time for CNF-E coated boards with 5% CMC and NaPA additions. The grease and mineral oil barrier for CNF-E + CMC coated board is higher when compared to pure CNF-E or CNF-E + NaPA coated boards. SEM surface images (Figure 4.20) reveal cracked surfaces for CNF-E and CNF-E + NaPA coated boards, while CNF-E + CMC coated board displays a comparatively smoother surface, which would explain it's higher barrier performance. The cracks could arise from a combination of factors, including faster thixotropy recovery times,

reduced water retention, and a higher yield-stress power exponent (discussed in the Rheology subsection; refer also to Figures 4.3b, 4.9b, and 4.10a) for CNF-E and CNF-E + NaPA suspensions compared to CNF-E with CMC.

Table 4.3 HVTR, KIT, and grease barrier for CNF-E (12.5%) coated samples with 5% CMC and NaPA addition.

Coating	**HVTR** ($g.m^{-2}.day^{-1}$)	**KIT**	**Grease penetration**[1] (h)
CNF-E	500 ± 70	5	< 0.2
CNF-E + 5% CMC	below detection limit	12	1 - 31
CNF-E + 5% NaPA	450 ± 50	5	< 0.8

[1]Failure time given as range (min. - max.) based on three parallel samples.

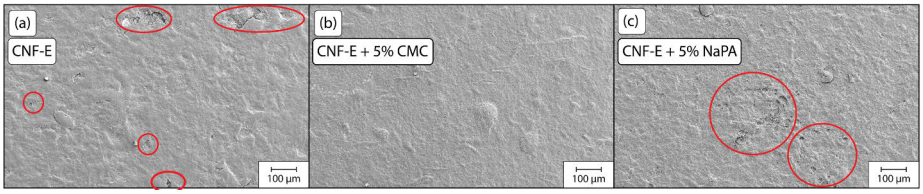

Figure 4.20 SEM surface images of: (a) CNF-E, (b) CNF-E + 5% CMC, and (c) CNF-E + 5% NaPA coated samples (the solid content for all suspensions was 12.5%).

The grease penetration time for CNF-E + CMC coated board is less than 31 hours which is much lower than other CNF coated samples (Figure 4.19). One plausible explanation is the higher probability of coating defects due to shorter and stiffer fibrils in CNF-E compared to other CNF grades. Additionally, the use of high suspension solid content (12.5%) and the resulting high viscosity might trap air that is difficult to remove, potentially leading to pinholes in the coating structure. Nonetheless, the coating of such high solid content nanocellulose grades holds promise for potential industrial applications, and future work should concentrate on improving the coating quality and barrier properties of such high solid content CNFs.

Concluding Remarks

Packaging serves a crucial role in our lives. Efficient packaging protects the food, extends its shelf life, and contributes to the reduction of food waste. Conventional food packaging involves the use of multiple layers composed of fossil-fuel-based plastics and metals for achieving water vapor, oxygen, and grease barriers. However, most of these designs are non-biodegradable and pose challenges during recycling. Nanocellulose is a bio based and biodegradable material that has excellent barrier against oxygen, oils, and grease, and therefore has a potential to be used as a sustainable barrier packaging material.

Six different nanocellulose grades were studied in this thesis. The primary emphasis was placed on understanding the factors that influence the roll-to-roll processability of nanocelluloses on a large scale, along with their resulting barrier properties. These grades cover the entire spectrum of nanocellulose sizes. This range included mechanically produced coarse fibrils found in CNF-M, chemically pre-treated finer fibrils in CNF-C and CNF-S, enzymatically pre-treated and twin-screw extruded short and stiff fibers as seen in CNF-E. Additionally, two variations of cellulose nanocrystals, CNC-M and CNC-C, were also incorporated. The solid contents of these suspensions spanned from 2% to 12.5%.

Nanocellulose suspensions display high yield stress due to inter-fibril hydrogen bonds and fiber entanglement. This can lead to cavitation during pumping, non-yielding regions in the coating head, causing defects and loss of barrier properties. Dispersants like CMC and NaPA reduce yield stress. CMC's optimal addition was found to be 5%, while NaPA should stay below 2% to prevent flocculation, which could otherwise lead to coating defects. Yield stress relates to solid concentration via a power function. CMC addition reduces the yield stress power exponent which will have a positive impact on the coating quality as the wet coated layer immobilizes slowly compared to the original suspension.

Nanocellulose suspensions exhibit shear thinning behavior, causing viscosity to decrease significantly (by 4 orders of magnitude) when shear rates rise from 0.1 to 1000 s^{-1}. The viscosity profile of CNFs shows three distinct zones: low-shear, intermediate, and high-shear. Consequently, conventional viscosity models are inadequate for precise data fitting. To address this, a novel Casson-Power-Cross model was introduced, that accurately fits the CNF viscosity data across a wide shear rate range, as well as for various solid contents and dispersant additions. The model's calculated yield stresses closely aligns with experimental measurements. This model can be a useful tool for computational fluid dynamics for the design and optimization of novel coating applicators tailored for nanocellulosic materials. Additionally, this model enables the extraction of vital characteristic parameters (yield stress, transition shear rate, and power-law index at high shear rates) from a single flow curve. In contrast, CNC suspensions lack a transition zone in their viscosity curve due to fewer fibril entanglements, making the Herschel-Bulkley model a suitable fit. Additionally, high-shear pipe and slot viscometers were constructed to understand the rheology of CNF suspensions at high shear rates. Shear rates up to 240 000 and 37 000 s^{-1} were achieved for slot and pipe rheometers, respectively. Viscosity values from these viscometers agree well with rotational rheometer results at low shear rates and with the proposed Casson-Power-Cross model at high shear rates.

CNF suspensions display thixotropic behavior, swiftly restoring their elastic modulus after shear forces are withdrawn. CMC addition extends this recovery period by up to five-fold, potentially enhancing coating quality. CNC suspensions exhibit gradual thixotropic recovery in contrast to CNF suspensions, due to the high charge and reduced mechanical interlocking of CNCs, which slows down the rate of structure reformation. CMC addition also increases the water retention of nanocellulose suspensions and therefore will have positive impact on coater runnability. In contrast, NaPa lowers the water retention due to the formation of strong nanocellulose flocs possibly due to excess dispersant addition. Based on these findings, 5% CMC was added to all CNF suspensions for roll-to-roll coating.

The substrate choice significantly affects the coating quality of nanocellulose suspensions. Several primers, including CMC, cationic starch, pigments, latex, and polymers, were tested for their impact on nanocellulose coating quality. A hydrophilic surface is essential for even wetting and spreading of the nanocellulose layer. Porous substrates allow for drying from the paper's backside. A smooth surface necessitates less nanocellulose material

for filling in the surface volume, facilitating full coverage at low coat weights. Positively charged surfaces enhance adhesion of the negatively charged nanocellulose layer. Therefore, a pigment-coated paperboard with a thin cationic starch primer coat was chosen as the base substrate for nanocellulose coatings.

The different nanocellulose suspensions were successfully applied onto the baseboard using a slot-die applicator in a roll-to-roll process. The dry coat weights ranged from 7 to 24 $g.m^{-2}$, and the coating speeds varied between 3 to 6 $m.min^{-1}$. SEM cross sections revealed uniform layers and full coverage for all nanocellulose coated samples. This demonstrates the slot-die's suitability as a coating applicator to handle a wide spectrum of nanocelluloses and solid contents.

To protect nanocellulose from moisture, several biodegradable thermoplastics and water-based dispersions were coated on top of nanocellulose-coated boards using extrusion or reverse gravure coating methods. The multilayer coatings reduced the water vapor permeance of nanocellulose-coated boards by over 70%, and closed any defects in the nanocellulose layer, thereby improving the oxygen and grease barriers. Oxygen permeance values for these multilayer-coated boards were similar (or even lower) to those for pure nanocellulose films.

Plasticizers such as glycerol and sorbitol further improved the oxygen barrier of the multilayer paperboards. Blending kaolin into nanocellulose improved the adhesion at the nanocellulose-thermoplastic interface. This raised the oxygen permeance, but the ratio of kaolin could be controlled to tailor the oxygen barrier properties for specific end-use scenarios. Applying a moisture barrier coating on the reverse side of the baseboard protects the nanocellulose layer against humidity-induced moisture intrusion. However, elevated oxygen permeance persisted especially at high humidity due to moisture seeping in through the baseboard's cross-section. Sandwiching nanocellulose layer in-between two moisture barrier materials could potentially protect the nanocellulose at high humidity.

This work provides insight into understanding how yield stress, dispersant type and loading, thixotropy, and water release influence coatability of different grades of nanocelluloses during high-throughput coating processes. Moreover, the approach of processing nanocellulose and moisture barrier materials together into multilayer structures complements the shortcomings of each other and produces a paperboard with superior barrier properties that is both bio-based and biodegradable.

Future research should encompass the exploration of several key areas. This includes investigating the utilization of different rheology modifiers, varying their charge contents and molecular weights. This step will notably enhance the coatability of high viscosity nanocellulose suspensions. CFD modeling holds promise in customizing the coating applicator for high viscosity and high solid content nanocelluloses. Additionally, blending different nanocellulose grades could yield superior barrier properties or meet target values with reduced coat weights. Exploring crosslinkers' effects on limiting nanocellulose layer swelling under high humidities is imperative. To be industrially viable, higher coating solid contents and application speeds reflective of real-world scenarios should be tested and understanding the drying parameters' impact on nanocellulose quality is essential. Compatibility between nanocellulose and moisture barrier materials warrants further investigation, including barrier performance after various converting operations. In conclusion, nanocellulose stands as a potential barrier material for sustainable barrier packaging, but requires further research on its processability enhancement before it can be commercialized.

References

[1] J. Schmidt, L. Grau, M. Auer, R. Maletz, and J. Woidasky, "Multilayer packaging in a circular economy," *Polymers*, vol. 14, no. 9, p. 1825, 2022.

[2] B. A. Morris, "1 - introduction," in *The Science and Technology of Flexible Packaging* (B. A. Morris, ed.), Plastics Design Library, pp. 3–21, Oxford: William Andrew Publishing, 2017.

[3] S. Torres-Giner, K. J. Figueroa-Lopez, B. Melendez-Rodriguez, C. Prieto, M. Pardo-Figuerez, and J. M. Lagaron, "Emerging trends in biopolymers for food packaging," in *Sustainable Food Packaging Technology* (A. Athanassiou, ed.), ch. 1, pp. 1–33, John Wiley & Sons, Ltd, 2021.

[4] Future Market Insights, "Food packaging market outlook (2022-2032)," tech. rep., Future Market Insights, Inc., 2021.

[5] K. Kaiser, M. Schmid, and M. Schlummer, "Recycling of polymer-based multilayer packaging: A review," *Recycling*, vol. 3, no. 1, p. 1, 2017.

[6] A.-S. Bauer, M. Tacker, I. Uysal-Unalan, R. M. Cruz, T. Varzakas, and V. Krauter, "Recyclability and redesign challenges in multilayer flexible food packaging—a review," *Foods*, vol. 10, no. 11, p. 2702, 2021.

[7] B. A. Morris, "4 - commonly used resins and substrates in flexible packaging," in *The Science and Technology of Flexible Packaging* (B. A. Morris, ed.), Plastics Design Library, pp. 69–119, Oxford: William Andrew Publishing, 2017.

[8] T. Anukiruthika, P. Sethupathy, A. Wilson, K. Kashampur, J. A. Moses, and C. Anandharamakrishnan, "Multilayer packaging: Advances in preparation techniques and emerging food applications," *Comprehensive Reviews in Food Science and Food Safety*, vol. 19, no. 3, pp. 1156–1186, 2020.

[9] M. Fereydoon and S. Ebnesajjad, "5 - development of high-barrier film for food packaging," in *Plastic Films in Food Packaging* (S. Ebnesajjad, ed.), Plastics Design Library, pp. 71–92, Oxford: William Andrew Publishing, 2013.

[10] K. Marsh and B. Bugusu, "Food packaging—roles, materials, and environmental issues," *Journal of food science*, vol. 72, no. 3, pp. R39–R55, 2007.

[11] PlasticsEurope, "Plastics - the facts 2022," tech. rep., Plastics Europe, 2022.

[12] R. Geyer, J. R. Jambeck, and K. L. Law, "Production, use, and fate of all plastics ever made," *Science advances*, vol. 3, no. 7, p. e1700782, 2017.

[13] H. Ritchie and M. Roser, "Plastic pollution," *Our World in Data*, 2018. https://ourworldindata.org/plastic-pollution.

[14] R. M. Cruz, V. Krauter, S. Krauter, S. Agriopoulou, R. Weinrich, C. Herbes, P. B. Scholten, I. Uysal-Unalan, E. Sogut, S. Kopacic, *et al.*, "Bioplastics for food packaging: Environmental impact, trends and regulatory aspects," *Foods*, vol. 11, no. 19, p. 3087, 2022.

[15] Z. Tartakowski, "Recycling of packaging multilayer films: New materials for technical products," *Resources, Conservation and Recycling*, vol. 55, no. 2, pp. 167–170, 2010.

[16] K. Ragaert, L. Delva, and K. Van Geem, "Mechanical and chemical recycling of solid plastic waste," *Waste management*, vol. 69, pp. 24–58, 2017.

[17] N. Stark and L. Matuana, "Trends in sustainable biobased packaging materials: A mini review," *Materials Today Sustainability*, vol. 15, p. 100084, 2021.

[18] K. Eissenberger, A. Ballesteros, R. De Bisschop, E. Bugnicourt, P. Cinelli, M. Defoin, E. Demeyer, S. Fürtauer, C. Gioia, L. Gómez, *et al.*, "Approaches in sustainable, biobased multilayer packaging solutions," *Polymers*, vol. 15, no. 5, p. 1184, 2023.

[19] C. T. de Mello Soares, M. Ek, E. Östmark, M. Gällstedt, and S. Karlsson, "Recycling of multi-material multilayer plastic packaging: Current trends and future scenarios," *Resources, conservation and recycling*, vol. 176, p. 105905, 2022.

[20] E. Commission and D.-G. for Communication, *Circular economy action plan : for a cleaner and more competitive Europe*. Publications Office of the European Union, 2020.

[21] E. Commission and D.-G. for Environment, *Assessment of options for reinforcing the Packaging and Packaging Waste Directive's essential requirements and other measures to reduce the generation of packaging waste : final report*. Publications Office of the European Union, 2022.

[22] K. Ekaterina, "Revision of directive 94/62/ec on packaging and packaging waste," 2022.

[23] E. M. Foundation, "The global commitment 2021 progress report," tech. rep., Ellen MacArthur Foundation, 2021.

[24] Congress.gov, "Actions - s.5163 - 117th congress (2021-2022): Protecting communities from plastics act," 2022. Accessed on April 2, 2023.

[25] J. Gaffey, H. McMahon, E. Marsh, K. Vehmas, T. Kymäläinen, and J. Vos, "Understanding consumer perspectives of bio-based products—a comparative case study from Ireland and The Netherlands," *Sustainability*, vol. 13, no. 11, 2021.

[26] I. Delioglamnis, E. Kouzi, E. Tsagaraki, M. Bougiouklis, and I. Tollias, "D2.4 public perception of bio-based products – societal needs and concerns," tech. rep., BIOWAYS Deliverable D2.4, 2018.

[27] P. Tyagi, K. S. Salem, M. A. Hubbe, and L. Pal, "Advances in barrier coatings and film technologies for achieving sustainable packaging of food products–a review," *Trends in Food Science & Technology*, vol. 115, pp. 461–485, 2021.

[28] P. K. Kunam, D. Ramakanth, K. Akhila, and K. K. Gaikwad, "Bio-based materials for barrier coatings on paper packaging," *Biomass Conversion and Biorefinery*, pp. 1–16, 2022.

[29] K. E. Helanto, L. Matikainen, R. Talja, and O. J. Rojas, "Bio-based polymers for sustainable packaging and biobarriers: A critical review," *BioResources*, vol. 14, no. 2, pp. 4902–4951, 2019.

[30] M. Mujtaba, J. Lipponen, M. Ojanen, S. Puttonen, and H. Vaittinen, "Trends and challenges in the development of bio-based barrier coating materials for paper/cardboard food packaging; a review," *Science of the Total Environment*, p. 158328, 2022.

[31] C. L. Reichert, E. Bugnicourt, M.-B. Coltelli, P. Cinelli, A. Lazzeri, I. Canesi, F. Braca, B. M. Martínez, R. Alonso, L. Agostinis, *et al.*, "Bio-based packaging: Materials, modifications, industrial applications and sustainability," *Polymers*, vol. 12, no. 7, p. 1558, 2020.

[32] M. Asgher, S. A. Qamar, M. Bilal, and H. M. Iqbal, "Bio-based active food packaging materials: Sustainable alternative to conventional petrochemical-based packaging materials," *Food Research International*, vol. 137, p. 109625, 2020.

[33] S. S. Nair, J. Zhu, Y. Deng, and A. J. Ragauskas, "High performance green barriers based on nanocellulose," *Sustainable Chemical Processes*, vol. 2, pp. 1–7, 2014.

[34] M. A. Hubbe, A. Ferrer, P. Tyagi, Y. Yin, C. Salas, L. Pal, and O. J. Rojas, "Nanocellulose in thin films, coatings, and plies for packaging applications: A review," *BioResources*, vol. 12, no. 1, pp. 2143–2233, 2017.

[35] Y. Zhao, H. Sun, B. Yang, and Y. Weng, "Hemicellulose-based film: potential green films for food packaging," *Polymers*, vol. 12, no. 8, p. 1775, 2020.

[36] C. Laine, A. Harlin, J. Hartman, S. Hyvärinen, K. Kammiovirta, B. Krogerus, H. Pajari, H. Rautkoski, H. Setälä, J. Sievänen, *et al.*, "Hydroxyalkylated xylans–their synthesis and application in coatings for packaging and paper," *Industrial crops and products*, vol. 44, pp. 692–704, 2013.

[37] R. Shorey and T. H. Mekonnen, "Sustainable paper coating with enhanced barrier properties based on esterified lignin and pbat blend," *International Journal of Biological Macromolecules*, vol. 209, pp. 472–484, 2022.

[38] E.-L. Hult, J. Ropponen, K. Poppius-Levlin, T. Ohra-Aho, and T. Tamminen, "Enhancing the barrier properties of paper board by a novel lignin coating," *Industrial crops and products*, vol. 50, pp. 694–700, 2013.

[39] H. Wang, J. Qian, and F. Ding, "Emerging chitosan-based films for food packaging applications," *Journal of agricultural and food chemistry*, vol. 66, no. 2, pp. 395–413, 2018.

[40] D. Liu, P. Zhao, J. Chen, Y. Yan, and Z. Wu, "Recent advances and applications in starch for intelligent active food packaging: A review," *Foods*, vol. 11, no. 18, p. 2879, 2022.

[41] K. Chi, H. Wang, and J. M. Catchmark, "Sustainable starch-based barrier coatings for packaging applications," *Food Hydrocolloids*, vol. 103, p. 105696, 2020.

[42] C.-H. Gu, J.-J. Wang, Y. Yu, H. Sun, N. Shuai, and B. Wei, "Biodegradable multilayer barrier films based on alginate/polyethyleneimine and biaxially oriented poly (lactic acid)," *Carbohydrate polymers*, vol. 92, no. 2, pp. 1579–1585, 2013.

[43] Ł. Łopusiewicz, S. Macieja, M. Śliwiński, A. Bartkowiak, S. Roy, and P. Sobolewski, "Alginate biofunctional films modified with melanin from watermelon seeds and zinc oxide/silver nanoparticles," *Materials*, vol. 15, no. 7, p. 2381, 2022.

[44] S. Kopacic, A. Walzl, A. Zankel, E. Leitner, and W. Bauer, "Alginate and chitosan as a functional barrier for paper-based packaging materials," *Coatings*, vol. 8, no. 7, p. 235, 2018.

[45] K. Khwaldia, A. H. Basta, H. Aloui, and H. El-Saied, "Chitosan–caseinate bilayer coatings for paper packaging materials," *Carbohydrate polymers*, vol. 99, pp. 508–516, 2014.

[46] A. V. Samrot, S. K. Samanvitha, N. Shobana, E. R. Renitta, P. Senthilkumar, S. S. Kumar, S. Abirami, S. Dhiva, M. Bavanilatha, P. Prakash, *et al.*, "The synthesis, characterization and applications of polyhydroxyalkanoates (phas) and pha-based nanoparticles," *Polymers*, vol. 13, no. 19, p. 3302, 2021.

[47] N. Israni and S. Shivakumar, "Polyhydroxyalkanoates in packaging," in *Biotechnological Applications of Polyhydroxyalkanoates* (V. C. Kalia, ed.), pp. 363–388, Singapore: Springer Singapore, 2019.

[48] M. Schmid and K. Müller, "Chapter 11 - whey protein-based packaging films and coatings," in *Whey Proteins* (H. C. Deeth and N. Bansal, eds.), pp. 407–437, Academic Press, 2019.

[49] M. Schmid, K. Dallmann, E. Bugnicourt, D. Cordoni, F. Wild, A. Lazzeri, and K. Noller, "Properties of whey-protein-coated films and laminates as novel recyclable food packaging materials with excellent barrier properties," *International Journal of Polymer Science*, vol. 2012, 2012.

[50] M. Zubair and A. Ullah, "Recent advances in protein derived bionanocomposites for food packaging applications," *Critical reviews in food science and nutrition*, vol. 60, no. 3, pp. 406–434, 2020.

[51] S. Marano, E. Laudadio, C. Minnelli, and P. Stipa, "Tailoring the barrier properties of pla: a state-of-the-art review for food packaging applications," *Polymers*, vol. 14, no. 8, p. 1626, 2022.

[52] R. Auras, B. Harte, and S. Selke, "An overview of polylactides as packaging materials," *Macromolecular bioscience*, vol. 4, no. 9, pp. 835–864, 2004.

[53] F. Wu, M. Misra, and A. K. Mohanty, "Challenges and new opportunities on barrier performance of biodegradable polymers for sustainable packaging," *Progress in Polymer Science*, vol. 117, p. 101395, 2021.

[54] M. I. Peñas, R. A. Pérez-Camargo, R. Hernández, and A. J. Müller, "A review on current strategies for the modulation of thermomechanical, barrier, and biodegradation properties of poly (butylene succinate)(pbs) and its random copolymers," *Polymers*, vol. 14, no. 5, p. 1025, 2022.

[55] T. Abitbol, A. Rivkin, Y. Cao, Y. Nevo, E. Abraham, T. Ben-Shalom, S. Lapidot, and O. Shoseyov, "Nanocellulose, a tiny fiber with huge applications," *Current opinion in biotechnology*, vol. 39, pp. 76–88, 2016.

[56] A. F. Turbak, F. W. Snyder, K. R. Sandberg, *et al.*, "Microfibrillated cellulose, a new cellulose product: properties, uses, and commercial potential," in *Journal of Applied Polymer Science: Applied Polymer Symposium*, vol. 37, pp. 815–827, 1983.

[57] F. W. Herrick, R. L. Casebier, J. K. Hamilton, and K. R. Sandberg, "Microfibrillated cellulose: morphology and accessibility," in *Journal of Applied Polymer Science: Applied Polymer Symposium*, vol. 37, pp. 797–813, 1983.

[58] B. Thomas, M. C. Raj, J. Joy, A. Moores, G. L. Drisko, and C. Sanchez, "Nanocellulose, a versatile green platform: from biosources to materials and their applications," *Chemical reviews*, vol. 118, no. 24, pp. 11575–11625, 2018.

[59] S. S. Ahankari, A. R. Subhedar, S. S. Bhadauria, and A. Dufresne, "Nanocellulose in food packaging: A review," *Carbohydrate Polymers*, vol. 255, p. 117479, 2021.

[60] E. Pasquier, B. D. Mattos, H. Koivula, A. Khakalo, M. N. Belgacem, O. J. Rojas, and J. Bras, "Multilayers of renewable nanostructured materials with high oxygen and water vapor barriers for food packaging," *ACS Appl. Mater. Interfaces*, 2022.

[61] G. Fotie, S. Limbo, and L. Piergiovanni, "Manufacturing of food packaging based on nanocellulose: Current advances and challenges," *Nanomaterials*, vol. 10, no. 9, p. 1726, 2020.

[62] R. M. Cherian, A. Tharayil, R. T. Varghese, T. Antony, H. Kargarzadeh, C. J. Chirayil, and S. Thomas, "A review on the emerging applications of nano-cellulose as advanced coatings," *Carbohydr. Polym.*, p. 119123, 2022.

[63] S. Salimi, R. Sotudeh-Gharebagh, R. Zarghami, S. Y. Chan, and K. H. Yuen, "Production of nanocellulose and its applications in drug delivery: A critical review," *ACS Sustain. Chem. Eng.*, vol. 7, no. 19, pp. 15800–15827, 2019.

[64] F. Hoeng, A. Denneulin, and J. Bras, "Use of nanocellulose in printed electronics: a review," *Nanoscale*, vol. 8, no. 27, pp. 13131–13154, 2016.

[65] A. Chakrabarty and Y. Teramoto, "Recent advances in nanocellulose composites with polymers: a guide for choosing partners and how to incorporate them," *Polymers*, vol. 10, no. 5, p. 517, 2018.

[66] J. D. P. de Amorim, K. C. de Souza, C. R. Duarte, I. da Silva Duarte, F. d. A. S. Ribeiro, G. S. Silva, P. M. A. de Farias, A. Stingl, A. F. S. Costa, G. M. Vinhas, *et al.*, "Plant and bacterial nanocellulose: Production, properties and applications in medicine, food, cosmetics, electronics and engineering. a review," *Environmental Chemistry Letters*, vol. 18, no. 3, pp. 851–869, 2020.

[67] M.-C. Li, Q. Wu, R. J. Moon, M. A. Hubbe, and M. J. Bortner, "Rheological aspects of cellulose nanomaterials: Governing factors and emerging applications," *Advanced Materials*, vol. 33, no. 21, p. 2006052, 2021.

[68] C. Chen and L. Hu, "Nanocellulose toward advanced energy storage devices: structure and electrochemistry," *Acc. Chem. Res.*, vol. 51, no. 12, pp. 3154–3165, 2018.

[69] FutureMarkets, "The nanocellulose market, production and pricing report 2021," tech. rep., Future Markets Inc., 2021.

[70] A. Naderi, T. Lindström, and J. Sundström, "Carboxymethylated nanofibrillated cellulose: rheological studies," *Cellulose*, vol. 21, no. 3, pp. 1561–1571, 2014.

[71] G. C. Ciftci, P. A. Larsson, A. V. Riazanova, H. H. Øvrebø, L. Wågberg, and L. A. Berglund, "Tailoring of rheological properties and structural polydispersity effects in microfibrillated cellulose suspensions," *Cellulose*, vol. 27, no. 16, pp. 9227–9241, 2020.

[72] O. Nechyporchuk, M. N. Belgacem, and J. Bras, "Production of cellulose nanofibrils: A review of recent advances," *Industrial Crops and Products*, vol. 93, pp. 2–25, 2016.

[73] V. Kumar, A. Elfving, H. Koivula, D. Bousfield, and M. Toivakka, "Roll-to-roll processed cellulose nanofiber coatings," *Industrial & Engineering Chemistry Research*, vol. 55, no. 12, pp. 3603–3613, 2016.

[74] A. I. Koponen, "The effect of consistency on the shear rheology of aqueous suspensions of cellulose micro- and nanofibrils: a review," *Cellulose*, vol. 27, no. 4, pp. 1879–1897, 2020.

[75] M. A. Hubbe, P. Tayeb, M. Joyce, P. Tyagi, M. Kehoe, K. Dimic-Misic, and L. Pal, "Rheology of nanocellulose-rich aqueous suspensions: a review," *BioResources*, vol. 12, no. 4, pp. 9556–9661, 2017.

[76] M. Hashemzehi, B. Mesic, B. Sjöstrand, and M. Naqvi, "A comprehensive review of nanocellulose modification and applications in papermaking and packaging: Challenges, technical solutions, and perspectives.," *BioResources*, vol. 17, no. 2, 2022.

[77] Q. Wang, Q. Yao, J. Liu, J. Sun, Q. Zhu, and H. Chen, "Processing nanocellulose to bulk materials: A review," *Cellulose*, vol. 26, no. 13, pp. 7585–7617, 2019.

[78] R. A. Chowdhury, C. Clarkson, and J. Youngblood, "Continuous roll-to-roll fabrication of transparent cellulose nanocrystal (CNC) coatings with controlled anisotropy," *Cellulose*, vol. 25, no. 3, pp. 1769–1781, 2018.

[79] K. Shanmugam, "Spray coated cellulose nanofiber laminates on the paper to enhance its barrier and mechanical properties," *Journal of Sustainability and Environmental Management*, vol. 1, no. 1, pp. 10–17, 2022.

[80] D. Beneventi, E. Zeno, and D. Chaussy, "Rapid nanopaper production by spray deposition of concentrated microfibrillated cellulose slurries," *Industrial Crops and Products*, vol. 72, pp. 200–205, 2015. Special issue derived from International Conference on Bio-based Materials and Composites.

[81] D. Guerin, Y. Rharbi, P. Huber, and M. Valérie, "Process and device for manufacturing a laminated material comprising a fibrillated cellulose layer," 2020. US Patent no. US10618015B2, date 14-April 2020.

[82] K. L. Spence, R. A. Venditti, O. J. Rojas, Y. Habibi, and J. J. Pawlak, "A comparative study of energy consumption and physical properties of microfibrillated cellulose produced by different processing methods," *Cellulose*, vol. 18, no. 4, pp. 1097–1111, 2011.

[83] A. Ferrer, L. Pal, and M. Hubbe, "Nanocellulose in packaging: Advances in barrier layer technologies," *Industrial Crops and Products*, vol. 95, pp. 574–582, 2017.

[84] L. Dai, Z. Long, J. Chen, X. An, D. Cheng, A. Khan, and Y. Ni, "Robust guar gum/cellulose nanofibrils multilayer films with good barrier properties," *ACS Applied Materials & Interfaces*, vol. 9, no. 6, pp. 5477–5485, 2017.

[85] K. Zhao, W. Wang, A. Teng, K. Zhang, Y. Ma, S. Duan, S. Li, and Y. Guo, "Using cellulose nanofibers to reinforce polysaccharide films: Blending vs layer-by-layer casting," *Carbohydrate polymers*, vol. 227, p. 115264, 2020.

[86] C. Aulin and G. Ström, "Multilayered alkyd resin/nanocellulose coatings for use in renewable packaging solutions with a high level of moisture resistance," *Industrial & Engineering Chemistry Research*, vol. 52, no. 7, pp. 2582–2589, 2013.

[87] F. Vilarinho, A. Sanches Silva, M. F. Vaz, and J. P. Farinha, "Nanocellulose in green food packaging," *Critical reviews in food science and nutrition*, vol. 58, no. 9, pp. 1526–1537, 2018.

[88] A. Cherpinski, S. Torres-Giner, J. Vartiainen, M. S. Peresin, P. Lahtinen, and J. M. Lagaron, "Improving the water resistance of nanocellulose-based films with polyhydroxyalkanoates processed by the electrospinning coating technique," *Cellulose*, vol. 25, no. 2, pp. 1291–1307, 2018.

[89] E.-L. Hult, M. Iotti, and M. Lenes, "Efficient approach to high barrier packaging using microfibrillar cellulose and shellac," *Cellulose*, vol. 17, no. 3, pp. 575–586, 2010.

[90] C. C. Satam, C. W. Irvin, A. W. Lang, J. C. R. Jallorina, M. L. Shofner, J. R. Reynolds, and J. C. Meredith, "Spray-coated multilayer cellulose nanocrystal—chitin nanofiber films for barrier applications," *ACS Sustainable Chemistry & Engineering*, vol. 6, no. 8, pp. 10637–10644, 2018.

[91] C. Aulin, E. Karabulut, A. Tran, L. Wågberg, and T. Lindström, "Transparent nanocellulosic multilayer thin films on polylactic acid with tunable gas barrier properties," *ACS applied materials & interfaces*, vol. 5, no. 15, pp. 7352–7359, 2013.

[92] J. Vartiainen, T. Kaljunen, H. Nykänen, T. Malm, and T. Tammelin, "Improving multilayer packaging performance with nanocellulose barrier layer," in *Tappi Place Conference 2014*, pp. 763–790, TAPPI Press, 2014.

[93] I. Siró and D. Plackett, "Microfibrillated cellulose and new nanocomposite materials: a review," *Cellulose*, vol. 17, no. 3, pp. 459–494, 2010.

[94] Y. Zeng, M. E. Himmel, and S.-Y. Ding, "Visualizing chemical functionality in plant cell walls," *Biotechnology for biofuels*, vol. 10, no. 1, pp. 1–16, 2017.

[95] D. Klemm, B. Heublein, H.-P. Fink, and A. Bohn, "Cellulose: fascinating biopolymer and sustainable raw material," *Angewandte chemie international edition*, vol. 44, no. 22, pp. 3358–3393, 2005.

[96] A. N. Fernandes, L. H. Thomas, C. M. Altaner, P. Callow, V. T. Forsyth, D. C. Apperley, C. J. Kennedy, and M. C. Jarvis, "Nanostructure of cellulose microfibrils in spruce wood," *Proceedings of the National Academy of Sciences*, vol. 108, no. 47, pp. E1195–E1203, 2011.

[97] J.-L. Wertz, O. Bédué, and J. P. Mercier, *Cellulose science and technology*. EPFL press, 2010.

[98] R. J. Moon, A. Martini, J. Nairn, J. Simonsen, and J. Youngblood, "Cellulose nanomaterials review: structure, properties and nanocomposites," *Chemical Society Reviews*, vol. 40, no. 7, pp. 3941–3994, 2011.

[99] A. Isogai, T. Saito, and H. Fukuzumi, "Tempo-oxidized cellulose nanofibers," *Nanoscale*, vol. 3, no. 1, pp. 71–85, 2011.

[100] H. Liimatainen, M. Visanko, J. A. Sirviö, O. E. Hormi, and J. Niinimäki, "Enhancement of the nanofibrillation of wood cellulose through sequential periodate–chlorite oxidation," *Biomacromolecules*, vol. 13, no. 5, pp. 1592–1597, 2012.

[101] A. Naderi, T. Lindström, J. Sundström, T. Pettersson, G. Flodberg, and J. Erlandsson, "Microfluidized carboxymethyl cellulose modified pulp: a nanofibrillated cellulose system with some attractive properties," *Cellulose*, vol. 22, no. 2, pp. 1159–1173, 2015.

[102] M. Ghanadpour, F. Carosio, P. T. Larsson, and L. Wågberg, "Phosphorylated cellulose nanofibrils: a renewable nanomaterial for the preparation of intrinsically flame-retardant materials," *Biomacromolecules*, vol. 16, no. 10, pp. 3399–3410, 2015.

[103] M. Pääkkö, M. Ankerfors, H. Kosonen, A. Nykänen, S. Ahola, M. Österberg, J. Ruokolainen, J. Laine, P. T. Larsson, O. Ikkala, *et al.*, "Enzymatic hydrolysis combined with mechanical shearing and high-pressure homogenization for nanoscale cellulose fibrils and strong gels," *Biomacromolecules*, vol. 8, no. 6, pp. 1934–1941, 2007.

[104] M. Mariano, N. El Kissi, and A. Dufresne, "Cellulose nanocrystals and related nanocomposites: Review of some properties and challenges," *Journal of Polymer Science Part B: Polymer Physics*, vol. 52, no. 12, pp. 791–806, 2014.

[105] C. Chen, Y. Kuang, S. Zhu, I. Burgert, T. Keplinger, A. Gong, T. Li, L. Berglund, S. J. Eichhorn, and L. Hu, "Structure–property–function relationships of natural and engineered wood," *Nature Reviews Materials*, vol. 5, no. 9, pp. 642–666, 2020.

[106] J. Gustafsson, R. Alén, J. Engström, R. Korpinen, P. Kuusisto, A. Leavitt, K. Olsson, J. Piira, A. Samuelsson, and J. Sundquist, "Chapter 2 - pulping," in *Chemical Pulping Part 1, Fibre Chemistry and Technology* (P. Fardim, ed.), vol. 6, pp. 187–381, Paper Engineers' Association/Paperi ja Puu Oy, 2 ed., 2011.

[107] A. Dufresne, "Nanocellulose: a new ageless bionanomaterial," *Mater. Today*, vol. 16, no. 6, pp. 220–227, 2013.

[108] F. Rol, G. Banvillet, V. Meyer, M. Petit-Conil, and J. Bras, "Combination of twin-screw extruder and homogenizer to produce high-quality nanofibrillated cellulose with low energy consumption," *Journal of Materials Science*, vol. 53, no. 17, pp. 12604–12615, 2018.

[109] O. Nechyporchuk, F. Pignon, and M. N. Belgacem, "Morphological properties of nanofibrillated cellulose produced using wet grinding as an ultimate fibrillation process," *Journal of Materials Science*, vol. 50, pp. 531–541, 2015.

[110] Q. Wang, J. Zhu, R. Gleisner, T. Kuster, U. Baxa, and S. McNeil, "Morphological development of cellulose fibrils of a bleached eucalyptus pulp by mechanical fibrillation," *Cellulose*, vol. 19, pp. 1631–1643, 2012.

[111] P. A. Gane, J. Schoelkopf, D. Gantenbein, M. Schenker, M. Pohl, and B. Kübler, "Process for the production of nano-fibrillar cellulose suspensions," 2014. US Patent 8,871,057.

[112] J. C. Husband, P. Svending, D. R. Skuse, T. Motsi, M. Likitalo, and A. Coles, "Paper filler composition," 2010. WO2010131016A2.

[113] J. C. Osorio-Arias, O. Vega-Castro, and S. I. Martínez-Monteagudo, "3.15 - fundamentals of high-pressure homogenization of foods," in *Innovative Food Processing Technologies* (K. Knoerzer and K. Muthukumarappan, eds.), pp. 244–273, Oxford: Elsevier, 2021.

[114] M. E. Malainine, M. Mahrouz, and A. Dufresne, "Thermoplastic nanocomposites based on cellulose microfibrils from opuntia ficus-indica parenchyma cell," *Composites Science and Technology*, vol. 65, no. 10, pp. 1520–1526, 2005.

[115] H. Kargarzadeh, M. Mariano, D. Gopakumar, I. Ahmad, S. Thomas, A. Dufresne, J. Huang, and N. Lin, "Advances in cellulose nanomaterials," *Cellulose*, vol. 25, pp. 2151–2189, 2018.

[116] T. T. T. Ho, K. Abe, T. Zimmermann, and H. Yano, "Nanofibrillation of pulp fibers by twin-screw extrusion," *Cellulose*, vol. 22, pp. 421–433, 2015.

[117] F. Rol, B. Vergnes, N. El Kissi, and J. Bras, "Nanocellulose production by twin-screw extrusion: simulation of the screw profile to increase the productivity," *ACS Sustainable Chemistry & Engineering*, vol. 8, no. 1, pp. 50–59, 2019.

[118] T. Lindström, A. Naderi, and A. Wiberg, "Large scale applications of nanocellulosic materials-a comprehensive review," *Journal of Korea Technical Association of The Pulp and Paper Industry*, vol. 47, no. 6, pp. 5–21, 2015.

[119] L. Wågberg, G. Decher, M. Norgren, T. Lindström, M. Ankerfors, and K. Axnäs, "The build-up of polyelectrolyte multilayers of microfibrillated cellulose and cationic polyelectrolytes," *Langmuir*, vol. 24, no. 3, pp. 784–795, 2008.

[120] H. Liimatainen, M. Visanko, J. Sirviö, O. Hormi, and J. Niinimäki, "Sulfonated cellulose nanofibrils obtained from wood pulp through regioselective oxidative bisulfite pre-treatment," *Cellulose*, vol. 20, pp. 741–749, 2013.

[121] C. Aulin, E. Johansson, L. Wågberg, and T. Lindström, "Self-organized films from cellulose I nanofibrils using the layer-by-layer technique," *Biomacromolecules*, vol. 11, no. 4, pp. 872–882, 2010.

[122] M. Henriksson, G. Henriksson, L. Berglund, and T. Lindström, "An environmentally friendly method for enzyme-assisted preparation of microfibrillated cellulose (mfc) nanofibers," *European polymer journal*, vol. 43, no. 8, pp. 3434–3441, 2007.

[123] S. Ang, V. Haritos, and W. Batchelor, "Effect of refining and homogenization on nanocellulose fiber development, sheet strength and energy consumption," *Cellulose*, vol. 26, pp. 4767–4786, 2019.

[124] G. L. Berto and V. Arantes, "Kinetic changes in cellulose properties during defibrillation into microfibrillated cellulose and cellulose nanofibrils by ultra-refining," *International journal of biological macromolecules*, vol. 127, pp. 637–648, 2019.

[125] M. Ankerfors, *Microfibrillated cellulose: energy-efficient preparation techniques and applications in paper*. PhD thesis, KTH Royal Institute of Technology, 2015.

[126] R. Baati, A. Magnin, and S. Boufi, "High solid content production of nanofibrillar cellulose via continuous extrusion," *ACS Sustainable Chemistry & Engineering*, vol. 5, no. 3, pp. 2350–2359, 2017.

[127] J. Hiltunen, K. Kemppainen, and J. Pere, "Process for producing fibrillated cellulose material," 2018.

[128] N. J. Davis and S. L. Flitsch, "Selective oxidation of monosaccharide derivatives to uronic acids," *Tetrahedron Letters*, vol. 34, no. 7, pp. 1181–1184, 1993.

[129] A. De Nooy, A. Besemer, and H. Van Bekkum, "Highly selective tempo mediated oxidation of primary alcohol groups in polysaccharides," *Recueil des Travaux Chimiques des Pays-Bas*, vol. 113, no. 3, pp. 165–166, 1994.

[130] T. Saito, Y. Nishiyama, J.-L. Putaux, M. Vignon, and A. Isogai, "Homogeneous suspensions of individualized microfibrils from tempo-catalyzed oxidation of native cellulose," *Biomacromolecules*, vol. 7, no. 6, pp. 1687–1691, 2006.

[131] M. Zhao, J. Li, E. Mano, Z. Song, D. M. Tschaen, E. J. Grabowski, and P. J. Reider, "Oxidation of primary alcohols to carboxylic acids with sodium chlorite catalyzed by tempo and bleach," *Journal of Organic Chemistry*, vol. 64, no. 7, pp. 2564–2566, 1999.

[132] T. Saito, M. Hirota, N. Tamura, S. Kimura, H. Fukuzumi, L. Heux, and A. Isogai, "Individualization of nano-sized plant cellulose fibrils by direct surface carboxylation using tempo catalyst under neutral conditions," *Biomacromolecules*, vol. 10, no. 7, pp. 1992–1996, 2009.

[133] A. Tejado, M. N. Alam, M. Antal, H. Yang, and T. G. van de Ven, "Energy requirements for the disintegration of cellulose fibers into cellulose nanofibers," *Cellulose*, vol. 19, pp. 831–842, 2012.

[134] J. A. Sirviö, A. Kolehmainen, M. Visanko, H. Liimatainen, J. Niinimäki, and O. E. Hormi, "Strong, self-standing oxygen barrier films from nanocelluloses modified with regioselective oxidative treatments," *ACS applied materials & interfaces*, vol. 6, no. 16, pp. 14384–14390, 2014.

[135] T. Heinze and A. Koschella, "Carboxymethyl ethers of cellulose and starch – a review," *Macromolecular Symposia*, vol. 223, no. 1, pp. 13–40, 2005.

[136] L. Wågberg, L. Winter, L. Ödberg, and T. Lindström, "On the charge stoichiometry upon adsorption of a cationic polyelectrolyte on cellulosic materials," *Colloids and surfaces*, vol. 27, no. 4, pp. 163–173, 1987.

[137] I. Siró, D. Plackett, M. Hedenqvist, M. Ankerfors, and T. Lindström, "Highly transparent films from carboxymethylated microfibrillated cellulose: the effect of multiple homogenization steps on key properties," *Journal of Applied Polymer Science*, vol. 119, no. 5, pp. 2652–2660, 2011.

[138] T. Ho, T. Zimmermann, R. Hauert, and W. Caseri, "Preparation and characterization of cationic nanofibrillated cellulose from etherification and high-shear disintegration processes," *Cellulose*, vol. 18, pp. 1391–1406, 2011.

[139] H. Liimatainen, T. Suopajärvi, J. Sirviö, O. Hormi, and J. Niinimäki, "Fabrication of cationic cellulosic nanofibrils through aqueous quaternization pretreatment and their use in colloid aggregation," *Carbohydrate polymers*, vol. 103, pp. 187–192, 2014.

[140] A. Olszewska, P. Eronen, L.-S. Johansson, J.-M. Malho, M. Ankerfors, T. Lindström, J. Ruokolainen, J. Laine, and M. Österberg, "The behaviour of cationic nanofibrillar cellulose in aqueous media," *Cellulose*, vol. 18, pp. 1213–1226, 2011.

[141] S. Saini, Ç. Y. Falco, M. N. Belgacem, and J. Bras, "Surface cationized cellulose nanofibrils for the production of contact active antimicrobial surfaces," *Carbohydrate polymers*, vol. 135, pp. 239–247, 2016.

[142] A. Chaker and S. Boufi, "Cationic nanofibrillar cellulose with high antibacterial properties," *Carbohydrate polymers*, vol. 131, pp. 224–232, 2015.

[143] C. M. Payne, B. C. Knott, H. B. Mayes, H. Hansson, M. E. Himmel, M. Sandgren, J. Stahlberg, and G. T. Beckham, "Fungal cellulases," *Chemical reviews*, vol. 115, no. 3, pp. 1308–1448, 2015.

[144] S. Tangnu, "Process development for ethanol production based on enzymatic hydrolysis of cellulosic biomass," *Process Biochemistry*, vol. 17, no. 3, pp. 36–45, 1982.

[145] W. Bolaski, A. Gallatin, and J. Gallatin, "Enzymatic conversion of cellulosic fibers," 1962. US Patent 3041246.

[146] Y. Qing, R. Sabo, J. Zhu, U. Agarwal, Z. Cai, and Y. Wu, "A comparative study of cellulose nanofibrils disintegrated via multiple processing approaches," *Carbohydrate polymers*, vol. 97, no. 1, pp. 226–234, 2013.

[147] G. Siqueira, S. Tapin-Lingua, J. Bras, D. da Silva Perez, and A. Dufresne, "Morphological investigation of nanoparticles obtained from combined mechanical shearing, and enzymatic and acid hydrolysis of sisal fibers," *Cellulose*, vol. 17, pp. 1147–1158, 2010.

[148] J. Pere, T. Tammelin, P. Niemi, M. Lille, T. Virtanen, P. A. Penttilä, P. Ahvenainen, and S. Grönqvist, "Production of high solid nanocellulose by enzyme-aided fibrillation coupled with mild mechanical treatment," *ACS Sustain. Chem. Eng.*, vol. 8, no. 51, pp. 18853–18863, 2020.

[149] V. Arantes, I. K. Dias, G. L. Berto, B. Pereira, B. S. Marotti, and C. F. Nogueira, "The current status of the enzyme-mediated isolation and functionalization of nanocelluloses: production, properties, techno-economics, and opportunities," *Cellulose*, pp. 1–60, 2020.

[150] R. Nickerson and J. Habrle, "Cellulose intercrystalline structure," *Industrial & Engineering Chemistry*, vol. 39, no. 11, pp. 1507–1512, 1947.

[151] B. G. Rånby, "Fibrous macromolecular systems. cellulose and muscle. the colloidal properties of cellulose micelles," *Discussions of the Faraday Society*, vol. 11, pp. 158–164, 1951.

[152] Y. Habibi, L. A. Lucia, and O. J. Rojas, "Cellulose nanocrystals: chemistry, self-assembly, and applications," *Chemical reviews*, vol. 110, no. 6, pp. 3479–3500, 2010.

[153] H. El-Saied, A. H. Basta, and R. H. Gobran, "Research progress in friendly environmental technology for the production of cellulose products (bacterial cellulose and its application)," *Polymer-Plastics Technology and Engineering*, vol. 43, no. 3, pp. 797–820, 2004.

[154] C. Sharma and N. K. Bhardwaj, "Bacterial nanocellulose: Present status, biomedical applications and future perspectives," *Materials Science and Engineering: C*, vol. 104, p. 109963, 2019.

[155] P. Gatenholm and D. Klemm, "Bacterial nanocellulose as a renewable material for biomedical applications," *MRS bulletin*, vol. 35, no. 3, pp. 208–213, 2010.

[156] M. Chen, J. Parot, V. A. Hackley, S. Zou, and L. J. Johnston, "Afm characterization of cellulose nanocrystal height and width using internal calibration standards," *Cellulose*, vol. 28, pp. 1933–1946, 2021.

[157] A. Karppinen, T. Saarinen, J. Salmela, A. Laukkanen, M. Nuopponen, and J. Seppälä, "Flocculation of microfibrillated cellulose in shear flow," *Cellulose*, vol. 19, pp. 1807–1819, 2012.

[158] V. Kumar, B. Nazari, D. Bousfield, and M. Toivakka, "Rheology of microfibrillated cellulose suspensions in pressure-driven flow," *Applied Rheology*, vol. 26, no. 4, pp. 24–34, 2016.

[159] O. Nechyporchuk, M. N. Belgacem, and F. Pignon, "Current progress in rheology of cellulose nanofibril suspensions," *Biomacromolecules*, vol. 17, no. 7, pp. 2311–2320, 2016.

[160] M. Schenker, J. Schoelkopf, P. Gane, and P. Mangin, "Influence of shear rheometer measurement systems on the rheological properties of microfibrillated cellulose (mfc) suspensions," *Cellulose*, vol. 25, pp. 961–976, 2018.

[161] T. Turpeinen, A. Jäsberg, S. Haavisto, J. Liukkonen, J. Salmela, and A. I. Koponen, "Pipe rheology of microfibrillated cellulose suspensions," *Cellulose*, vol. 27, pp. 141–156, 2020.

[162] A. K. Jaiswal, V. Kumar, A. Khakalo, P. Lahtinen, K. Solin, J. Pere, and M. Toivakka, "Rheological behavior of high consistency enzymatically fibrillated cellulose suspensions," *Cellulose*, vol. 28, pp. 2087–2104, 2021.

[163] M.-C. Li, Q. Wu, K. Song, S. Lee, Y. Qing, and Y. Wu, "Cellulose nanoparticles: structure–morphology–rheology relationships," *ACS Sustainable Chemistry & Engineering*, vol. 3, no. 5, pp. 821–832, 2015.

[164] E. Saarikoski, T. Saarinen, J. Salmela, and J. Seppälä, "Flocculated flow of microfibrillated cellulose water suspensions: an imaging approach for characterisation of rheological behaviour," *Cellulose*, vol. 19, pp. 647–659, 2012.

[165] S. Wojno, G. Westman, and R. Kádár, "Gel point in cnc dispersion from ft rheology," *Annu Trans Nordic Rheol Soc*, vol. 27, pp. 179–184, 2019.

[166] T. Mezger, *The Rheology Handbook: 4th Edition*. European Coatings Tech Files, Vincentz Network, 2011.

[167] B. Nazari, V. Kumar, D. W. Bousfield, and M. Toivakka, "Rheology of cellulose nanofibers suspensions: boundary driven flow," *Journal of Rheology*, vol. 60, no. 6, pp. 1151–1159, 2016.

[168] H. A. Barnes, J. F. Hutton, and K. Walters, *An introduction to rheology*, vol. 3. Elsevier, 1989.

[169] V. Kumar, *Roll-to-roll processing of nanocellulose into coatings*. Doctoral thesis, Åbo Akademi University, Faculty of Science and Engineering, 2018.

[170] M. Fazilati, S. Ingelsten, S. Wojno, T. Nypelö, and R. Kádár, "Thixotropy of cellulose nanocrystal suspensions," *Journal of Rheology*, vol. 65, no. 5, pp. 1035–1052, 2021.

[171] G. Agoda-Tandjawa, S. Durand, S. Berot, C. Blassel, C. Gaillard, C. Garnier, and J.-L. Doublier, "Rheological characterization of microfibrillated cellulose suspensions after freezing," *Carbohydrate Polymers*, vol. 80, no. 3, pp. 677–686, 2010.

[172] E. Lasseuguette, D. Roux, and Y. Nishiyama, "Rheological properties of microfibrillar suspension of tempo-oxidized pulp," *Cellulose*, vol. 15, pp. 425–433, 2008.

[173] B. P. Sutliff, A. Das, J. Youngblood, and M. J. Bortner, "High shear capillary rheometry of cellulose nanocrystals for industrially relevant processing," *Carbohydrate polymers*, vol. 231, p. 115735, 2020.

[174] X. Sun, Q. Wu, S. Lee, Y. Qing, and Y. Wu, "Cellulose nanofibers as a modifier for rheology, curing and mechanical performance of oil well cement," *Scientific reports*, vol. 6, no. 1, p. 31654, 2016.

[175] X. Sun, Q. Wu, J. Zhang, Y. Qing, Y. Wu, and S. Lee, "Rheology, curing temperature and mechanical performance of oil well cement: Combined effect of cellulose nanofibers and graphene nano-platelets," *Materials & Design*, vol. 114, pp. 92–101, 2017.

[176] S. Iwamoto, S.-H. Lee, and T. Endo, "Relationship between aspect ratio and suspension viscosity of wood cellulose nanofibers," *Polymer journal*, vol. 46, no. 1, pp. 73–76, 2014.

[177] Y. Boluk, R. Lahiji, L. Zhao, and M. T. McDermott, "Suspension viscosities and shape parameter of cellulose nanocrystals (cnc)," *Colloids and Surfaces A: Physicochemical and Engineering Aspects*, vol. 377, no. 1-3, pp. 297–303, 2011.

[178] Q. Wu, X. Li, S. Fu, Q. Li, and S. Wang, "Estimation of aspect ratio of cellulose nanocrystals by viscosity measurement: influence of surface charge density and nacl concentration," *Cellulose*, vol. 24, pp. 3255–3264, 2017.

[179] B. Peng, J. Tang, P. Wang, J. Luo, P. Xiao, Y. Lin, and K. C. Tam, "Rheological properties of cellulose nanocrystal-polymeric systems," *Cellulose*, vol. 25, pp. 3229–3240, 2018.

[180] A. Puisto, X. Illa, M. Mohtaschemi, and M. Alava, "Modeling the rheology of nanocellulose suspensions," *Nordic Pulp & Paper Research Journal*, vol. 27, no. 2, pp. 277–281, 2012.

[181] N. Casson, "Rheology of disperse systems," *Flow Equation for Pigment Oil Suspensions of the Printing Ink Type. Rheology of Disperse Systems*, pp. 84–102, 1959.

[182] A. Sisko, "The flow of lubricating greases," *Industrial & Engineering Chemistry*, vol. 50, no. 12, pp. 1789–1792, 1958.

[183] W. vom Berg, "Influence of specific surface and concentration of solids upon the flow behaviour of cement pastes," *Magazine of concrete research*, vol. 31, no. 109, pp. 211–216, 1979.

[184] L. Onsager, "Viscosity and particle shape in colloid solutions," *Phys. Rev*, vol. 40, pp. 1028–1038, 1932.

[185] R. Simha, "The influence of brownian movement on the viscosity of solutions.," *The Journal of physical chemistry*, vol. 44, no. 1, pp. 25–34, 1940.

[186] G. Batchelor, "Slender-body theory for particles of arbitrary cross-section in stokes flow," *Journal of Fluid Mechanics*, vol. 44, no. 3, pp. 419–440, 1970.

[187] I. M. Krieger and T. J. Dougherty, "A mechanism for non-newtonian flow in suspensions of rigid spheres," *Transactions of the Society of Rheology*, vol. 3, no. 1, pp. 137–152, 1959.

[188] O. Nechyporchuk, M. N. Belgacem, and F. Pignon, "Rheological properties of micro-/nanofibrillated cellulose suspensions: wall-slip and shear banding phenomena," *Carbohydrate polymers*, vol. 112, pp. 432–439, 2014.

[189] M. Mohtaschemi, K. Dimic-Misic, A. Puisto, M. Korhonen, T. Maloney, J. Paltakari, and M. J. Alava, "Rheological characterization of fibrillated cellulose suspensions via bucket vane viscometer," *Cellulose*, vol. 21, pp. 1305–1312, 2014.

[190] M. Mohtaschemi, A. Sorvari, A. Puisto, M. Nuopponen, J. Seppälä, and M. J. Alava, "The vane method and kinetic modeling: shear rheology of nanofibrillated cellulose suspensions," *Cellulose*, vol. 21, pp. 3913–3925, 2014.

[191] H. A. Barnes, *A handbook of elementary rheology*, vol. 1. University of Wales, Institute of Non-Newtonian Fluid Mechanics Aberystwyth, 2000.

[192] J. Salmela, S. Haavisto, A. Koponen, A. Jäsberg, and M. Kataja, "Rheological characterization of micro-fibrillated cellulose fibre suspension using multi scale velocity profile measurements," in *Advances in Pulp and Paper Research, 15th Fundamental Research Symposium* (S. L'Anson, ed.), pp. 495–509, 2013.

[193] A. Karppinen, A.-H. Vesterinen, T. Saarinen, P. Pietikäinen, and J. Seppälä, "Effect of cationic polymethacrylates on the rheology and flocculation of microfibrillated cellulose," *Cellulose*, vol. 18, pp. 1381–1390, 2011.

[194] A. Sorvari, T. Saarinen, S. Haavisto, J. Salmela, M. Vuoriluoto, and J. Seppälä, "Modifying the flocculation of microfibrillated cellulose suspensions by soluble polysaccharides under conditions unfavorable to adsorption," *Carbohydrate polymers*, vol. 106, pp. 283–292, 2014.

[195] M. H. Korhonen, A. Sorvari, T. Saarinen, J. Seppälä, J. Laine, *et al.*, "Deflocculation of cellulosic suspensions with anionic high molecular weight polyelectrolytes," *BioResources*, vol. 9, no. 2, pp. 3550–3570, 2014.

[196] M. Schenker, J. Schoelkopf, P. Mangin, and P. Gane, "Rheological investigation of complex micro and nanofibrillated cellulose (mnfc) suspensions: discussion of flow curves and gel stability," *Tappi Journal*, vol. 15, no. 6, pp. 405–416, 2016.

[197] N. Butchosa and Q. Zhou, "Water redispersible cellulose nanofibrils adsorbed with carboxymethyl cellulose," *Cellulose*, vol. 21, pp. 4349–4358, 2014.

[198] S. Ahola, P. Myllytie, M. Österberg, T. Teerinen, and J. Laine, "Effect of polymer adsorption on cellulose nanofibril water binding capacity and aggregation," *BioResources*, vol. 3, no. 4, pp. 1315–1328, 2008.

[199] M.-P. Lowys, J. Desbrieres, and M. Rinaudo, "Rheological characterization of cellulosic microfibril suspensions. role of polymeric additives," *Food Hydrocolloids*, vol. 15, no. 1, pp. 25–32, 2001.

[200] K. L. Spence, R. A. Venditti, O. J. Rojas, Y. Habibi, and J. J. Pawlak, "The effect of chemical composition on microfibrillar cellulose films from wood pulps: water interactions and physical properties for packaging applications," *Cellulose*, vol. 17, pp. 835–848, 2010.

[201] P. Lahtinen, S. Liukkonen, J. Pere, A. Sneck, and H. Kangas, "A comparative study of fibrillated fibers from different mechanical and chemical pulps," *BioResources*, vol. 9, no. 2, pp. 2115–2127, 2014.

[202] T. Lindström, "Aspects on nanofibrillated cellulose (nfc) processing, rheology and nfc-film properties," *Current Opinion in Colloid & Interface Science*, vol. 29, pp. 68–75, 2017.

[203] M. Delgado Aguilar, I. González Tovar, J. A. Tarrés Farrés, M. Alcalà Vilavella, M. À. Pèlach Serra, and P. Mutjé Pujol, "Approaching a low-cost production of cellulose nanofibers for papermaking applications," *© Bioresources, 2015, vol. 10, núm. 3, p. 5435-5355*, 2015.

[204] Y. Chu, Y. Sun, W. Wu, and H. Xiao, "Dispersion properties of nanocellulose: a review," *Carbohydrate polymers*, vol. 250, p. 116892, 2020.

[205] B. Ong, Y.-K. Leong, and S. Chen, "Yield stress-zeta potential relationship of oxide dispersions with adsorbed polyacrylate—steric effect and zeta potential at the flocculated-dispersed transition state," *Powder Technol.*, vol. 186, no. 2, pp. 176–183, 2008.

[206] E.-J. Teh, Y.-K. Leong, Y. Liu, B. Ong, C. Berndt, and S. Chen, "Yield stress and zeta potential of washed and highly spherical oxide dispersions—critical zeta potential and hamaker constant," *Powder Technol.*, vol. 198, no. 1, pp. 114–119, 2010.

[207] A. Ferrer, I. C. Hoeger, X. Lu, and O. J. Rojas, "Reinforcement of polypropylene with lignocellulose nanofibrils and compatibilization with biobased polymers," *Journal of Applied Polymer Science*, vol. 133, no. 34, 2016.

[208] M. P. Arrieta, E. Fortunati, F. Dominici, J. López, and J. M. Kenny, "Bionanocomposite films based on plasticized pla–phb/cellulose nanocrystal blends," *Carbohydrate polymers*, vol. 121, pp. 265–275, 2015.

[209] E. Fortunati, F. Luzi, D. Puglia, F. Dominici, C. Santulli, J. Kenny, and L. Torre, "Investigation of thermomechanical, chemical and degradative properties of pla-limonene films reinforced with cellulose nanocrystals extracted from phormium tenax leaves," *European Polymer Journal*, vol. 56, pp. 77–91, 2014.

[210] M. Martinez-Sanz, A. Lopez-Rubio, and J. M. Lagaron, "Optimization of the dispersion of unmodified bacterial cellulose nanowhiskers into polylactide via melt compounding to significantly enhance barrier and mechanical properties," *Biomacromolecules*, vol. 13, no. 11, pp. 3887–3899, 2012.

[211] M. Martínez-Sanz, A. Lopez-Rubio, and J. M. Lagaron, "Nanocomposites of ethylene vinyl alcohol copolymer with thermally resistant cellulose nanowhiskers by melt compounding (i): Morphology and thermal properties," *Journal of applied polymer science*, vol. 128, no. 5, pp. 2666–2678, 2013.

[212] M. Martínez-Sanz, A. Lopez-Rubio, and J. M. Lagaron, "Nanocomposites of ethylene vinyl alcohol copolymer with thermally resistant cellulose nanowhiskers by melt compounding (ii): Water barrier and mechanical properties," *Journal of applied polymer science*, vol. 128, no. 3, pp. 2197–2207, 2013.

[213] M. Ö. Seydibeyoğlu and K. Oksman, "Novel nanocomposites based on polyurethane and micro fibrillated cellulose," *Composites Science and Technology*, vol. 68, no. 3-4, pp. 908–914, 2008.

[214] M. Ankerfors, T. Lindström, and D. Söderberg, "The use of microfibrillated cellulose in fine paper manufacturing–results from a pilot scale papermaking trial," *Nordic Pulp & Paper Research Journal*, vol. 29, no. 3, pp. 476–483, 2014.

[215] I. González Tovar, S. Boufi, M. À. Pèlach Serra, M. Alcalà Vilavella, F. Vilaseca Morera, and P. Mutjé Pujol, "Nanofibrillated cellulose as paper additive in eucalyptus pulps," *© BioResources, 2012, vol. 7, núm. 4, p. 5167-5180*, 2012.

[216] T. Taipale, M. Österberg, A. Nykänen, J. Ruokolainen, and J. Laine, "Effect of microfibrillated cellulose and fines on the drainage of kraft pulp suspension and paper strength," *Cellulose*, vol. 17, pp. 1005–1020, 2010.

[217] Ø. Eriksen, K. Syverud, and Ø. Gregersen, "The use of microfibrillated cellulose produced from kraft pulp as strength enhancer in tmp paper," *Nordic Pulp & Paper Research Journal*, vol. 23, no. 3, pp. 299–304, 2008.

[218] S. Ahola, M. Österberg, and J. Laine, "Cellulose nanofibrils—adsorption with poly (amideamine) epichlorohydrin studied by qcm-d and application as a paper strength additive," *Cellulose*, vol. 15, pp. 303–314, 2008.

[219] Z. Fang, H. Zhu, C. Preston, and L. Hu, "Development, application and commercialization of transparent paper," *Translational Materials Research*, vol. 1, no. 1, p. 015004, 2014.

[220] C. Aulin, M. Gällstedt, and T. Lindström, "Oxygen and oil barrier properties of microfibrillated cellulose films and coatings," *Cellulose*, vol. 17, pp. 559–574, 2010.

[221] M. Minelli, M. G. Baschetti, F. Doghieri, M. Ankerfors, T. Lindström, I. Siró, and D. Plackett, "Investigation of mass transport properties of microfibrillated cellulose (mfc) films," *Journal of Membrane Science*, vol. 358, no. 1-2, pp. 67–75, 2010.

[222] V. Kumar, R. Bollström, A. Yang, Q. Chen, G. Chen, P. Salminen, D. Bousfield, and M. Toivakka, "Comparison of nano-and microfibrillated cellulose films," *Cellulose*, vol. 21, pp. 3443–3456, 2014.

[223] M. Henriksson, L. A. Berglund, P. Isaksson, T. Lindström, and T. Nishino, "Cellulose nanopaper structures of high toughness," *Biomacromolecules*, vol. 9, no. 6, pp. 1579–1585, 2008.

[224] K. Syverud and P. Stenius, "Strength and barrier properties of mfc films," *Cellulose*, vol. 16, pp. 75–85, 2009.

[225] K. Larsson, L. A. Berglund, M. Ankerfors, and T. Lindström, "Polylactide latex/nanofibrillated cellulose bionanocomposites of high nanofibrillated cellulose content and nanopaper network structure prepared by a papermaking route," *Journal of Applied Polymer Science*, vol. 125, no. 3, pp. 2460–2466, 2012.

[226] T. Tammelin, U. Hippi, and A. Salminen, "Method for the preparation of mfc films on supports," 2013. WO2013/030934A2.

[227] R. Pihko and V. Kunnari, "Method for the production of a film comprising microfibrillated cellulose, a film and a paper or paperboard product," 2019. US2019/0226149A1.

[228] V. Kumar and A. Jaiswal, "Method for manufacturing films from high consistency nanocellulose suspensions," 2020. WO2020/201627A1.

[229] S. M. Mazhari Mousavi, E. Afra, M. Tajvidi, D. Bousfield, and M. Dehghani-Firouzabadi, "Cellulose nanofiber/carboxymethyl cellulose blends as an efficient coating to improve the structure and barrier properties of paperboard," *Cellulose*, vol. 24, pp. 3001–3014, 2017.

[230] N. Lavoine, I. Desloges, B. Khelifi, and J. Bras, "Impact of different coating processes of microfibrillated cellulose on the mechanical and barrier properties of paper," *Journal of Materials Science*, vol. 49, pp. 2879–2893, 2014.

[231] E. Afra, S. Mohammadnejad, and A. Saraeyan, "Cellulose nanofibils as coating material and its effects on paper properties," *Progress in Organic Coatings*, vol. 101, pp. 455–460, 2016.

[232] C. J. Ridgway and P. A. Gane, "Constructing nfc-pigment composite surface treatment for enhanced paper stiffness and surface properties," *Cellulose*, vol. 19, pp. 547–560, 2012.

[233] M. A. Herrera, J. A. Sirviö, A. P. Mathew, and K. Oksman, "Environmental friendly and sustainable gas barrier on porous materials: Nanocellulose coatings prepared using spin-and dip-coating," *Materials & Design*, vol. 93, pp. 19–25, 2016.

[234] G. Fortunato, T. Zimmermann, J. Lübben, N. Bordeanu, and R. Hufenus, "Reinforcement of polymeric submicrometer-sized fibers by microfibrillated cellulose," *Macromolecular materials and engineering*, vol. 297, no. 6, pp. 576–584, 2012.

[235] M. S. Peresin, Y. Habibi, A.-H. Vesterinen, O. J. Rojas, J. J. Pawlak, and J. V. Seppälä, "Effect of moisture on electrospun nanofiber composites of poly (vinyl alcohol) and cellulose nanocrystals," *Biomacromolecules*, vol. 11, no. 9, pp. 2471–2477, 2010.

[236] J. P. de Mesquita, C. L. Donnici, and F. V. Pereira, "Biobased nanocomposites from layer-by-layer assembly of cellulose nanowhiskers with chitosan," *Biomacromolecules*, vol. 11, no. 2, pp. 473–480, 2010.

[237] Y. Boissard, "MFC for paper surface treatment," Master's thesis, Luleá University of Technology, Department of Engineering Sciences and Mathematics, 2017.

[238] F. Richmond, *Cellulose nanofibers use in coated paper*. Doctoral thesis, The University of Maine, 2014.

[239] K. Kinnunen-Raudaskoski, T. Hjelt, E. Kenttä, and U. Forsström, "Thin coatings for paper by foam coating," *Tappi J*, vol. 13, no. 7, pp. 9–19, 2014.

[240] K. Jung, Y. Ji, T.-J. Jeong, P. N. Ciesielski, J. C. Meredith, and T. A. Harris, "Roll-to-roll, dual-layer slot die coating of chitin and cellulose oxygen barrier films for renewable packaging," *ACS Applied Materials & Interfaces*, vol. 14, no. 39, pp. 44922–44932, 2022.

[241] M. Vähä-Nissi, H. M. Koivula, H. M. Räisänen, J. Vartiainen, P. Ragni, E. Kenttä, T. Kaljunen, T. Malm, H. Minkkinen, and A. Harlin, "Cellulose nanofibrils in biobased multilayer films for food packaging," *Journal of Applied Polymer Science*, vol. 134, no. 19, 2017.

[242] J. Fernández-Santos, C. Valls, O. Cusola, and M. B. Roncero, "Improving filmogenic and barrier properties of nanocellulose films by addition of biodegradable plasticizers," *ACS Sustainable Chemistry & Engineering*, vol. 9, no. 29, pp. 9647–9660, 2021.

[243] P. Cazón, M. Vázquez, and G. Velazquez, "Cellulose-glycerol-polyvinyl alcohol composite films for food packaging: Evaluation of water adsorption, mechanical properties, light-barrier properties and transparency," *Carbohydrate polymers*, vol. 195, pp. 432–443, 2018.

[244] K. Spence, Y. Habibi, and A. Dufresne, "Nanocellulose-based composites," in *Cellulose Fibers: Bio- and Nano-Polymer Composites: Green Chemistry and Technology* (S. Kalia, B. S. Kaith, and I. Kaur, eds.), pp. 179–213, Berlin, Heidelberg: Springer Berlin Heidelberg, 2011.

[245] C. Aulin, G. Salazar-Alvarez, and T. Lindström, "High strength, flexible and transparent nanofibrillated cellulose–nanoclay biohybrid films with tunable oxygen and water vapor permeability," *Nanoscale*, vol. 4, no. 20, pp. 6622–6628, 2012.

[246] L. Alves, E. Ferraz, and J. Gamelas, "Composites of nanofibrillated cellulose with clay minerals: A review," *Advances in Colloid and Interface Science*, vol. 272, p. 101994, 2019.

[247] M. Al-Gharrawi, R. Ollier, J. Wang, and D. W. Bousfield, "The influence of barrier pigments in waterborne barrier coatings on cellulose nanofiber layers," *Journal of Coatings Technology and Research*, vol. 19, no. 1, pp. 3–14, 2022.

[248] G. L. Robertson, "1 - introdcution to food packaging," in *Food packaging: principles and practice*, pp. 1–10, CRC press, 3 ed., 2016.

[249] T. Lindström and F. Österberg, "Evolution of biobased and nanotechnology packaging–a review," *Nordic Pulp & Paper Research Journal*, vol. 35, no. 4, pp. 491–515, 2020.

[250] D. S. An, J. H. Lee, and D. S. Lee, "Water vapor and oxygen barrier estimation in designing a single-serve package of powdered infant formula for required shelf life," *Journal of Food Process Engineering*, vol. 41, no. 1, p. e12592, 2018.

[251] J. Lange and Y. Wyser, "Recent innovations in barrier technologies for plastic packaging—a review," *Packaging Technology and Science: An International Journal*, vol. 16, no. 4, pp. 149–158, 2003.

[252] A. Adibi, B. M. Trinh, and T. H. Mekonnen, "Recent progress in sustainable barrier paper coating for food packaging applications," *Progress in Organic Coatings*, vol. 181, p. 107566, 2023.

[253] J. Wang, D. J. Gardner, N. M. Stark, D. W. Bousfield, M. Tajvidi, and Z. Cai, "Moisture and oxygen barrier properties of cellulose nanomaterial-based films," *ACS Sustainable Chemistry & Engineering*, vol. 6, no. 1, pp. 49–70, 2018.

[254] J. Lyytikäinen, *Interaction and barrier properties of nanocellulose and hydrophobically modified ethyl (hydroxyethyl) cellulose films and coatings*. Doctoral thesis, Lappeenranta-Lahti University of Technology LUT, 2021.

[255] D. Kyllönen, "Cellulose products for paperboard barrier coatings," Master's thesis, Aalto University, School of chemical engineering, 2022.

[256] A. Miettinen, G. Chinga-Carrasco, and M. Kataja, "Three-dimensional microstructural properties of nanofibrillated cellulose films," *International journal of molecular sciences*, vol. 15, no. 4, pp. 6423–6440, 2014.

[257] C. A. Cozzolino, G. Cerri, A. Brundu, and S. Farris, "Microfibrillated cellulose (MFC): Pullulan bionanocomposite films," *Cellulose*, vol. 21, pp. 4323–4335, 2014.

[258] M. Österberg, J. Vartiainen, J. Lucenius, U. Hippi, J. Seppälä, R. Serimaa, and J. Laine, "A fast method to produce strong nfc films as a platform for barrier and functional materials," *ACS applied materials & interfaces*, vol. 5, no. 11, pp. 4640–4647, 2013.

[259] G. I. for Standardization, "Requirements for packaging recoverable through composting and biodegradation - test scheme and evaluation criteria for the final acceptance of packaging," Standard DIN EN 13432, German Instiute for Standardization, Berlin, Germany, 2000.

[260] M. Vikman, J. Vartiainen, I. Tsitko, and P. Korhonen, "Biodegradability and compostability of nanofibrillar cellulose-based products," *Journal of Polymers and the Environment*, vol. 23, pp. 206–215, 2015.

[261] B. P. Frank, C. Smith, E. R. Caudill, R. S. Lankone, K. Carlin, S. Benware, J. A. Pedersen, and D. H. Fairbrother, "Biodegradation of functionalized nanocellulose," *Environmental Science & Technology*, vol. 55, no. 15, pp. 10744–10757, 2021.

[262] I. Leppänen, M. Vikman, A. Harlin, and H. Orelma, "Enzymatic degradation and pilot-scale composting of cellulose-based films with different chemical structures," *Journal of Polymers and the Environment*, vol. 28, pp. 458–470, 2020.

[263] K. Shanmugam, H. Nadeem, S. Varanasi, G. Gamier, and W. Batchelor, "Effect of recycling on the properties of nanocellulose-barrier and mechanical properties," in *Paper Conference and Trade Show 2019*, pp. 1401–1403, TAPPI Press, 2019.

[264] H. Nadeem, M. Naseri, M. Dehghani, M. Pazirofteh, V. Raghuwanshi, G. Garnier, and W. Batchelor, "Spray deposited cellulose nanofibril films: a recyclability study," *Waste and Biomass Valorization*, pp. 1–14, 2023.

[265] S. Ang, D. Ghosh, V. Haritos, and W. Batchelor, "Recycling cellulose nanofibers from wood pulps provides drainage improvements for high strength sheets in papermaking," *Journal of Cleaner Production*, vol. 312, p. 127731, 2021.

[266] A. Naderi, T. Lindström, J. Sundström, G. Flodberg, and J. Erlandsson, "A comparative study of the properties of three nanofibrillated cellulose systems that have been produced at about the same energy consumption levels in the mechanical delamination step," *Nordic Pulp & Paper Research Journal*, vol. 31, no. 3, pp. 364–371, 2016.

[267] J. F. Steffe, *Rheological methods in food process engineering*. Freeman press, 1996.

[268] N. Elton, L. Gate, and J. Hooper, "Texture and orientation of kaolin in coatings," *Clay Miner*, vol. 34, no. 1, pp. 89–98, 1999.

[269] R. Bollström, R. Nyqvist, J. Preston, P. Salminen, and M. Toivakka, "Barrier properties created by dispersion coating," *Tappi Journal*, vol. 12, no. 4, pp. 45–51, 2013.

[270] P. Miettinen, S. Auvinen, J. Kuusipalo, and S. Haakana, "Validity of traditional barrier-testing methods to predict the achievable benefits of the new generation water based barrier coatings for packaging materials," in *PTS Coating Symposium*, pp. 328–342, 2015.

[271] G. Drage, O. Tammn, and J. Husband, "Pigments," in *Pigment coating and surface sizing of paper* (J. Paltakari, ed.), vol. 11, pp. 72–190, Paper Engineers' Association/Paperi ja Puu Oy, 2 ed., 2009.

[272] M. Singhvi and D. Gokhale, "Biomass to biodegradable polymer (pla)," *RSC advances*, vol. 3, no. 33, pp. 13558–13568, 2013.

[273] S. Rafiqah, A. Khalina, A. S. Harmaen, I. A. Tawakkal, K. Zaman, M. Asim, M. Nurrazi, and C. H. Lee, "A review on properties and application of bio-based poly (butylene succinate)," *Polymers*, vol. 13, no. 9, p. 1436, 2021.

[274] K. W. Meereboer, M. Misra, and A. K. Mohanty, "Review of recent advances in the biodegradability of polyhydroxyalkanoate (pha) bioplastics and their composites," *Green Chemistry*, vol. 22, no. 17, pp. 5519–5558, 2020.

[275] U. Witt, T. Einig, M. Yamamoto, I. Kleeberg, W.-D. Deckwer, and R.-J. Müller, "Biodegradation of aliphatic–aromatic copolyesters: evaluation of the final biodegradability and ecotoxicological impact of degradation intermediates," *Chemosphere*, vol. 44, no. 2, pp. 289–299, 2001.

[276] E. Rudnik, "11 - biodegradability testing of compostable polymer materials," in *Handbook of Biopolymers and Biodegradable Plastics* (S. Ebnesajjad, ed.), Plastics Design Library, pp. 213–263, Boston: William Andrew Publishing, 2013.

Rajesh Koppolu

High-throughput Processing of Nanocelluloses into Barrier Coatings

A Focus on Nanocellulose Rheology and Multilayer Barrier Properties

Our modern lives are heavily reliant on packaging, particularly for food, where complex multi-layered structures ensure freshness, extended shelf life, and minimized waste. However, the single-use nature of most packaging necessitates sustainable and bio-based materials, alongside designs favoring recyclability or biodegradability. This thesis explores high-throughput processing methods to leverage nanocellulose, a natural and biodegradable polymer, as a coating for effective barrier properties in packaging. The complex rheology of nanocelluloses hinders its industrial use, and therefore, this work examines their properties and develops efficient coating methods to process them into barrier coatings. By systematically studying the role of the substrate, nanocellulose additives, coating conditions, and interlayer adhesion on paperboard substrates, all coatings were conducted via a roll-to-roll process mimicking industrial conditions. In addition, multilayer coatings with a moisture barrier top coat containing different bio-based and biodegradable polymers were also produced using traditional methods, and these nanocellulose-based multilayer structures showed barrier properties comparable to conventional references. This research brings nanocellulose closer to real-world application as a sustainable and high-performance barrier material for food packaging.

ISBN 978-952-12-4358-5